LINAG phase I

W. Mittig

LINAG Phase I

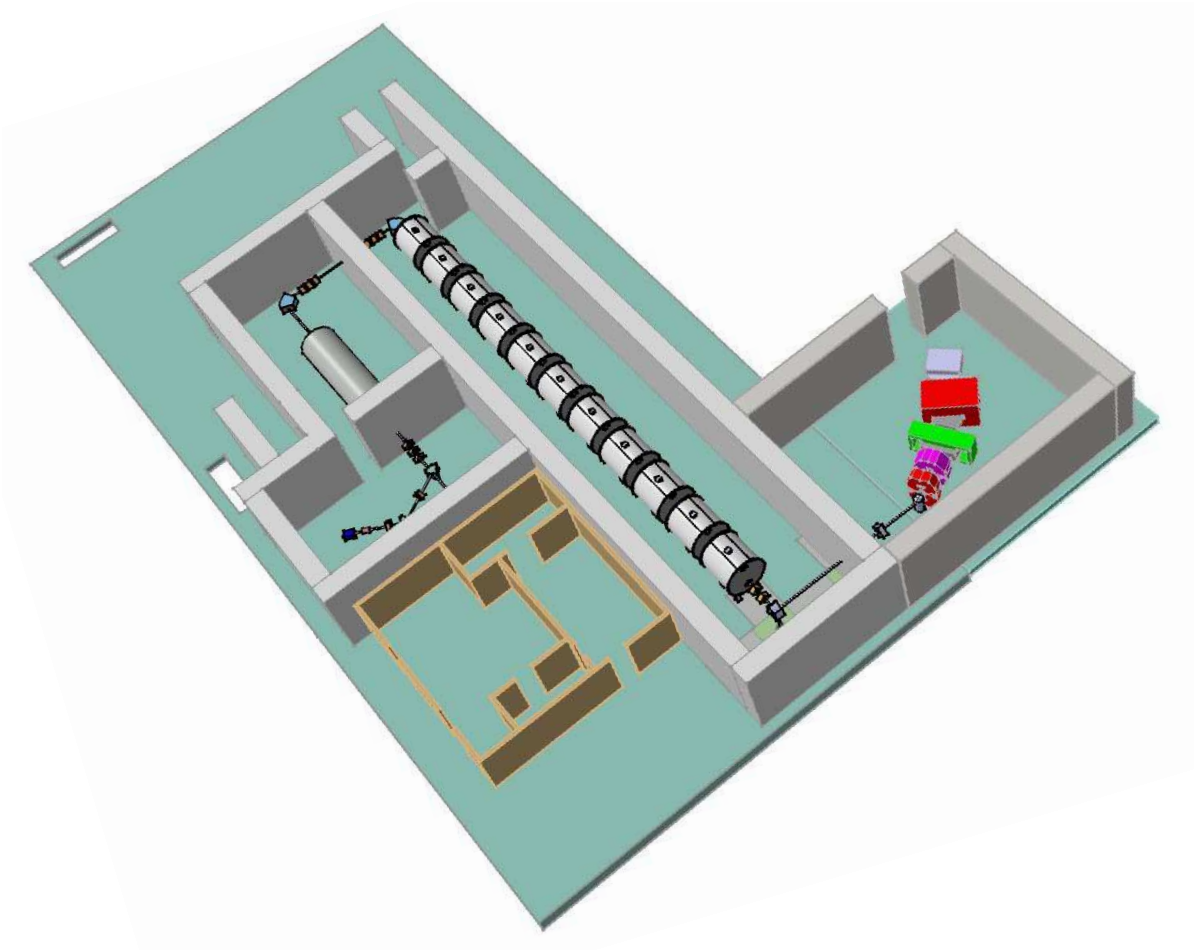

A Technical Report

Version : 1.3

GANIL, June 27, 2002

Chapter I : Introduction

In a first report [ref. 1] the possibility of a high intensity accelerator at GANIL, producing secondary beams of unprecedented intensity, was considered. As was outlined in that report, LINAG I, a low energy high intensity linear accelerator constituting a first phase of this more general project, could produce secondary beams either from fission products, or from fusion-evaporation or deep inelastic reactions. The Scientific Council and Directors of GANIL recommended a more detailed technical study of LINAG I as a possible option for the SPIRAL II project [ref. 2], to be compared to the photofission option. This is the objective of the present report. We will first remind readers of the general context.

The systematic and very successful use of high energy fragmentation at GANIL, (the first operational high intensity heavy ion accelerator in the 50-100 MeV/nucleon domain) for exploring the structure of nuclei far from stability, triggered the question of how to proceed even further in this domain. The study of nuclei far from stability has become one of the major activities at GANIL, and is one of its domains of excellence. In near future, the possibility of producing and accelerating radioactive beams by the ISOL method will become available. For this reason the Directors and the Scientific Council of GANIL decided about four years ago to initiate a study of long range perspectives. The results of the working groups can be found in the minutes of the Scientific Council, and the physics case will be published soon.

A pre-project study named SPIRAL II [ref. 2, 3], was undertaken in order to add medium-mass nuclei to the ones available with SPIRAL. In this project, fission induced by light particles (e, p, d, etc...) is proposed to produce the radioactive ions, with an aim of 10^{13} fissions/s at least, with and without a converter (an intermediate target for producing high fluxes of neutrons).

It is clear that the final intensities of RIBs will determine the domains of the nuclear chart that will be accessible to experiments. This implies a need for high intensity primary beams and versatile production techniques. Following these scientific needs, GSI is considering an upgrade of its facility, to provide 10^{12} ions/s from p to U at 1.5 GeV. The USA project RIA is planning to use several hundreds of kW of primary beams—from protons to U—at about 400 MeV/nucleon. The ISAC facility at TRIUMF uses already 20 µA (1.2×10^{14} p/s) of protons at 500 MeV for spallation production of ISOL beams, and will be able to use 5 times higher intensities in the future. The UK has proposed a high intensity proton accelerator for fission and fusion-evaporation reactions. RIKEN in Japan is starting an energy and intensity upgrade. In Europe, a study group is considering various solutions for EURISOL, an eventual European ISOL facility for provision of intense radioactive ion beams. The LNL laboratory in Legnaro, Italy, is considering a high intensity low energy proton driver, called SPES. Links to these projects can be found in [ref. 4].

In this context of fast evolution on the European and international level we consider here the possibility of an intensity upgrade of GANIL in its domain of excellence, i.e. beams in the energy domain of about 100 MeV/nucleon for low- to medium-mass nuclei (A<100). We have evaluated the possibility of producing beams of several hundreds of kilowatts, i.e. of the order of 1 mA, corresponding to 6×10^{15} particles/s for light particles and 3×10^{14}/s for heavier particles. The present accelerator configuration consisting of three cyclotrons in a cascade will not be capable of furnishing such high intensities. At present, the highest beam powers reached are in the 2–6 kW domain, or 2×10^{13} particles/s. It is not realistic to expect a very significant increase with respect to such values. With present technologies, only linear accelerators are capable of producing such high intensities. Moreover, recent progress in high intensity ion sources for high charge states is another important feature to be taken into account. For this reason, we are considering the possibility of the construction of a very high intensity linear accelerator at GANIL in this energy and mass domain. Such a possibility would be complementary to the RIKEN, GSI and RIA projects, optimised in a different mass-energy domain.

The project, as outlined below, can be constructed in various phases, starting at low energy. It would cover a broad range of possibilities of primary and secondary beams. Very high intensity primary beams would be available from below the Coulomb barrier to 100 MeV/n from deuterons to mass 100 nuclei. Even intense heavy beams like U could be accelerated to somewhat lower energy. These beams could be used for the production of intense secondary beams by all reaction mechanisms (fusion, fission, fragmentation, spallation, etc.) and technical methods (recoil spectrometers, ISOL, IGISOL, etc.). Thus, the most advantageous method for a given problem of physics could be chosen. In the first phase, this corre-

sponds to an acceleration potential of about 40 MV, with fission induced by neutrons from a converter, or by direct beams such as d, ^{3}He or ^{4}He, and fusion-evaporation reactions would be available.

The present work was done, as stated in the title, as an internal consideration of the possibilities of producing these high intensity beams at GANIL. It is clear that any project has to be integrated in a European and international context. In particular, we need to be aware of the EURISOL project, at present still a site-independent study, and the possibilities for LINAG—or some sections of it—to form part of this future project. For example, the EURISOL post-accelerator, planned for accelerating very heavy ions to some 100 MeV/u, has essentially the same specifications as that proposed here for the primary LINAG driver.

References

1) http//www.ganil.fr/research/sp/reports/files/linag.pdf
2) M.G. Saint Laurent et al. , SPIRAL phase II European RTD report, GANIL R 01-03 2001.
3) http//www.ganil.fr/spiral2/spiral_phaseII.pdf
4) http://www.ganil.fr/eurisol/eurisollinks.html

Chapter II : Production of RIBs by fragmentation and ISOL

II.1) GENERAL REMARKS

To achieve high intensities of RIBs, whilst reaching very far from stability regions, it will be of fundamental importance to take advantage of various strategies in the production scheme. Therefore, modern "next-generation" exotic ion beam facilities should consider all available techniques for the production of radioactive elements. Only a multi-beam heavy ion driver offers the possibility of adapting the best production method to the requested radioactive ion beam specifications. This is the main asset of the present GANIL laboratory, as this unique facility offers both thin-target (in-flight) and thick-target (ISOL) methods.

The facility considered in this document represents an intensity upgrade of the present GANIL laboratory, with the same characteristics of the production systems and a factor of 100–500 higher primary beam intensity. This new facility could provide an upgrade of the RIB final intensity of the same order of magnitude, i.e. 100–500 higher.

If one considers an improved separator with characteristics similar to the new A1900, recently commissioned at MSU [ref. 1], the final intensity of in-flight RIBs can be increased of another factor 10 to 100 as compared to present devices at GANIL such as SISSI and LISE.

All possible production schemes potentially available in such a facility are shown in figure II.1, with the two main branches of thin-target (in-flight) and thick-target (ISOL) methods. Primary beams are shown in green, ion beams in red and neutral particles in black.

In the in-flight method, the primary beam hits a thin target so that the reaction products escape from the target with energies close to that of the beam. Such fragmentation reactions are favourable when high-energy heavy ions hit a suitable target. The fragments are directed forward in a narrow cone at considerable energy, but with a large momentum spread. As much as possible of the beam is accepted into a separator and a particular isotope selected. The energy from the reaction is usually high enough for many nuclear physics experiments at intermediate energy (see the GANIL reports since 1987).

In the ISOL method—presently in use at SPIRAL—the primary beam hits a thick target : the reaction products are stopped in the target material and diffuse out to the surface. Then they pass through the target voids (effuse) and eventually reach the ioniser and are extracted as an ion beam. The beam is mass-analysed and the selected isotope transmitted to the experiment or to a post-accelerator. A variation of the ISOL method is to use protons or deuterons into a neutron-producting "converter" target, from which the neutrons then interact with a thick production target. The converter and the production target can also be one and the same target.

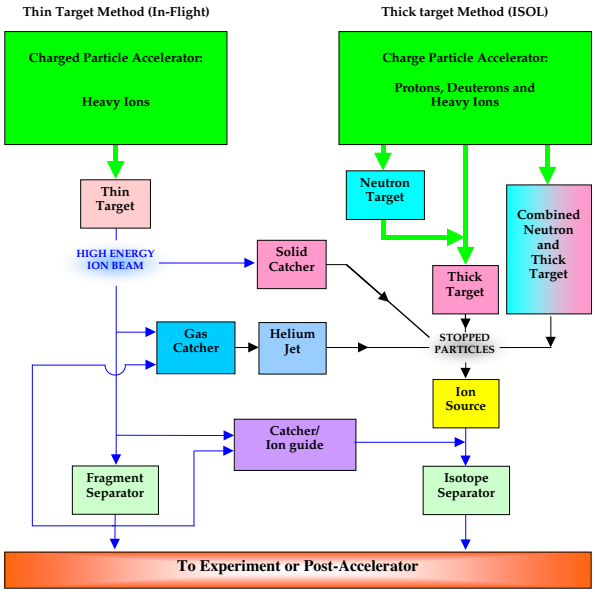

Figure II-1 : All potential RIB production methods with a heavy ion driver [ref. 2]. GANIL has already developed and routinely uses most of the branches shown.

The thin-target and thick-target methods can be combined ; the particles from the thin fragmentation target are stopped in a thick target and then pass into the rest of the ISOL system. Alternatively the particles can be stopped in a gas catcher and passed into the ion source via a helium gas jet. Another variation on this is to stop the energetic particles in a gas and then have a helium gas ion-guide system or IGISOL (Ion-Guide Isotope Separator On-Line). The particles emerge from the IGISOL as singly charged ions, avoiding the need for a separate ioniser.

With the use of a thin target technique, all the particles are released instantaneously, whereas in the thick-target technique, where all the particles are stopped, there may be

considerable delay in the release. This is due to the slow diffusion out of the target and effusion through the target void to the ioniser. In addition, many particles stick physically or chemically to the surfaces. If the effusion time is longer than the lifetime of the radioactive particles, they will decay before reaching the ioniser.

The combination of these two techniques allows one to have a complementary and complete range of radioactive species available for experiments in a large energy range. The obvious extra advantage of this concept is that the GANIL team has already the know-how for the various production schemes proposed in this document. It is a straightforward upgrade of the present facility.

For a more detailed comparison between production methods and yields see [ref. 3].

II.2) PRODUCTION OF ACCELERATED ISOL-RIBs FROM FISSION AND COMPARISON WITH PHOTO-INDUCED FISSION.

Fission yields from 40 MeV deuterons with converter as compared to the fission yield from electrons

Deuterons of 40 MeV will produce in the converter neutrons centered at around 14 MeV that will induce fission of the compound nucleus ^{239}U at an excitation energy of about 19 MeV. Electrons will induce fission centered at the giant dipole resonance (GDR) in ^{238}U at about 15 MeV of excitation energy. Thermal neutrons on ^{235}U induce fission at an excitation energy equal to the binding energy of the neutron, 6.54 MeV. Fast neutrons from fission are centered around 2 MeV. We will present the results of two model calculations for the different reactions. The first one is from [ref. 4]. The fission yields for neutron-induced fission were obtained from http://isotopes.lbl.gov/fission.html, and are commonly used and adopted for reactor physics. The same data tables are used by the CINDER'90 activation code coupled to the LAHET high energy code. Fission yields for gamma-induced fission were calculated with the fission model by V. Rubchenya at Jyväskylä, Finland.

In figure II.2, the mass yield for different reactions is shown. As is well known, the valley in the mass yield is filled in with increasing excitation energy and the “wings” become broader. Figure II.3 shows, as an example, the yield of Kr isotopes per fission. The same tendencies are obtained for other isotope chains. Full calculations taking into account the energy variation and geometry for the deuterons with converter are available (ref. 5 and see chapter V). Owing to the extra neutron in the compound nucleus, and the broader fission distributions, the yield of neutron-rich isotopes is higher for 14 MeV neutron-induced fission. This of course implies a lower branching ratio to isotopes on the maximum of the distribution.

The ratio of fission yields for neutrons and gammas is shown in figure II.4 As can be seen, the relative yield for isotopes near the maximum is about a factor of 2 lower on the fission peak, whereas it is a factor 10 to 100 higher for the most neutron rich isotopes.

In order to check the model dependence of such a calculation, we may compare them with the calculations of J. Benliure et al. [ref. 6]. The photofission was calculated using GEANT 3.21 for the geometry and bremsstrahlung and the atomic interactions with converter of a W cylinder 0.2 cm x

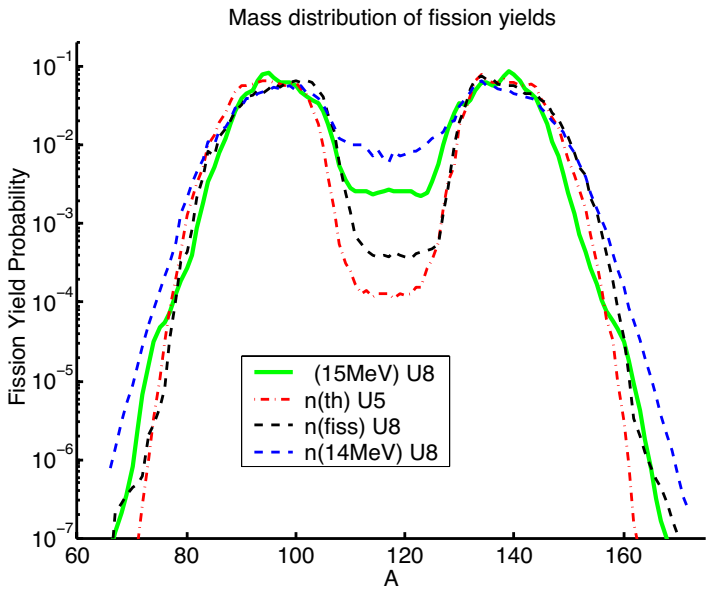

Figure II.2 : Mass yields for different reactions.

1 cm radius and a target in the form of a cylinder of ^{238}U 10cm long, and 1 cm radius. The GSI code [ref.7] for gamma capture for evaporation and fission was used. For the fast neutrons, the Serber model for deuteron breakup was used together with GEANT 3.21 for the geometry, and atomic

interactions and neutron propagation, based on the code FLUKA. The GSI code was used for neutron capture and evaporation and fission. The converter was a Be cylinder, 1 cm long, and 1 cm radius. The same target geometry as above was used. The deuteron energy was 40 MeV. The isotopic distributions obtained are shown on figures II.5a and II.5b.

There is a good quantitative agreement with the preceding calculations. As can be seen, with the only exception of Ag, the neutron-induced fission gives higher yields for neutron-rich isotopes as compared to electrons.

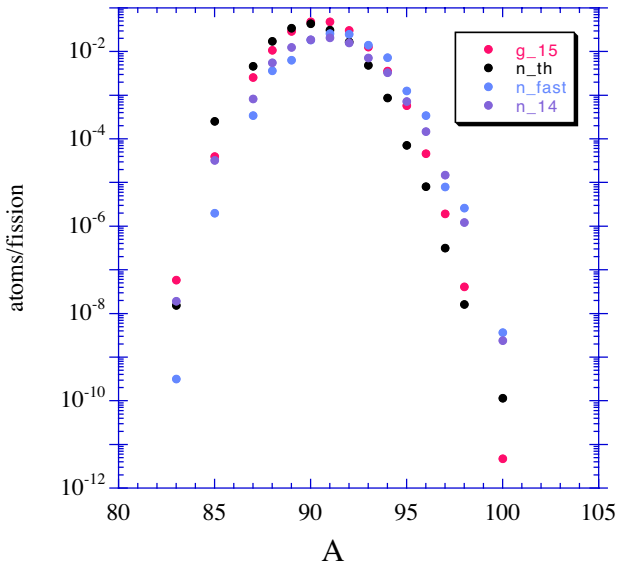

Figure II.3 : In-target yields of Kr isotopes for different reactions (from D.Ridikas, private communication)

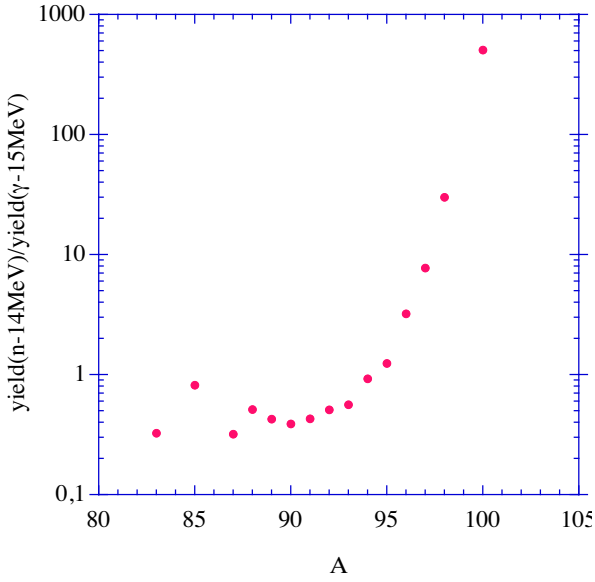

Figure II.4 : Ratio of yields from neutron- and electron-induced fission for Kr isotopes.

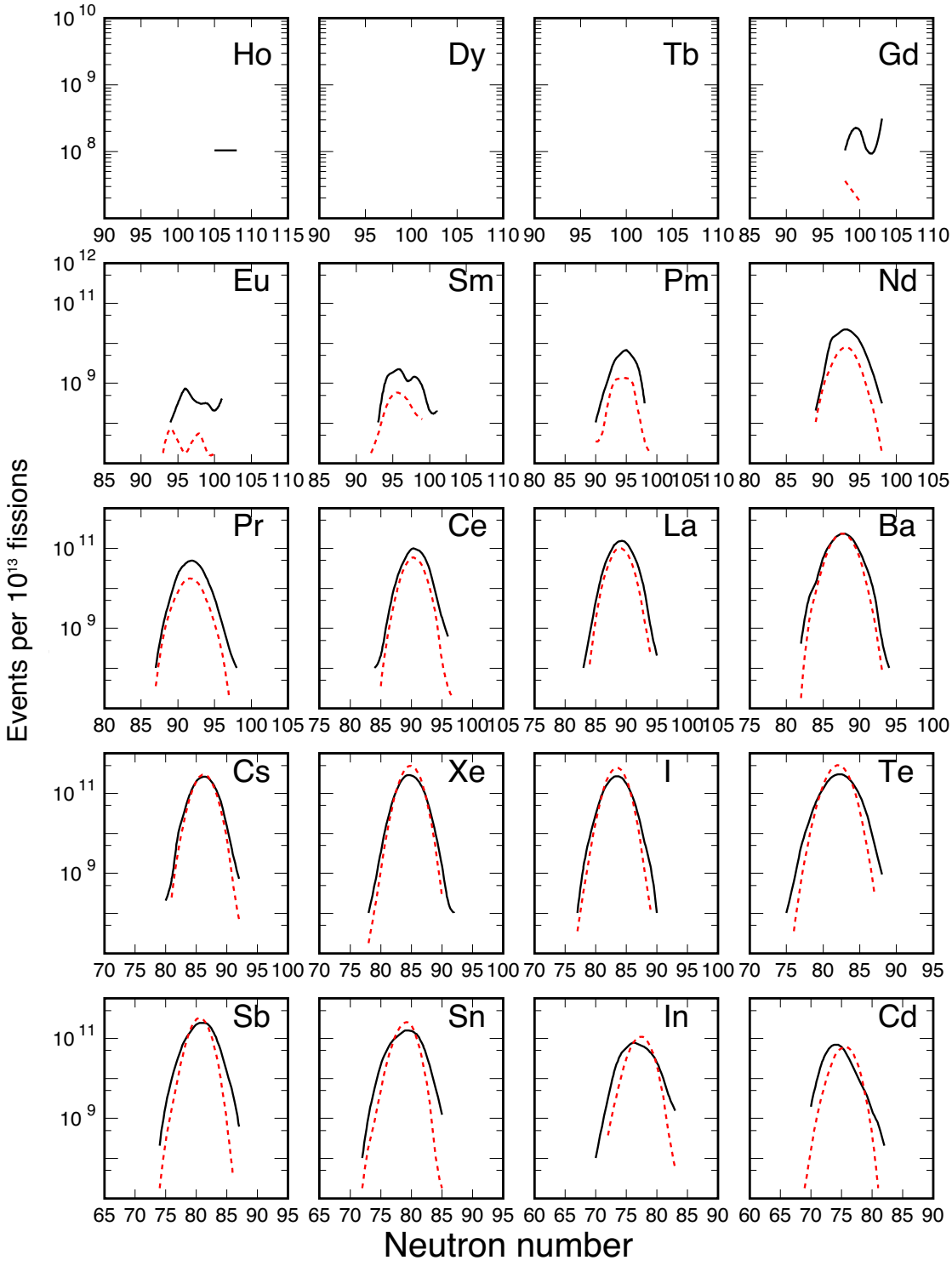

Figure II.5a : Isotopic yields for neutron- and electron-induced fission, for 10^{13} fissions, for Ho to Cd. Continuous black line for neutrons, broken red line for electrons (from ref. 6 and J. Benliure, private communication).

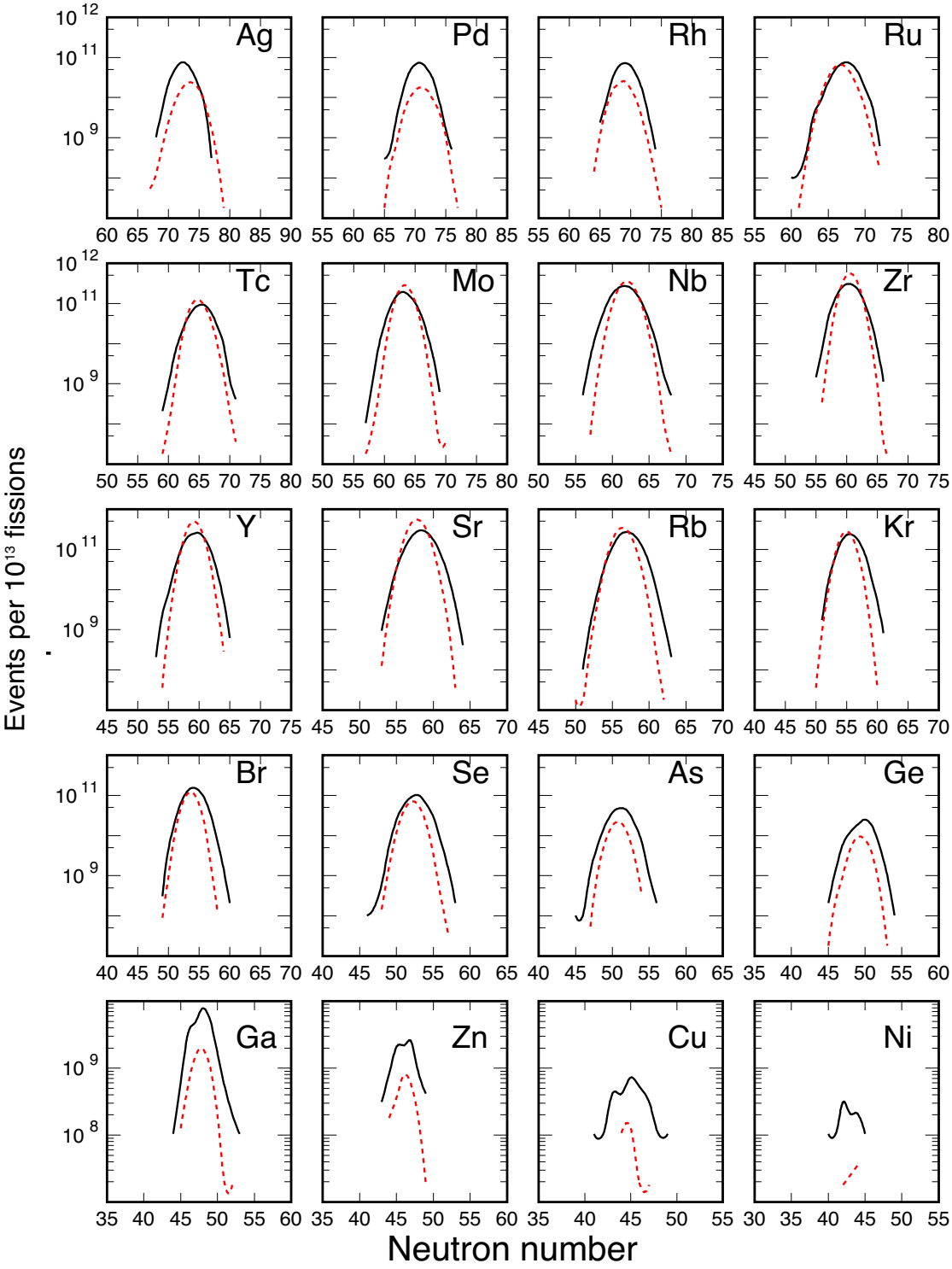

Figure II.5b : Isotopic yields for neutron- and electron-induced fission, for 10^{13} fissions, for Ag to Ni. Continuous black line for neutrons, broken red line for electrons (from ref. 6 and J.Benliure, private communication).

Similar conclusions were reached by [ref 8], as can be seen in particular in their figures II.4 and 5.

We can conclude that fission yields are similar from electron- and deuteron-induced fission near the maximum of the fission yield. The deuteron-induced fission has a higher yield by 1–2 orders of magnitude as one moves away from this region, either to more neutron-rich nuclei, or/and to lighter or heavier masses.

Fission induced without converter.

With the LINAG I accelerator, fission may be induced directly using deuterons without a converter. In this case the beam power will be deposited in the fissile material. With deuterons or protons of about 40 MeV, to reach 10^{13} fissions/s a beam power of 12 kW (corresponding to 0.3 mA) is necessary. In principle, only a very small amount of target material is needed, owing to the short range in UC_x. The total range of 40 MeV deuterons is 1540 mg/cm^2, corresponding to only 8 mm for a low-density UC_x, implying the need for a very compact geometry, and thus a small target and consequently a fast release. However, the power density is extremely high, mainly in the Bragg peak region. In order to overcome this problem, one could divide the target into two pieces. The first one, of UC_2, would be used for the production of radioactive species and diffusion. The second one, of pure C, would act as a cooled beam-stop. In this case, the last 3 mm of the range are useless for the fission production and, therefore, a slightly larger intensity is necessary in order to achieve 1 x 10^{13} fission/s. This corresponds to approximately 0.5 mA of deuteron beam. It is clear that in both cases a special geometry of the UC_2 target is necessary in order to spread the beam power over a large volume. A solution similar to the cone-shaped target of SPIRAL can be very suitable. A specific study is needed to define a realistic design.

Other projectiles can be used for induction of fission: $^{3,4}He$ 1^+ or 2^+, ^6Li 2^+, ^{12}C 4^+, etc..., corresponding to maximum kinetic energies of 40, 80, 80, and 160 MeV, respectively. Beams of up to 1 mA could be used, and a broader range of masses would be covered, owing to the high excitation energy.

IGISOL methods for the production of refractive element beams.

The high intensity flux of neutrons could be used to induce fission in thin foils, embedded in a He gas that captures the fission products (IGISOL method). At present the efficiency reached for 10 µA of protons of 30 MeV is 0.02% at Jyväskyla. It is believed that the rather low value of the efficiency is mainly due to the ionisation of the He gas by the beam. This could be avoided by using neutrons from the converter. With a neutron yield of 0.006 n/d in a 30-degree cone, this would lead to 1.5 x 10^9 fissions/s. The IGISOL method is chemically completely unselective, so refractive elements are accessible. Assuming an efficiency of 10%, as seems possible with this method, and a fission branching ratio of 1%, 1^+ beams of 10^6 ions/s could be extracted. This number could be improved using a multi-target device.

Fusion evaporation reactions.

The neutron-rich fission products could be complemented by nuclei near the proton drip line. It is well known that highest cross sections in this region are provided by fusion-evaporation reactions. Because of the nearly infinite number of combinations possible, it is difficult to give an exhaustive list. We shall just give one example :

The cross section in the reaction $^{24}Mg+^{58}Ni$ leading to ^{80}Zr has been measured to be 10±5 µb [ref. 9] at 3.3 MeV/n. Taking a rotating target wheel such as was developed for the search of super-heavy elements at GANIL, we can estimate that a beam of 200 µA of $^{24}Mg^{8+}$ should be possible without melting the Ni target. This will lead to some 8 x 10^4 atoms of ^{80}Zr per second, an unprecedented production rate. With a recoil spectrometer having 30% transmission, 2 x 10^4/s could be delivered to an experimental device.

Other possible beams are ^{16}O, ^{20}Ne, ^{32}S, etc. on targets of Ca, Fe, Ni, etc. This opens up the possibility of a broad range of experiments on N=Z nuclei.

References.

1) http://www.nscl.msu.edu
2) Adapted from R. Bennet and A.C.C. Villari, FINA report (2001).
3) GANIL report R0102.
4) D. Ridikas and W. Mittig, GANIL report P9822 and D. Ridikas, private communication.
5) M.G. Saint Laurent et al., SPIRAL phase II European RTD report, GANIL R 01-03 2001.
6) J. Benlluire, private communication.
7) J. Benlluire et al., Nucl.Phys. A700(2002) 469, and ref. cited.
8) J. Aysto et al., Europ. Phys. Journal A, 13(2002)109.
9) Gelletly et al Acta Physica Pol.B26(95)323.

Chapter III : Hight intensity multi-charge ion sources for LINAG I

III.1) CONSTRAINTS

We have focused our attention on the ion sources dedicated to the production of heavy ions with Q/A equal to 1/3 at the level of 1 mA. The source will function in CW mode at a voltage close to 60 kV and the emittance of the source must be lower than the acceptance of the RFQ, i.e. around 200 π mm.mrad

III.2) MULTI-CHARGED ION SOURCES.

III.2.1) Current state of the art

Rapid strides have been made recently in several parts of the world in the development of ion sources capable of producing ion beams in high charge states. For example, one of the more promising sources for producing high current ion beams at present is the 28 GHz PHOENIX ion source from SSI/ISN (Fig. III.1).

The highest current that has been produced up to the present with this source is a beam of 0.6 mA of Xe^{20+} in pulsed mode (10 ms at 10 Hz with afterglow and at 60 kV). This beam corresponds to 15 mA of total current extracted from the source and 10.4 mA transferred through the beam line. A rough estimation of the emittance leads to a value of 150–200 π.mm.mrad. This means that in term of beam characteristics the requested beam of LINAG has already been achieved, and the feasibility of a source operating at 60 kV has been proved. It is thought that an upgrade up to 100 kV is feasible.

However, this source operates in pulsed mode at present, although an extension of its operation to the CW region has also been contemplated. This can be done through a short and relatively low-cost development program on the present PHOENIX source, simply by the introduction of a new FeNdB hexapole (1.5 T instead of 1.2 T), a new extractor and insulator, and a diagnostic system for beam emittance measurement. [This program is called A-PHOENIX].

To give an overview of the state of the art more generally, table III.1 summarizes the best currents which have been obtained to date with different ECR ion sources all over the world :

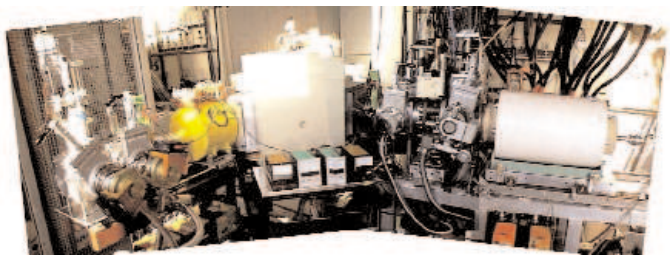

Fig. III.1 : PHOENIX 28 GHz / 60 kV on its test bench

ION	Q/A	Ionisation Potential	Maximum. Current	Source	frequency
		eV	μA		GHz
18 O 6+	0.333	122	1000	Riken Artemis ECR4M	18 14 14
20 Ne 6+	0.300	164	360	ECR4M	14
22 Ne 7+	0.318	222	270	AECRU	10+14
36 Ar 12+	0.333	614	200	AECRU SERSE Riken GTS	10+14 14+18 18 18
40 Ar 13+	0.325	689	120	AECRU SERSE Riken GTS	10+14 14+18 18 18
86 Kr 27+	0.314	2728	8	AECRU SERSE	10+14 14+18
86 Kr 28+	0.325	2900	2	AECRU SERSE	10+14 14+18
129 Xe 38+	0.29	2630	0.9	SERSE	14+18
"	"	"	8	Test SERSE	28
129 Xe 44+	0.33	3390	0.04	Extrapolation for SERSE	14+18
129 Xe 20+	0.155	642	600	Phoenix*	28*

** Obtained in pulsed mode with afterglow*

Table III.1 : Best currents published (or to be published) by MSU, USA (Artemis), GANIL, France (ECR4M), Berkeley, USA (AECRU), LNS-Catania, Italy, (SERSE), RIKEN, Japan (RIKEN SOURCE), SSI-ISN, France (PHOENIX), CENGrenoble, France (GTS).

The present state of the art in ECR sources shows that the 1 mA intensity with Q/A=1/3 has been obtained for the light ions like $^{18}O^{6+}$. For heavier masses up to argon, this goal is probably within reach if some further developments are made, including the use of high frequencies (28 GHz or more). For krypton or xenon, the charge states achieved are respectively 28^{+} and 44^{+}, corresponding to ionisation potentials of 2900 eV and 3390 eV, respectively. A current of the order of 1 mA of such high charge states does not seem to be attainable in the next 10 years. However some tens of μA are probably achievable.

III.2.2) Beam characteristics

The total current extracted from the source can reach some 15 mA, owing to the global spectrum (Ar and O ions). Such high currents induce an increase of the emittance of the beams. However, the results obtained at GANIL with ECR4M have been obtained on a test bench with an acceptance less than 200 π mm.mrad while the emittance of Xe beam produced at SSI-ISN with PHOENIX 28 GHz (see table III.1) is estimated to be lower than 200 π mm.mrad. These values are compatible with the requirement of the RFQ.

III.2.3) Cost estimate and time-scale

The construction program must be preceded by a development program to finalize the type and the characteristics of the source necessary for the 1 mA beam at 60 kV. An intermediate stage with a room temperature source will permit us to define the final structure of the source that will eventually be installed on the accelerator.

If we observe some limitations concerning the Q/A we know that we have two other options for the design of the source :

- The first is a hybrid version with SC-HTS coils and the FeNdB hexapole. The interesting aspect of the design is the possibility of retaining a compact plasma chamber while maintaining the production of high current density with good use of the UHF power.
- The second is to choose a fully superconducting device. For information, we note that the next SC source that will start operation is the Berkeley source that has cost 2.5 M€ and required 7 years of development.

	Room temperature source (k€)	**Hybrid source (k€)**	**SC source (k€)**
Source	90	530	1000
Power supply	110	30	76
Transmitter (28 GHz)	230	230	230
Total	**430**	**790**	**>1306**
Time-scale	**1 year**	**2 years**	**>3 years**

Chapter IV : The linear accelerator

IV.1.) GENERAL LAYOUT OF THE LINEAR ACCELERATOR

The proposed LINAG 1 driver has the ability to accelerate a 5 mA D^+ beam up to 20 A MeV ; nevertheless, the different parameters are optimised for q/A=1/3 ions up to 14.5 A MeV in order to preserve a long-term evolution towards a heavy ion driver. It is a continuous wave (CW) mode machine, designed for maximum efficiency in the transmission of intense beams of heavy ions. It consists in an injector (ECR source + radio-frequency quadrupole), which accelerates the beam up to 0.75 A MeV, followed by a superconducting linear accelerator based on independently phased quarter-wave resonators (QWR).

A schematic layout of the linear accelerator is presented below :

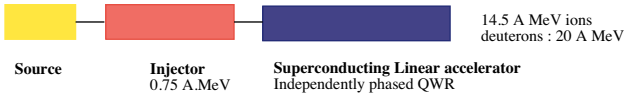

Figure IV.1 : Layout of the LINAG

IV.2) SOURCE AND LOW ENERGY BEAM TRANSPORT LINE

D^+ ion source characteristics.

The D^+ source chosen for the accelerator is of SILHI type [ref. 1, 2, 3]. The SILHI source has been developed in the frame of the IPHI project, and routinely produces an 80-mA proton beam at 95 keV, in an RMS normalised emittance of 0.3 π.mm.mrad, without charge compensation. In the LINAG phase I case, the extraction energy is chosen to be 20 A keV, which means an extraction voltage of 40 kV for the deuteron beam. The choice of the voltage, i.e. 40 kV for deuterons (and 60 kV for heavy ions) was made for the following reasons :

- There is no need of an isolated platform for these voltages. Several high intensity sources work at this level, without any problems (ISN, Los Alamos…). It would also greatly reduce problems which would otherwise exist if we choose to install a superconducting source in the future.
- The design of the bunching section of the RFQ is simpler at lower source voltages.
- The activation of the LEBT by the deuterons is reduced at a lower energy [ref. 4].

The 5 mA intensity is obtained by reducing the extraction hole diameter (from 9 to 3 mm), which also compensates the emittance increase due to a lower extraction voltage (40 kV instead of 100 kV), and maintains the normalised RMS emittance at under 0.2 π.mm.mrad. A new extraction system that will fit these requirements is at a preliminary design stage.

Low energy beam transport (LEBT).

The LEBT for the D^+ beam is mainly based on the use of 2 solenoids, to transport and match the beam at the entrance of the RFQ [6]. For the initial design, one has to take into account the future installation of a LEBT that transports q/A=1/3 ions to the same RFQ [4], so that both lines are compatible.

A possible transfer line has been studied, considering a D^+ beam with a normalised RMS emittance of 0.2 π.mm.mrad, which is certainly over-estimated (the effective emittance for the deuterons beam will be smaller, and this will just give a higher margin of safety for this preliminary design). Figure IV.2 presents the beam line structure, and one possible tuning for the 5 mA D^+ beam (including space

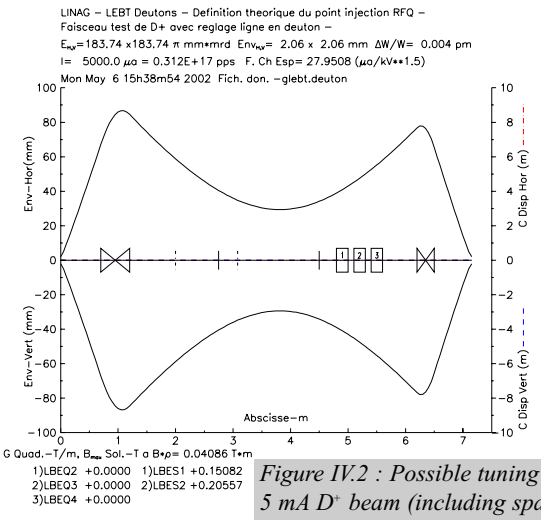

Figure IV.2 : Possible tuning for a 5 mA D^+ beam (including space charge)

charge) ; the transmission in the line is 100%, and parasitic beams like protons or H_3^{1+} are defocused along the line, long before the RFQ entrance. A scheme for the ion transport has also been studied, and figure IV.3. presents the structure of the line and ion beam envelopes.The overall layout of the

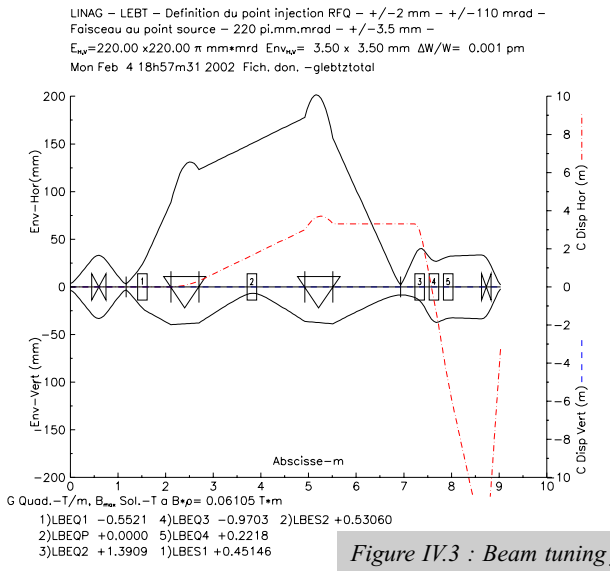

Figure IV.3 : Beam tuning for a 1 mA ion beam (q/A= 1/3)

LEBT is shown in section IV.5 below, including the optional heavy ion line.

Cost evaluation (beam line elements, vacuum, diagnostics).

The D^+ source price is evaluated from SILHI (with an extraction system matched to 40 kV), considering that the coil and its power supply will be replaced by a permanent magnet.

Item	Cost in k€
Source body and accessories (permanent magnet)	32
RF system 2.45 GHz	30
Extraction system at 40 kV	87
Pumps and pressure probes	26
Mechanics	10
TOTAL SOURCE COST	**185**
2 solenoids and power supplies	55
Vacuum, water cooling, diagnostics, installation: 6m @ 29 k€/m	174
TOTAL LEBT (D^+)	**229**
5 quadrupoles and power supplies	76
5 dipoles and power supplies	76
Vacuum, water cooling, diagnostics, installation: 6m @ 29 k€/m	174
TOTAL LEBT(IONS)	**326**

IV.3) THE RFQ INJECTOR.

Main parameters

The RFQ must operate in CW mode. Its frequency has been chosen equal to 87.5 MHz, sub-harmonic frequency of 350 MHz (power sources availability). This quite low value has been determined for the following reasons :
- the RF power density is quite low at this frequency, and allows a solution based on a formed-metal technology, leading to a cheap mechanical solution [ref. 7].
- At lower frequency, the inter-vane distance is larger, and allows a higher margin for the mechanical tolerances.

The RFQ output energy, 0.75 A MeV, has been determined by the fact that the first cavities of the SC linac must allow a possible evolution of the machine for q/A= 1/5 or 1/6 ions, which means that their beta values have to remain quite low (≈ 0.06).

The RFQ parameters are described in detail in [ref. 8]. The following table presents a summary of the main design parameters. In particular, the maximum peak field value is kept to a conservative level, lower than LEDA and Chalk River RFQs, which also work in CW mode.

Parameters	Values
Length	6.076 m
Minimum aperture (a)	5.1 - 7.5 mm
Mean aperture (R_0)	6.9 - 7.5 mm
Modulation (m)	1 - 1.8
Frequency	87.5 MHz
Voltage	90 - 101 kV
Peak field	1.43 - 1.66 Kp
Synchronous phase	-90 -30 deg

Mechanical design

As described above, a formed copper-plated stainless steel solution has been recently studied, and gives very interesting results, mainly from the point of view of cost and realisation schedule. The inner extremities of the vanes are in bulk copper, and the tolerances on the vanes are ±0.2 mm (fig. IV.4). It is assumed that the copper coating will be made at GSI, before welding, with the participation of GANIL personnel. The preliminary study is described in [ref. 3].

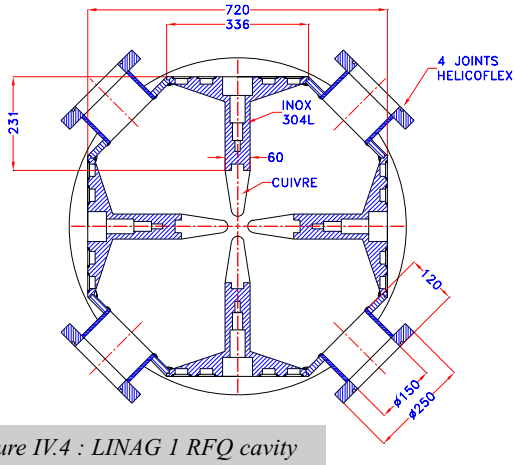

Figure IV.4 : LINAG 1 RFQ cavity

Beam dynamics

Beam dynamics calculations have been performed, and are described in detail in [ref. 8]. The ion beam, with an RMS normalised emittance of 0.4 π.mm.mrad, has been considered for the RFQ parameter and geometry definition, and the deuteron beam, with an RMS normalised emittance of 0.2 π.mm.mrad, has then been transported in the RFQ : the transport efficiency is 100% in both cases. Figures IV.5 and IV.6 summarise the results obtained for the D^+ beam.

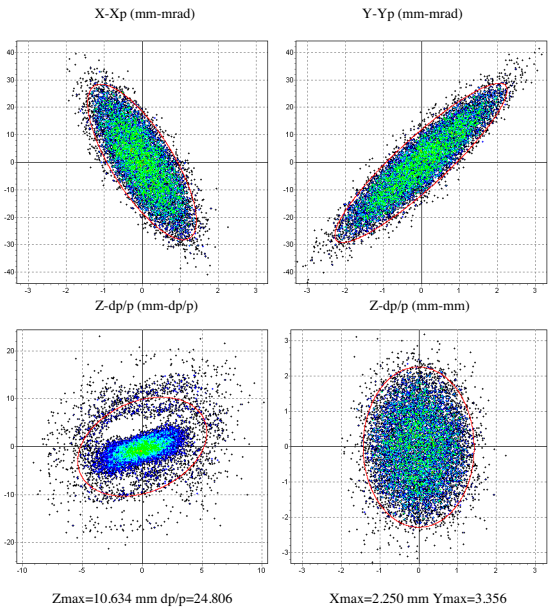

Figure IV.5 : Output phase space distribution for D^+ beam

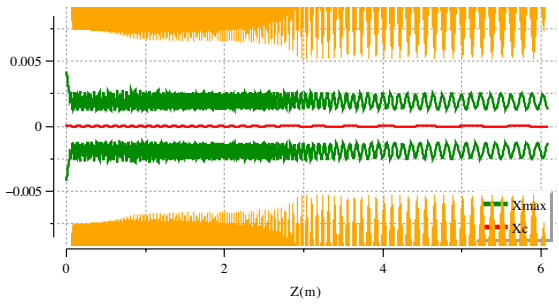

Figure IV.6 : Horizontal envelope of D^+ beam.

Error simulations have been performed [ref. 8], considering mechanical tolerance of ± 0.1 mm on machining of the vanes and ± 0.2 mm on misalignment. The results confirm that the deuteron beam transmission remains very close to 100%, (only 5.10^{-5} loss rate) as shown in figures IV.7 and 8. This gives quite a comfortable safety margin: losses of up to 3% have been considered for radioprotection purposes.

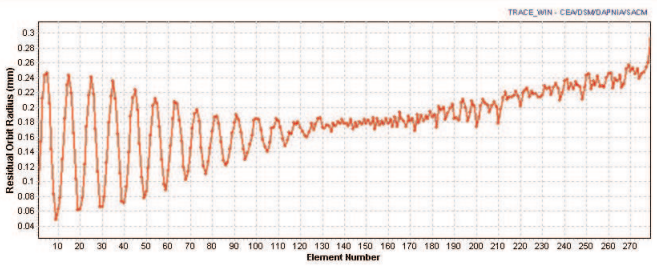

Figure IV.7 : Oscillation of the beam centroid along the proposed LINAG RFQ, with full error combination.

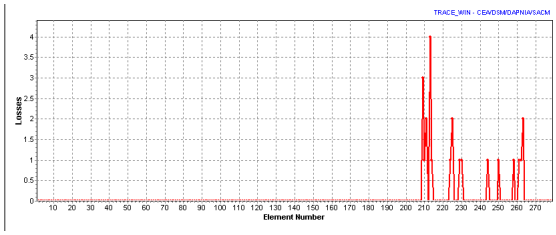

Figure IV.8 : Distribution of losses in the proposed LINAG RFQ with full error combination. The number of hits for 500,000 particles is plotted on the vertical axis.

Cost evaluation (cavity, vacuum, cooling, RF, low-level RF)

	Cost in k€
Cavity	**1000**
Power Transmission Line:	**100**
(includes power coupler:40 k€)	
Power Amplifier 200 kW:	**1200**
Water Cooling	**150**
Control loops	**15**
Vacuum	**170**
TOTAL (without installation)	**2635**

IV.4) THE SUPERCONDUCTING LINEAR ACCELERATOR

Main parameters

The linac must have the ability to accelerate D^+ and q/A=1/3 ions with the maximum energy gain, and must also be able to be extended to accelerate heavy ions in future. A linac based on independently phased superconducting quarter-wave resonators (QWR) is thus proposed.

The linac design requires accelerating voltages of the order of one MV per cavity and two beta values, around 0.06 and 0.12, at sub-harmonic frequencies of 350 MHz (available power sources). The starting frequency was chosen as 87.5 MHz, not too high for the lowest beta cavity and not too low for the RFQ.

Technical choices

Cavities

Low-beta superconducting (SC) cavities in the beta range 0.04 to 0.2 are typically quarter-wave resonators (QWR), operated at 4.2 K as the frequency is less than 500 MHz. Two technologies for these cavities have been analysed up to now : bulk niobium and sputtered niobium on a copper layer : Nb/Cu. Both kinds are presently used in heavy ion accelerators : at Argonne [ref. 9], Legnaro [ref. 10, 11], and JAERI [ref. 12], but only those of the first two laboratories have been analysed. The cavities from Argonne and Legnaro can be immediately identified by their shape : the Argonne type (figure IV.9) takes greater care of the field symmetry in the beam axis region, with a conical stem and a cylindrically shaped drift tube. The Legnaro QWRs are characterised by a very simple design (figure IV.10) reducing the manufacturing costs : perfectly cylindrical stem, terminated by a half sphere, more or less squeezed to suit the cavity beta, cylindrical outer walls coaxial with beam tube, and noses added to match the transit-time factor at different betas. The Legnaro resonators are built in both technologies while the Argonne cavities are solid niobium.

Figure IV.9 : Argonne QWR 115 MHz β=0.15. (Courtesy of K.Shepard.)

Figure IV.10 : Legnaro QWR. (Courtesy of A.Facco.)

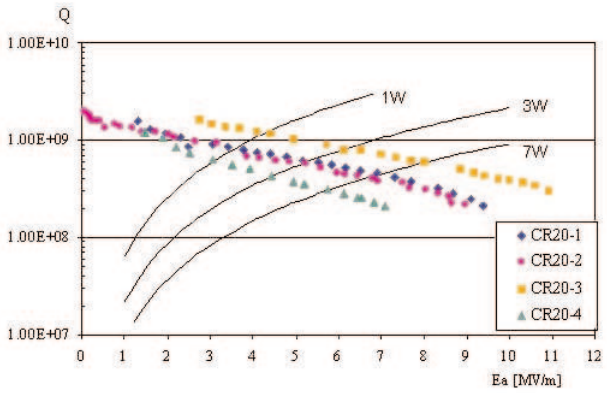

Figure IV.11 : Performance of the LNL Nb/Cu cavities (Coutersy of A.Porcellato).

The most important difference in the two technologies is in the thermo-mechanical stability of the resonator. Super-conducting cavities are very demanding in this respect, owing to their very narrow natural bandwidth of < 0.1 Hertz, and any mechanical vibration or variation in the helium bath pressure can produce a de-tuning that shifts the cavity away from the operating frequency.

This is less of a problem in Nb/Cu cavities that are sensitive only to pressure differences higher than 100 mbar. On the other hand, Nb resonators present a higher sensitivity to pressure variation and need mechanical dampers and/or fast tuners in order to compensate the mechanical vibration effects. Fast tuners have been developed and have routinely been used at Argonne for a decade and today they are extremely reliable, while there is very little operational experience yet with the new Legnaro type of solid-Nb QWRs, using a mechanical damper of the electrode stem that should avoid the need for fast tuners. Slow tuners, dampers and fast tuners are important accessories for the cavities as they strongly affect the operating reliability and ease of operation, as well as the cost. Also of interest is that the assembling of these cavities does not require a “clean room”, but only an area equipped with a laminar airflow.

For of the accelerating field, both Legnaro type cavities can be operated with almost 7 MV/m at 7 watts and performances of Nb/Cu QWR are presented in figure IV.11.

The beam dynamics calculations and cost evaluations have been made for this conceptual design, using the Nb/Cu QWR of the Legnaro type, as they provide the required accelerating field at the best price.

Cryostats

The cryostats for LINAG 1 cavities include a liquid helium tank connected to the upper parts of the superconducting resonators, like those at LNL. Gaseous helium (in a 7-bar circuit) is used to cool the radiation shields of the cryostat. Each cryostat is isolated by two vacuum valves mounted on the beam line.

Two solutions are proposed for the vacuum system :

- The vacuum inside the cryostat is both for insulation and beam transport. In this case the vacuum system must reach low pressure (~ 10^{-5} Pa) according to the beam line vacuum requirements. This pressure level must be obtained before starting the cooling process, to avoid contamination on the cavity surfaces during warming up of the cryostat. That is why “superinsulation” or other materials cannot be used in the cryostats (to limit the outgassing rate). On the other hand, the main advantage of this solution consists in its mechanical design (since dismounting of cryostats is easier).
- The insulation vacuum is independent. The cryostat design and its vacuum system are conventional. With this solution, the cavities can stay under vacuum during the cryostat maintenance.

Power couplers

There is no existing experience on multi-kW power couplers with SC QWRs, but the design for power of less than 10 kW should not present any particular problems, as power level more than a factor 10 higher are already handled on SC cavities. Nevertheless, this element will complicate the design of both the cavity and the cryostat, adding some extra

costs. A 7 kW coupler for the 350 MHz spoke cavity is under development at Argonne and the first results could be available next year.

Owing to the large variety of beam intensities to be handled, a variable coupler could be necessary in order to reduce the RF power consumption when working with low intensities. Calculations [ref. 13] show that the over-coupling required with maximum beam intensity when the power P is completely absorbed by the beam, demands a power P/4 to produce the same accelerating field without beam. This amount of power is of the order of 1.5 kW, and could be difficult to handle, and a variable coupler could reduce it by a factor 10 to 20, resulting in reduced operating costs.

RF amplifiers

Solid state amplifiers are currently used at Argonne and Legnaro owing to the better gain linearity at different power levels and the better behaviour versus ageing than that obtained with amplifiers using tube technology. Nevertheless, solid-state amplifiers are today limited to power levels of a few kW and, at our frequencies, the costs are not competitive with the tube amplifiers. There seems therefore to be no choice other than tube amplifiers [ref. 14].

Low-level RF

The scheme of the self-oscillating loop will be used [ref. 14], as it simplifies the setting of the slow tuner position by giving a feedback signal even when the cavity is not yet at the operating frequency. This scheme is already used in both the laboratories mentioned above, and no particular innovations are required.

Solenoids and steerers

For the beam focusing, SC solenoids have been chosen. They are located in the cryostats together with the cavities, and the necessary magnetic fields remain under 10 tesla. The fringing field is reduced either by shielding, or by compensation coils.

For the beam alignment, necessary to compensate for any element-positioning uncertainties and the QWR steering effect, SC steerers are chosen. They are located with the solenoids (a prototype is presently under construction at Argonne).

Beam diagnostics

The use of classical diagnostics is chosen for the machine tuning, which will be done at very low intensity (with a pepper-pot in the LEBT line), as well as for the machine survey : secondary-electron-emission beam profile monitors for observing the transverse profiles of the beam (used only at low intensities, and not with the deuteron beam), residual-gas micro-channel plates for measuring the transverse beam profiles once the beam alignment has been done, capacitive probes for determining the beam centre-of-gravity position and capacitive probes for observing the longitudinal characteristics of the beam (central phase, time of flight). These probes and monitors will be placed along the SC linac in multi-box systems, in order to minimise the drift lengths between cryostats. The QWR cavities can also be used as beam phase monitors, for the tuning of the synchronous phase. In the survey mode, the non-interceptive diagnostics will control the full-intensity beam. Some of them will also be connected to the safety control system, in order to guarantee perfect control of the beam variations and losses.

Command-Control

The control system of the LINAG accelerator can be based on the Experimental Physics and Industrial Control System (EPICS) [ref. 15]. This platform, available in the public domain, is used in a large variety of accelerators including KEKB, CEBAF, SLS, LANL and SNS, as well as several detectors and telescopes. The EPICS architecture consists of front-end computers using a real-time system, which can communicate with a variety of buses and operator consoles. The software is ported into Unix, Solaris and Windows. The main advantage in EPICS is its wide user community, which facilitates debugging and collaborations through the Web, and the fact it works on a huge number of hardware architectures and operating systems.

Cryogenic Plant

The LINAG-I cryogenic system will have to supply 44 superconducting resonators mounted in 11 cryostats (a group of four resonators and a superconducting solenoid per cryostat). Cavities and solenoids are operated at 4.2K and cooled by means of liquid helium provided by an on-line liquefier-refrigerator system.

The LINAG-I refrigeration plant must provide 800

W @ 4.2K (with a safety factor of 40%). For the thermal shielding an average value of 0.5 kW @ 60K will be necessary. If gaseous helium is used for pre-cooling operations, an average value is 1.5 kW @ 60K.

Cryogenic power requirement at 4.2K

Cavity dynamic losses	10 W/cavity	44	440 W
Cryostat static losses	5 W/ cryostat	11	55 W
Cryogenic lines static losses	2 W/m	44	88 W

The cryogenic plant is composed of a cold-box module, the cryogenic distribution system, and a gas storage circuit (figure IV.11). A screw compressor compresses the helium at 16 bars and sends it to the cold-box for refrigeration. An outlet from the cold-box at 60K (provided from the first turbine of the refrigerator) can be used to cool the cryostats and transfer lines thermal shields (gaseous helium at 7 bars). With a slight reduction in efficiency of liquid helium production (~5%), this solution avoid the need for liquid nitrogen for the thermal shields.

The liquid helium produced from the last stage of the cold-box (J-T valve), is stored in a dewar before transfer to the cryostats.

Cryogenic transfer lines can use a coaxial-shield configuration, or four independent pipes super-isolated in vacuum. Each cryostat can be fed independently from a local distribution box by cryogenic valves (liquid-He inlet and returning gas, gaseous-He inlet at 60 K and return). This configuration allows removal of a cryostat without interrupting the cryogenic distribution. The return circuits are connected to the cold-box and to a storage gas circuit.

Beam dynamics

Two types of beam dynamics calculations have been performed. The first one [ref.16], using the code TRACK [ref. 17], has been performed at Argonne, in order to show the feasibility and the performances of the SC linac. 3D field maps of the Legnaro type QWRs, calculated with Micro Wave Studio, are used for the beam dynamics calculations

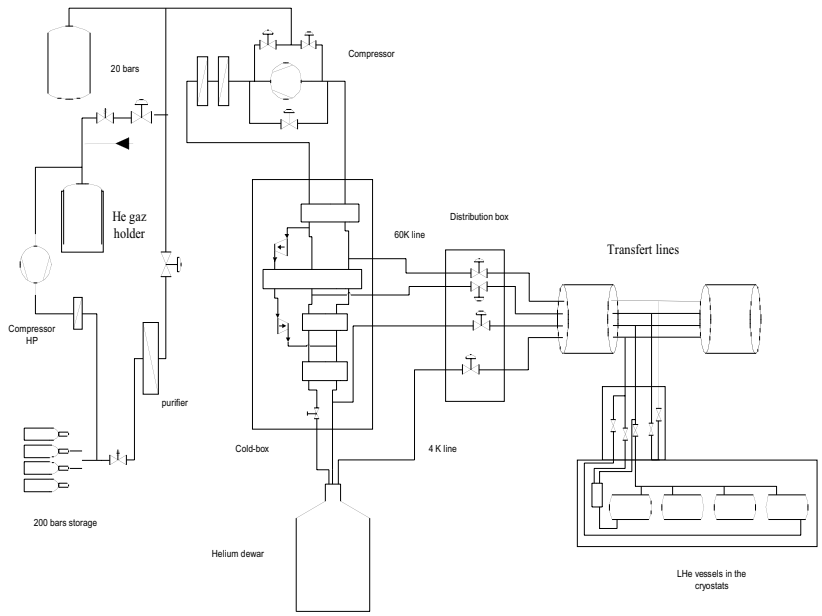

Figure IV.12 : Principle layout of the cryogenic plant.

Estimated cost of the cryogenic system

Components	Comments	Unit price (k€)
Cold-box	800W@4K (with compressor)	1300
Helium dewar	2000 litres	30
Distribution box		60
Transfer lines		180
Local distribution boxes	10 units	165
Gas vessel	20 bars – 50m^3	50
Gas holder	50 m^3	20
Compressor	200 bars – 50 m^3/h	50
Storage	200 bars – 12 m^3	60
Purifier	Cryogenic	100
Pipes and valves		20
Gas analyser		30
Installation	12 man-months	100
	Total	**2165**

(including all the field dissymetries proper to these cavities and magnetic fields), so that the QWR steering effect is taken into account [ref. 18, 19]. Accelerating fields of 6 MV/m are considered. The space charge effects are not included in the calculations ; according to the experts in SC linacs, they should not be a problem for a 5-mA beam, this point is being checked. Halo and error simulations are being study in details [ref. 20]. The solution is based on quite a high number of solenoids, and figure IV.13 show the beam envelopes for the full emittance beam.

Another type of solution is under design, with a lower number of solenoids, and a structure containing shorter cryostats ("Legnaro" type cryostats). Even if the calculations are still in progress, this second solution has been considered for the cost evaluation, just because the prices and cryogenic performances of the "Legnaro" type cryostats were precisely known. The remaining uncertainty concerns the exact number of solenoids, which will not greatly affect the total price of the SC linac.

Tuning procedure

The first high intensity beam tests will be performed with H_2^{1+} or He^{2+} beams, before accelerating a D^+ beam. The SC linac and the RFQ are tuned first with a low intensity CW beam, by inserting a rotating pepper-pot in the LEBT line. This pepper-pot is connected to a remote-handling system, for the case of activation by the deuteron beam. The cavity phases are tuned one by one, on intermediate time-of-flight diagnostics (those placed in the inter-cryostats drifts) or by using the cavity as a beam phase monitor, and the solenoids are tuned using beam profile monitors. The cavity phases can also be tuned by an energy measurement after magnetic deviations placed regularly along the SC linac. (This option has not been retained for the cost evaluation). The intensity is then increased slowly, step by step (by rotating the pepper-pot), and parameters are optimised at each step, using then non-interceptive diagnostics.

Medium Energy Beam Transport (MEBT)

The Medium Energy Beam Transport line has not been designed in detail, but we have chosen to include an analysing section in order to retain the possibility of easy addition of a second RFQ injector in future. The transverse and longitudinal beam matching are performed respectively by quadrupoles and rebunchers (1 or 2). The layout of this line is presented in section (e).

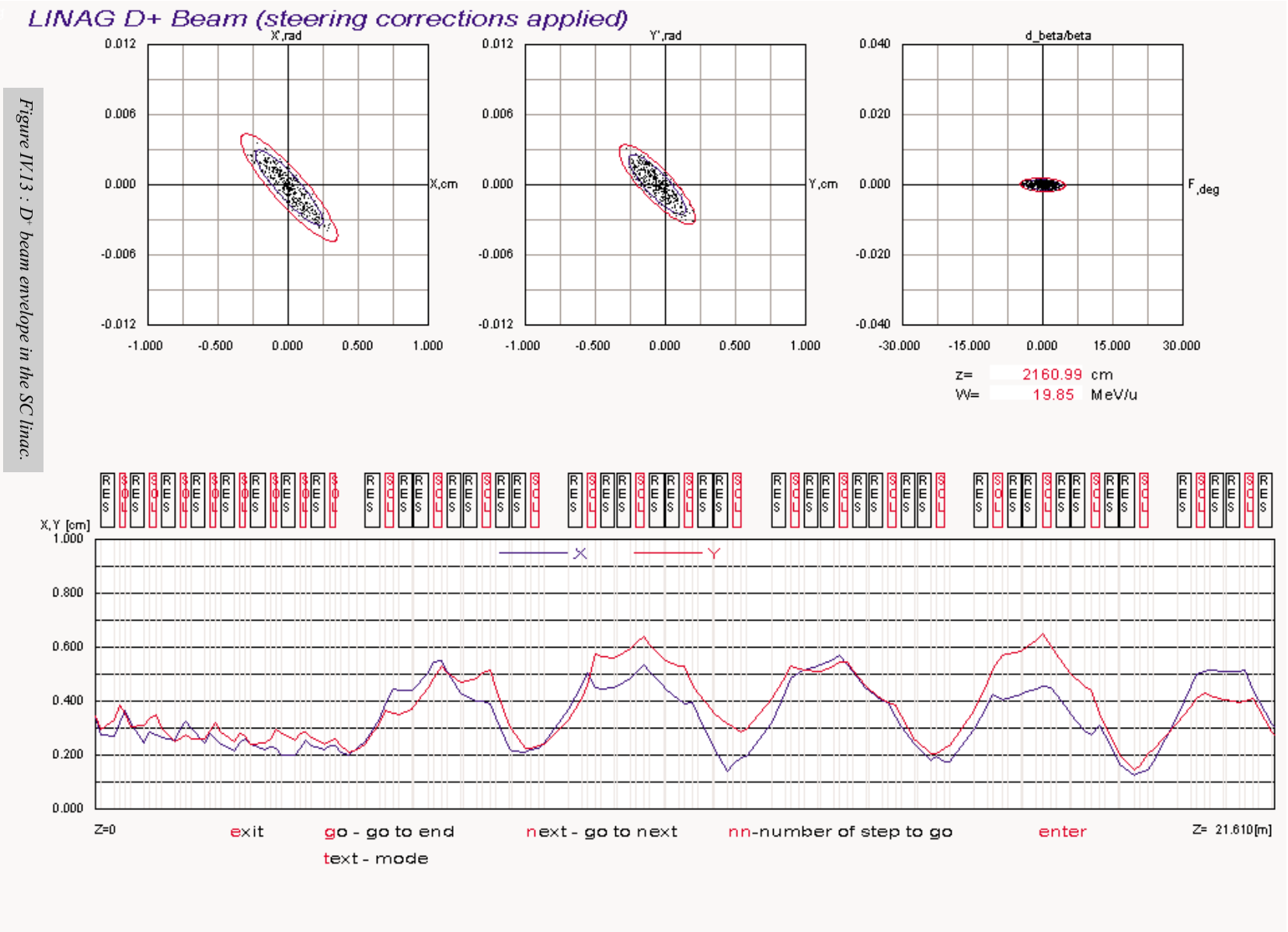

Figure IV.13 : D^+ beam envelope in the SC linac.

Cost evaluation

The following table presents the SC LINAG cost evaluation without the cryogenic plant and installation.

SC LINAC: Cost evaluation (without cryogenic plant)	**k€**
1 cryostat , assembled and including vacuum pumps (35 or 25 k€ depending on same or separated vacuum) and thermometry	230
4 Nb/Cu QWR with slow tuner, coupler, pick-up, connectors etc.	100
4 circulators or extra-cost for variable power coupler	60
4 directional couplers and transmission lines	30
1 solenoid with liquid-He housing and power supply	60
1 cabinet of control electronics for the QWR	40
4 5 kW, RF power amplifiers with 100 W preamplifier	200
Cost of the single module for 4 MV, 5 mA and focusing	720
MEBT (≈10 m+ rebuncher)	610
10 inter-cryostat transfer line	210
TOTAL SC LINAC (44 MV, 5 mA, focusing, transfer lines)	**8740**

Cost evaluation

IV.5) LAYOUT OF THE DRIVER

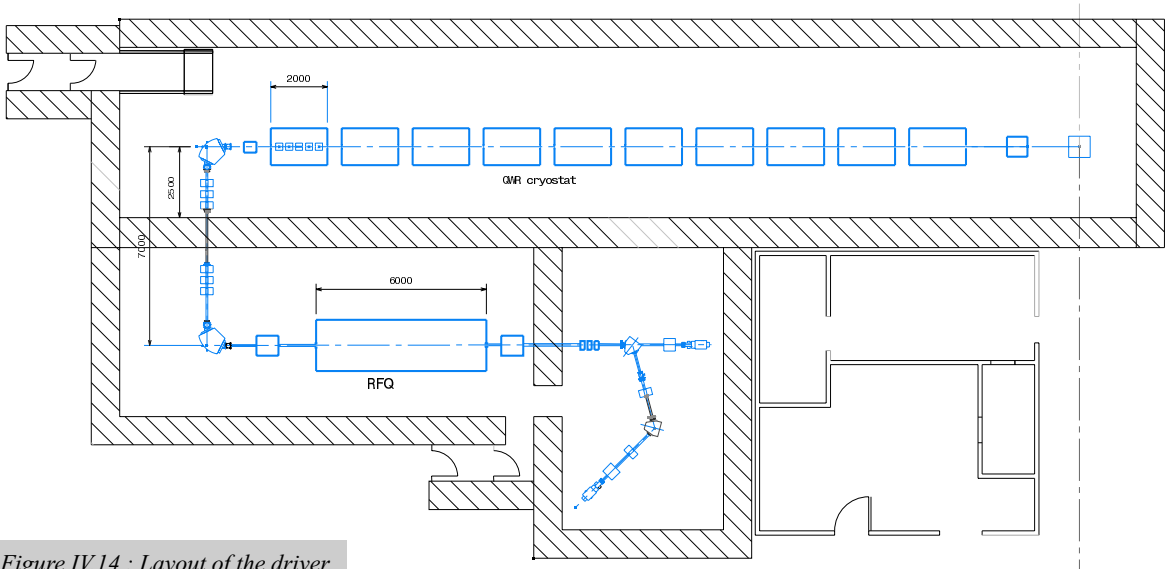

Figure IV.14 : Layout of the driver.

IV.6) REVIEW OF THE DRIVER COST EVALUATION.

The following table present a review of the costs of the differents parts of the driver. The additional electrical power needed for the operation of this driver is around 1,5 MW. This power is available at GANIL electrical power station input, though it would be necessary to adapt the electricity distribution.

	Cost in k€
D^+ source	**185**
LEBT	**275**
RFQ	**2635**
SC LINAC:	
MEBT	**610**
CRYOMODULES (11)	**8130**
CRYOGENIC PLANT	**2150**
DIAGNOSTICS	**400**
COMPUTER-CONTROL	**400**
TOTAL	**14785**

References

1) Compte rendu de réunion du 18 mars 2002, R. Gobin, R. Ferdinand, R. Duperrier, P. Lehérissier, et C. Barué.
2) Détermination et caractéristiques des sources d'ions pour LINAG, Document de synthèse, P. Lehérissier, C. Barué
3) R. Duperrier, R. Ferdinand, R. Gobin, M. Painchault, DSM/DAPNIA/SACM 2002/19, Rapport d'étape du projet LINAG.
4) M. Martone et al, RT/ERG/FUF/96/11, IFMIF Conceptual Design Activity Final Report
5) F. Varenne, GTM/NOTE/LINAG/06-05-02/FV/003, internal report on D+ LEBT
6) F. Varenne, GTM/LINAG/NOTE/01-02-02/FV/001, internal report on ions LEBT
7) M. Di Giacomo, GTM/LINAG1/NOTE/20-03-02/MDG/001, Considérations sur la technologie du RFQ, internal report
8) R. Duperrier, D. Uriot, RFQ beams dynamics studies in favor of the LINAG project, CEA/DSM/DAPNIA/SACM internal report, may 2002.
9) M.P. Kelly et al., Superconductive RF activities at Argonne National Laboratory, Proccedings of the 10th Workshop on RF Supercontivity, Tsukuba, 2001
10) A.M. Porcellato et al., Operation Experience with ALPI Resonators, Proceedings of the 10th Workshop on RF Superconductivity, Tsukuba, 2001
11) A. Facco et al., Superconducting RF Activites at LNL, Proceedings of the 10th Workshop on RF Superconductivity, Tsukuba, 2001
12) S. Takeuchi et al., Nucl. Inst. Meth. A382, 153-160 (1996)
13) J-L. Biarotte, "Flexibilité en puissance de LINAG, internal report IPNO.
14) J. Lesrel, IPNO, Note interne : Etude préliminaire des systèmes RF de LINAG 1
15) L. Dalesio, EPICS: Recent applications and future directions, Proceedings of the 2001 PAC, Chicago, 2001
16) P. Ostroumov, ANL, private communication
17) P. Ostroumov, TRACK: a code for beam dynamics simulation in superconducting linac with 3D electric and magnetic fields, Technical Note, March 2002
18) P. Ostroumov, K. Shepard, ANL, Correction of beam-steering effects in low-velocity superconducting quarter-wave cavities, Physical Review Special Topics, Accelerators and Beams, Vol.4, 110101 (2001)
19) A. Facco, V. Zviagintsev, LNL, Study on beam steering in intermediate-b Superconducting quarter-wave resonators, Proccedings of the 2001 Particle Accelerator Conference, Chicago, 2001
20) J.M. Lagniel, Halos and chaos in space charge dominated beams. Proceedings of the 1996 European Particle Conference, Barcelone (1996).

Chapter V : The Target and Ion Source

The LINAG phase-I project offers the possibility of producing intermediate-mass radioactive ions by neutron-induced fission – using a 40 MeV deuteron beam – or other reactions, such as fusion-evaporation and transfer. Moreover, two alternative possibilities can be used for producing fission fragments, by directly bombarding a uranium carbide target with a beam of deuterons or another heavier ion, or indirectly with neutrons from d-n converter. In this chapter, we will discuss in detail only the converter technique, which is considered the most reliable option for achieving the required number of fissions per second in the uranium carbide target.

The principal specifications chosen for the production system are shown in the following table :

Primary beam energy (Deuterons)	40 MeV
Maximum primary beam power	200 kW
Fission rate in the target	> 10^{13} fissions per second
Reliability of the production system	3 months
Ion production	1+ close to the target
Charge breeding	n+ far away from the irradiation zone

The choice between different technical solutions for the production and automatic handling system has been dictated by the security and safety conditions around the target. From these considerations, an automatic handling system has been chosen based on the known "target-plug" technology – as will be described in the following sessions – used successfully at ISIS, RAL [ref.1], ISAC, TRIUMF [ref.2] and other high intensity beams in fixed-target facilities.

V.1) THE PRODUCTION OF FISSION FRAGMENTS

The technique proposed for LINAG phase-I has been already discussed in the SPIRAL-II EU-RTD report [ref. 3], consisting in the use of energetic neutrons to induce fission of ^{238}U. The neutrons are generated by the break-up of deuterons in a thick target, the so-called "converter", of sufficient thickness to prevent charged particles from escaping.

The energetic forward-going neutrons impinge on a thick production target of fissionable material, i.e. Uranium carbide UC_x. The resulting fission products accumulating in the target diffuse to the surface from which they evaporate, are ionised, mass-selected, eventually charge-bred and finally post-accelerated. This method has several advantages. The material of the highly activated converter can be chosen to withstand the power of the beam without constraints concerning the diffusion of radioactive atoms. Moreover, the temperature of the converter does not affect the neutron flux. As projectiles, neutrons do not contribute to the heating of the target material directly, nor of the entrance window, which can therefore be very thick, and they do not present any special security issue. Neutrons bombard the target, losing energy mostly in useful nuclear interactions. They also have a high penetrating power, which allows very thick targets to be used.

The choice of the deuteron bombarding energy – 40 MeV – and the nature of the converter – carbon – has been made taking into consideration four main factors :

(i) the production rate of neutrons at forward angles as a function of energy,

(ii) the angular distribution of the neutrons,

(iii) the excitation energy of uranium, which defines the fission fragment distribution and

(iv) the cost of the project.

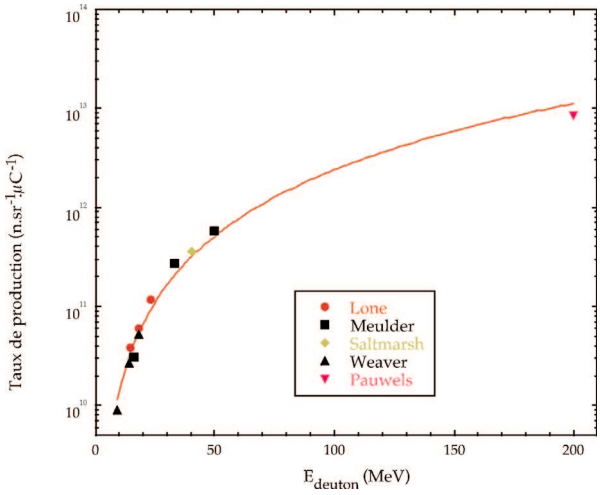

Figure V.1 : Production of neutrons at forward angles.

We examine each of these briefly :

(i) The production of neutrons at forward angles is illustrated in figure V.1, which shows the experimental neutron yield at 0° as a function of the incident energy of the deuterons for a Be-converter.

(ii) The strong forward peaking of the yield of high-energy neutrons (see figure V.2) shows that an approach with compact geometry, consisting of a converter to produce the neutrons followed by a second target containing the fissionable material, is well suited to the task.

(iii) The energy distribution of the neutrons produced in the deuteron break-up (that determines the excitation energy of Uranium) is centered at about 40% of the energy of the incident deuterons and has at 0° a width between one-third and one-half of the energy of the incident deuterons.

(iv) The neutron energy and angular distributions are similar for light converters. The yield for a carbon converter is only 30% smaller and it is slightly less forward peaked than for a beryllium converter, and therefore carbon has been chosen as the converter in our case.

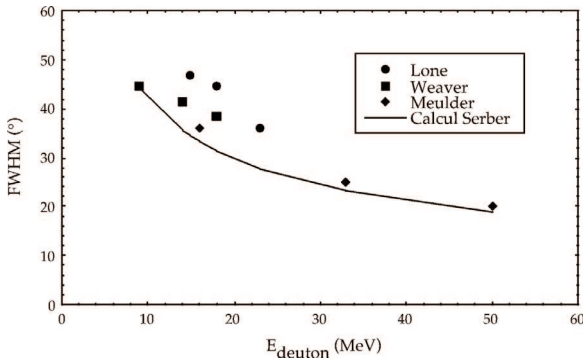

Figure V.2 : Neutron distribution width as a fonction of deuteron energy.

V.1.1) The rotating target/converter

During the studies of SPIRAL-II EU RTD, simulations of neutron spectra for several beam-converter configurations have been performed with the LAHET high-energy transport code combined with Monte Carlo N-Particle MCNP code for low-energy transport. Deuteron Coulomb dissociation has been added to the more standard processes, the forward peaked break-up and direct reactions and the rather isotropic evaporation of low-energy neutrons [ref. 4]. The simulations performed at GANIL [ref. 3] were compared with experimental angular distributions measured at energies of 80, 160 and 200 MeV for carbon and beryllium converters.

The LAHET-MCNP code reproduces the order of magnitude of the differential cross sections without any adjusted parameter. Some systematic deviations can be noted. Nevertheless, these deviations do not change the conclusions of the simulations, within 30% of confidence level.

The neutron yield is only one of the factors to be taken in consideration for the choice of the converter material. Other aspects in the evaluation are :

i) thermal properties that allow a compact geometry of the converter and the production target,

ii) toxicity and material properties of the converter,

iii) production of long-lived radioactive nuclides, and

iv) cost of operation.

Our conclusions regarding these aspects are summarised below :

A beryllium converter produces the largest amount of neutrons, however, its low melting point (1278° C), does not allow the use of high-intensity deuteron beams, nor placing of the converter very close to the hot target.

Liquid lithium is a more robust converter with respect to deposited beam power than beryllium or carbon. However, the flow of hot liquid lithium containing some amount of radioactive products requires special care in the design, especially from safety considerations. A converter designed along these lines, originally described by Grand and Goland [ref. 5], is probably not to be considered in the context of LINAG phase I, but could be of interest for a “next-generation” facility, e.g. EURISOL since it can stand extremely high beam power.

The above-mentioned properties clearly favour carbon as converter material. It is non-toxic, easy to handle and has a high melting point of 3632 °C. These excellent properties allow high beam intensities with a rotating wheel cooled mainly by thermal radiation.

For LINAG-I the main parameters of the rotating carbon wheel have been obtained by simulations using the code SYSTUS [ref. 6]. The quality of the carbon has been chosen for its conductivity. POCO [ref. 7] graphite PLS has a thermal conductivity exceeding 40 W/m°C at high temperatures. This is important for reducing the size of the wheel. For the simulations, an infinite rotation velocity was used, in a first approach. Once the main characteristics were chosen, the temperature variation with respect of the beam impact was calculated for a real angular velocity of 1000 RPM. The

thermal shock for which graphite achieves the ultimate strength (break-down condition) is for about 50°C in our conditions, therefore a maximum temperature variation of 20-30°C per revolution has been considered. The results of four different calculations are presented in table V.1. In the first column, the internal and external radii of the wheel are quoted with its total weight. In the second column, the mean beam radius and the vertical size of the beam is indicated – the horizontal size has been taken as 10 mm in all calculations. The maximum converter temperature is shown in column 3 and the temperature variation over one turn is quoted in column 4.

The evaporation ratio of the carbon is dependent of the graphite saturated vapour pressure. Experiments performed at GANIL and IPN-Orsay [ref. 8] for a specific carbon from POCO and Carbon Lorraine industries show that the evaporation ratio of carbon is in agreement with the values found in literature. The evaporation rate obtained experimentally is shown in the figure V.3. The evaporation rate for

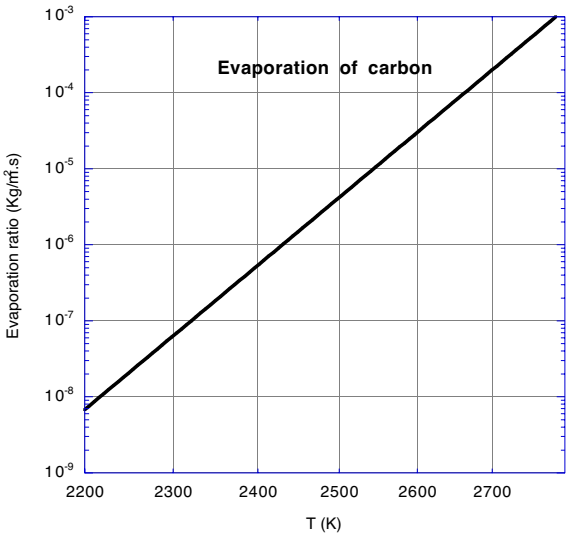

Figure V.3 : Carbon evaporation rate.

R_{int} R_{ext} converter (weight)	X_{beam} = 10 mm (scanning target)	T_{max} target	ΔT (with w=1000tr/mn)
290-350mm (1.5kg)	320mm (20mm)	2280°C	33°C
290-350mm (1.5kg)	320 (30mm)	2120°C	22°C
290-350mm (1.5kg)	320 (44mm)	2000°C	<20°C
340-400mm (1.75kg)	370mm (20mm)	2160°C	29°C

Table V.1 : Maximum target temperature with different target radius and different sizes of beam scanning.

evaporating 1 mm thickness of the carbon wheel in a period of 2000 hours is 2.6 x 10^{-7} kg/m²s. It corresponds to a temperature of 2085°C. This consideration fixes the sizes of the wheel and the beam spot on the carbon converter; i.e. 350 mm of radius for a beam spot of 10 x 35 mm.

The precise size of the beam can be achieved by applying a fast scanning of the beam in one direction and/or by having an angle in the converter. We suggest the solution with a beam profile such as 10 x 30 mm with a converter angle of 30°. A sketch of the converter-target design is shown in figure V.4, for two alternative configurations.

A similar study with equal results [ref. 9] has been made in the framework of the SPES project, Legnaro, Italy. The difference between both projects is that, in the latter case, the beam considered was proton of 10 MeV, with a total beam power of 100 kW.

V.1.2) The target and ion source production system

The target and ion source production system is placed just behind the rotating carbon converter. With 1 x 10^{13} fissions per second, the total power produced in the UC_x target is 310 W. As mentioned above, the production target is not influenced by the primary beam. The target temperature is completely controlled by an independent heating system, with a power of about 5 kW.

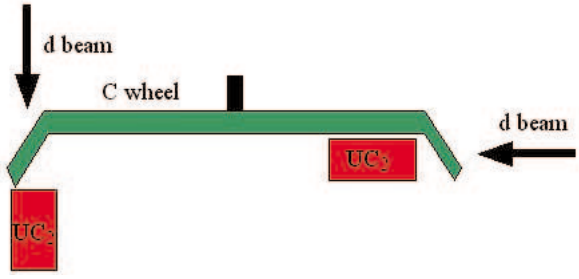

Figure V.4 : Sketch of converter-target design.

The production target

Two possibilities have been considered in this study for the fissile targets. The first one of UC_x with 2.3 g/cm^3, using the successful technology developed over many years at CERN-ISOLDE [ref. 10]. Oxide of uranium is mixed with carbon powder in a small container, pressed and heated at 2000°C for about 24 hours. The chips produced have generally around 1 mm thickness and a diameter of 20 mm. Larger diameters do not seem to be a problem, but smaller thickness could be very difficult to produce. We have assumed in our calculations of production yields a thickness of 1 mm. Any development which could reduce this value would be welcome.

The second possibility is the use of a high-density UC_2 target (11 g/cm2) already developed at Gatchina in Russia. The high-density UC_2 allows us either to reduce the size of the target considerably or to increase the yields by a factor of around 5 (for a given geometry). Preliminary results show that the diffusion properties of high-density UC_2 are similar to the low-density UC_x. The following yield estimations were done for both possibilities.

The geometry adopted in the simulations is not the optimum. The best would be to have a UC_x targets of conical shape, with an angle of approximately of 30–40°, as proposed in [ref. 11]. In order to simplify the simulations, a simple cylindrical geometry has been adopted in all cases. Moreover, a reasonable size of the UC_x target has been adopted. Therefore, the in-target yields calculated here can be considered as lower limits for all cases.

In the simulations the beam profile was 2 cm in diameter. The UC_x fission target of 6 cm diameter is placed at 2 cm behind the converter. It consists of slices of 1 mm thickness, separated by 0.5 mm, distributed over a length of 8.5 cm, corresponding to a total of 360 g of low-density UC_x or 1.8 kg of uranium for the high-density material. This target could be made of self-supported disks (if mechanically possible) or with a combination of several smaller targets in a suitable geometry. Concerning high-density UC_2 a design proposed for LINAG made by V. Panteleev and collaborators is shown in fig. V.5. Prototypes of both low-density (1.6-cm diameter) and high-density (1 cm diameter) materials already exist and have been tested at PARRNe2 and also at the Gatchina on-line mass separator.

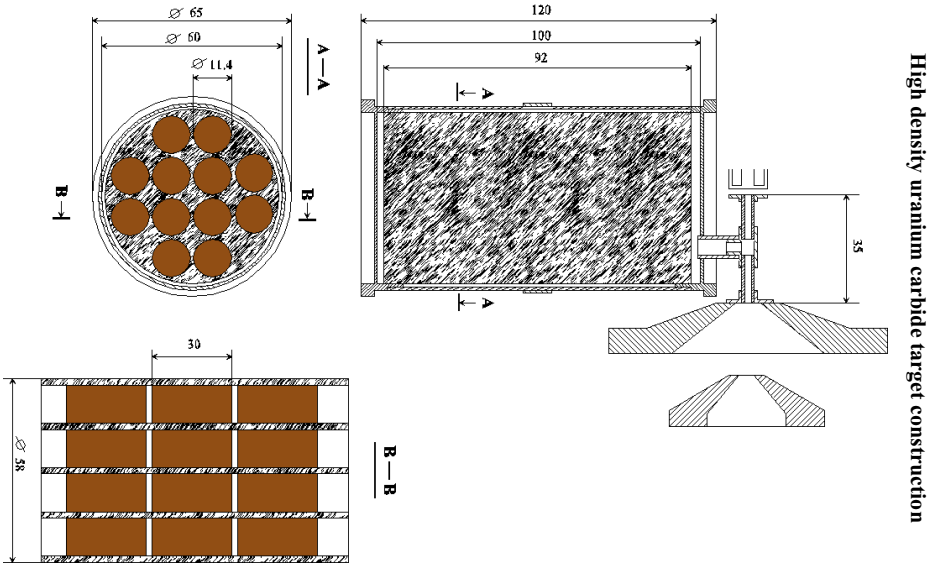

Figure V.5 : High density UC_2 target assembly proposed by V. Panteleev and collaborators

Ion sources

The ionisation source will be installed in a module as close as possible to the target. The chemical features of the selected radioactive element will define the type of the ion source regarding its efficiency. The main methods considered are surface ionisation for alkali elements, an electron-cyclotron-resonance ion source for noble gases or for volatile mono-atomic or molecular elements, and a laser ion

source for refractory elements. A new kind of electron-beam ion source, developed at Gatchina is another attractive possibility. Corresponding existing sources for radioactive ion production are respectively described in [ref. 12, 13, 14, 15]. The design of the target and ion source system should, in particular, take into account the parameters which have an effect on the global efficiency, i.e. the diffusion of the radioactive atoms out of the target, their effusion up to the source and the ionisation efficiency.

Different experiments and developments [ref. 16, 17, 18] were carried out at GANIL for the target-source system of SPIRAL. The experience acquired in that work, and the knowledge of how to design such production systems, are of paramount importance in achieving good design and performance for LINAG.

Original work was recently carried out in the SPIRAL framework in order to maximise the efficiency of the target/source system for diffusion, effusion and ionisation at low cost [ref. 19, 20, 21]. Specially dedicated to gases, a new, inexpensive, fully permanent-magnet ECRIS has been developed [ref. 22]. The final design of such a source is now complete and its construction is under way (see fig. V.6). The first tests should be carried out in June 2002. A new version of this ion source with coils (with better radiation hardness) is now under development. Special radiation-resistant coils will be tested soon in a different ECRIS at TRIUMF. The combination of the technological developments at GANIL and the know-how of TRIUMF should lead to significant increases in the reliability and efficiency of radioactive ion production.

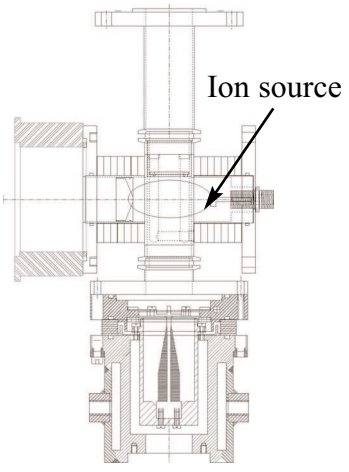

Figure V.6 : Minimono target ion source with a SPIRAL target.

It will be possible to install any one of the proposed sources in the production module at SPIRAL, the ECRIS being the largest one. In all cases, the useful lifetime of the production system is considered to be about 3 months. The replacement of the whole production system will be performed in a hot cell, specially designed for such an operation.

Charge breeding

The charge breeding ($1^+/n^+$ transformation) will increase the charge-state of the singly charged incoming ion to a charge-state compatible with acceleration by the CIME cyclotron or by the C0 injector. For a heavy nucleus like ^{144}Xe, it is necessary to produce a 23^+ charge-state, in order to be able to accelerate the ions in CIME (at the maximum energy), and such a charge-state leads to an energy of around 6 MeV/n after acceleration.

An ECR charge booster has been developed by the SSI group at ISN Grenoble (France) based on the use of a PHOENIX ion source at 14 GHz. The present results with this source are summarised in the table V.2.

The most abundant charge-state can be shifted to higher values by using higher UHF frequency. Therefore, the PHOENIX ion source is currently being upgraded by increasing the radial magnetic field up to 1.6 T, with a corresponding increase in the plasma volume. It will allow operation at a UHF frequency of 18 GHz.

	Charge-breeding efficiency (for the most abundant charge state)	Overall efficiency
Noble gas	10%	50 to 70%
Condensable elements	6%	45%

Table V.2 : Order of magnitude of charge-breeding characteristics with stable elements.

Other solutions could also be considered, like the use of superconducting ion sources (SERSE or GYROSERSE). For details see [ref. 23, 24]

V.1.3) Production rates

Calculations have been performed with the LAHET+MCNP+CINDER code for of the yield of fission fragments obtained from ~5 mA deuteron beam of 40 MeV energy on a carbon converter, followed by a UC_x target. Two UC_x densities were considered:

Case 1 : a low-density target, with $\rho(^{238}U) = 2.3 g/cm^3$, and 1 atom of U for 9 atoms of C as used in the first PARRNe2 experiment.
Case 2 : a high-density target, with $\rho(^{238}U) = 11 g/cm^3$, and 1 atom of U for 2 atoms of C, as developed by V. Panteleev in Gatchina.

The geometry used for the yield calculations is as

follows : the deuteron beam of 2 cm diameter hits a carbon converter of 1.8 g/cm^3 density with an effective length of 0.7 cm, in order to stop the deuterons and also protons from stripping reactions. The UC_x fissile target of 6 cm diameter is placed at 2 cm behind the converter. The target is composed of 56 slices of 1 mm thickness separated by 0.5 mm, distributed over a length of 8.5 cm. (For simplicity of calculation, this target was approximated by one cylinder of 8.5 cm length with density reduced by a factor 2/3 in the LAHET code. This gives the correct solid angle for neutron impact and the correct ^{238}U quantity). It contains 360 g of ^{238}U for the low-density target, or 1800 g for the higher-density target.

For such a target, 10^{13} fission/s could be obtained with a deuteron beam of 3.8 mA for the low-density UC_x target and with 1 mA for the higher density, as shown in table V.3.

The gain in the number of fissions when using the higher density is not exactly proportional to the density ratio.

Target density	2.3 g/cm^3	11 g/cm^3
Intensity for 10^{13} fission/s	3780 μA	947 μA
Fission per 5 mA	1.32 10^{13}	5.28 10^{13}

Table V.3 : Required primary beam intensity for 10^{13} fission/s and total number of fission for 5 mA deuterons for 2 different densities.

This effect is probably due to high-energy neutrons, as seen in table V.4. These neutrons are produced in the converter and are probably mostly absorbed in the higher-density UC_2 target. A more important proportion of lower energy neutrons are directly produced inside the UC_x target from fission of U, corresponding to a neutron source inside the target, and are

	Density	Fission (s^{-1}) n>20MeV	Fission (s^{-1}) n<20MeV	Total number of fission (s^{-1})
Target 1	2.3g/cm^3	1.24 10^{11}	1.4 10^{11}	2.64 10^{11}
Target 2	11g/cm^3	3.98 10^{11}	6.57 10^{11}	1.055 10^{12}
Ratio	4.78	3.21	4.69	3.99

Table V.4 : Total number of fission for 100μA deuterons.

then less sensitive to the effective length of the target.

In-target production rates

The expected cumulative yields for fission products, parent and direct production calculated with LAHET+MCNP+CINDER codes are reported in table V.8 (see end of this chapter) for the conditions described in the preceding section, and for the high-density UC_2 case. The cumulative yield is deduced from the activities (in Becquerel units) at saturation for each nucleus or after 6 months of irradiation for long-lived elements. The direct production is the difference between cumulative and parent yields. The choice between direct or cumulative yield for the in-target production depends on the chemical nature of the element and of the respective parent. It is a function of diffusion times associated with both elements. This makes a difference mainly for the less neutron-rich isotopes (those closest to stability) for which the production parent could be important, when compared to direct production.

Negative values can be present in the direct yields calculated as described in the paragraph above. This is a statistical effect coming from the Monte Carlo simulation, and such values should be re-evaluated.

Release of the products

Theoretically, the diffusion, effusion and ionisation processes are well-known phenomena, provided the particular properties of the selected element are known. However, despite a large experimental and theoretical effort, the diffusion and effusion behaviour of ions implanted into some materials, including the details of their thermal transport or their trapping in the temperature range relevant to ISOL system, remains unknown. In particular, the Arrhenius diffusion coefficients have been measured for numerous elements, but mainly in a W, Ta, Re or C-matrix. To our knowledge, these coefficients are not known for different tracers in uranium carbide matrices of different densities. A European RTD project "TARGISOL" N° HPRI-2001-50063 has been proposed and accepted recently in order to make progress in this critical field.

In the case of the LINAG-I study, two different approaches have been considered for the evaluation of final beam intensities :

The first one is based on a comparison of the predicted in-target production yields (using the Ficner code and the known cross-sections) and those measured after diffusion-effusion and ionisation in the PARRNe2 experiment. This work, done by the Orsay groups, [ref.25] gives a good indication of the diffusion efficiency for different elements in a uranium carbide target and with an ion-transfer pipe of small diameter.

The second one, performed at GANIL and based on a theoretical simulation of the diffusion-effusion process,

provides some idea of the influence of the target-source geometry. However, since the diffusion-effusion parameters for uranium carbide are not known, as was mentioned above, diffusion-effusion parameters for a C or Ta-matrix are used instead.

The expected radioactive beam intensities (after diffusion, effusion, ionisation and acceleration) are shown in the following plots (fig. V.13 to V.21, see end of this chapter) for some elements, viz. Kr, Xe, I and Cd, using the first method, and for Zn, Kr, Sr, Sn Sb and Xe using the second one. The in-target production yields are those calculated using the LAHET-MCNP-CINDER codes. The assumed 1^+ and $1^+/n^+$ ionisation efficiencies are 90% (1^+) and 12% ($1^+/n^+$) respectively for Kr and Xe, but only 30% (1^+) and 4% ($1^+/n^+$) respectively for Zn, Sr, Sn, I and Cd. The assumed transmission through the CIME cyclotron is 50%.

V.2) RADIOPROTECTION AND TARGET HANDLING

The dose rate immediately after the end of irradiation with the primary beam is estimated to be 32 Sv/h at 1 m from the target, after an irradiation time of 3 months. One year later, the radiation rate is still 34 mSv/h. (Refer Table V.5) This high level of radiation does not permit manual intervention near the target itself. Automatic handling is therefore necessary. The high level of radiation also imposes heavy demands on critical parts of the production system, like insulators, o-rings, etc. Where α-activity is concerned, Table V.6 shows the isotopes which would be produced at levels above the threshold allowed presently for an irradiation time of 10 days, 3 months and 6 months, respectively.

	ρ=2.3g/cm^3	ρ=11g/cm^3
Total activity (Bq)	$6.77\ 10^{13}$	$3.16\ 10^{14}$
Total activity alpha (Bq)	$4.13\ 10^{12}$	$1.82\ 10^{13}$
Total activity tritium (Bq)	$4.28\ 10^{6}$	$3.76\ 10^{8}$
Total activity beta-gamma (Bq)	$6.58\ 10^{13}$	$3.07\ 10^{14}$
Dose gamma max (μSv/h)	$6{,}83\ 10^{6}$	$3.20\ 10^{7}$
Total activity ^{235}U* (Bq)	$3\ 10^{10}$	$1.21\ 10^{11}$
Total activity ^{237}U (Bq)	$4{,}13\ 10^{12}$	$1.81\ 10^{13}$
Total activity ^{238}U (Bq)	$4.5\ 10^{6}$	$2.15\ 10^{7}$
Total activity 1 year after beam stop (Bq)	$1.44\ 10^{11}$	$6.88\ 10^{11}$
Total alpha activity 1year after beam stop, without ^{238}U (Bq)	$2.15\ 10^{6}$	$1.89\ 10^{7}$
Equivalent gamma dose 1 year after beam stop (μSv/h)	$6.76\ 10^{3}$	$3.39\ 10^{4}$

Table V.5

Description of the "target-plug" solution

The target and the ion source will be placed in a parallelepiped module (called the "plug" in what follows) which is surrounded by at least 2 m of concrete and iron shielding. The same principle has been applied at the ISAC facility at TRIUMF (Vancouver, Canada), for 100 mA of 500 MeV protons. Presently, two alternative possibilities are under study for LINAG phase I : the first one considers a vertically incident primary beam, while the second one considers a horizontal scenario. These two solutions will be studied in details during the next months and the final approach will be selected after considering the advantages and the disadvantages of each one. Figures V.7-11 show the sketch of both possibilities.

The advantages of a vertical beam scenario are mainly that :

i) the most important flux of neutrons is directed at zero degree, i.e. into the ground,

ii) the high-energy focussing elements and diagnostics are placed in the same plug, i.e. the production plug, and

iii) a horizontal rail-based guided dismounting system is envisaged, which might be preferred by the licensing authorities.

Concerning the horizontal beam solution, the main advantages are :

i) total protection of equipment and personnel in the area where the connections are made (above the plug) even during irradiation, and

ii) more reliable installation of a double vacuum system, since the vertical removal movement does not require rails.

The 2 m thickness of concrete reduces the dose rate at the top of the plug to 7.5 mSv/h when the beam is stopped, allowing people to come and work on the equipment located at this place.

In both approaches, the turbo-molecular pumps and all the insulators are located on the top of the plug, where they are protected from radiation. This increases the lifetime of the various components and permits the manual disconnection of the electrical power, etc. The target/ion-source system is immersed in the vacuum chamber, pumped by two turbo molecular pumps located on the plug. The plug can be closed off at the entrance and exit by two plates moved by air-actuators. The plug itself is contained in a large vacuum

Nucleus		10days	3 months	6 months	Threshold (Bq)
Pm145	17.7 a.		44.3	205.7	10^3
Gd151	120 j			2.4	10^3
Bi211	2.17 m		11.87	12.5	10^3
Bi212	25-60 m	< 5	79.9	192.25	10^3
Bi213	46 m		27.66	28.78	10^3
Po214	0.164 ms			1.21	10^3
Po216	0.15 s	< 5	79.47	192.24	10^3
At217	0.03s		27.66	28.78	10^3
Rn219	3.96 s		11.9	12.5	10^3
Rn220	55 s	< 5	79.5	192.24	10^3
Fr221	4.9 m		27.66	7828	10^3
Ra223	21.8 m		11.87	12.5	10^3
Ra224	3.66 j	< 5	79.5	192.24	10^3
Ac225	10 j		27.66	28.78	10^3
Th227	18.72 j		1.22	1.27	10^4
Th228	1.9 a	< 5	79.	192.79	10^3
Th229	7880a		27.66	28.78	10^3
U232	68.9 a	4.82	50.1	186.9	10^3
U234	$2.45\ 10^5$	3.64	31.36	63.2	10^4
U236	$2.34\ 10^7$	1.05	9.53	19.1	10^4
U238	$4.47\ 10^9$	21535.9	21535.9	21535	10^3
Np233	36 m			1.41	10^3
Np235	396 j	16.94	3862.4	16334	10^3
Np237	$2.13\ 10^6$	160	1447.2	2893	10^3
Pu236	2.86 a		20.38	87.6	10^4
Pu238	88a		16.18	67.1	10^4
Pu239	$2.41\ 10^4$ a	150.9	1386.4	2669.3	10^4
Nuclei over threshold		12	24	28	

Table V.6 : List of isotopes which would be produced at levels above the threshold allowed presently for α emitters.

tank with concrete packed tightly around the components, in order to minimise air activation. This tank contains four modules. Module 1, in the horizontal scenario, contains the diagnostics to measure the profile and the position of the primary beam in front of the target. Module 2 contains the target/ion-source system and the radioactive nuclear beam extraction electrodes. Modules 3 and 4 the contain electrode, beam profile monitors, and slits to monitor, transport and adjust the beam characteristics of the RNB from the ion source to the mass separator. The vacuum connections between the modules do not need seals as the plug is in vacuum.

After three month of irradiation, the different connections to the plug (electrical, primary pumping, water, etc...) can be manually removed. The plug is then removed from the production cave with a remote-controlled system and is evacuated to a storage cell. After a delay, and depending on the state of the target ion source system, the plug can either be re-used or moved to a hot cell where the elements at the bottom of the module can be replaced, using master/slave manipulators.

The handling system

A dedicated handling system will be studied for the manipulation of the plugs, taking into account the different risks induced by this action. In particular, the risk of anything being dropped, and the consequent risk of dispersion of contamination, should be carefully studied.

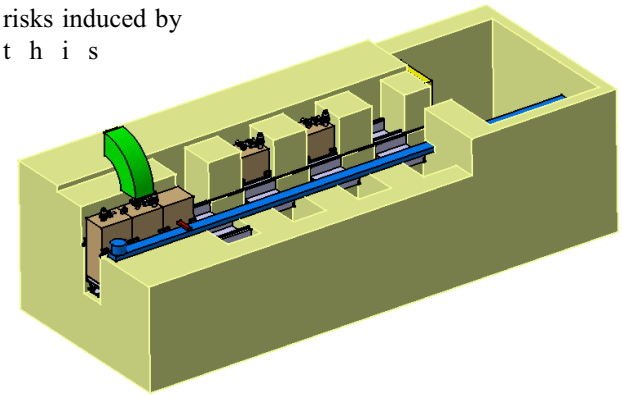

Figure V.7 : View of the plugs for the vertical beam scenario

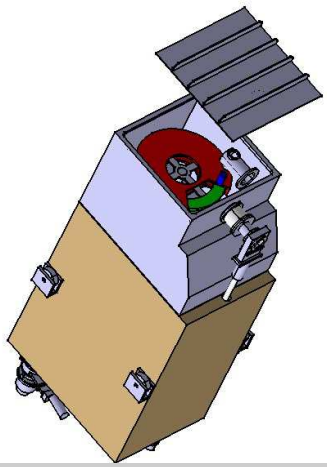

Figure V.8 : Internal view of the production plug for the vertical beam scenario

Air activation

As mentioned above, air activation is reduced to a minimum, as the plug and the target-ion-source production system are both under vacuum. Nevertheless, the small volume of air surrounding the target tanks will be considered to be at the same level as the hot cell inner volume and the building. They are thus a "radiation zone" and air should be sampled and monitored.

Gas storage

All pumps exhaust into a series of tanks where the activity can be sampled and evaluated, similarly to the present SPIRAL system. This activity is mainly due to the rare gas nuclei (i.e. ^{85}Kr, with a half time of 11 years, and ^{133}Xe). Table V.7 show an estimation of this activity after 1 month and 30 years, respectively. The storage time depends on the approved level of activity for release permitted by the

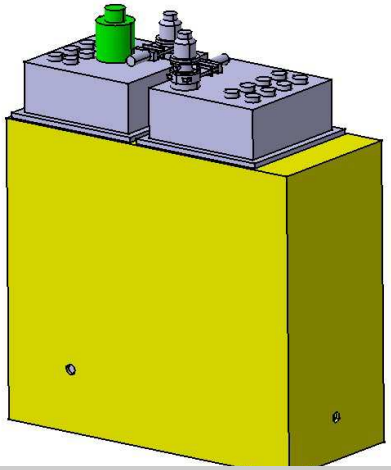

Figure V.9 : View of the first two plugs for the horizontal beam scenario

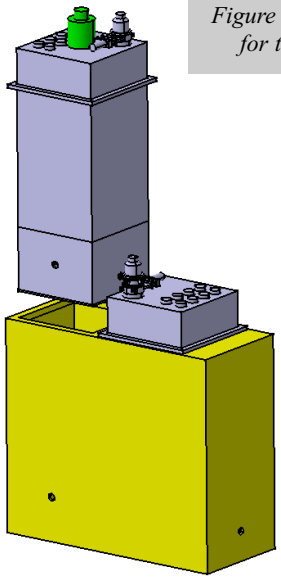

Figure V.10 : Plug being removed vertically in the horizontal beam scenario

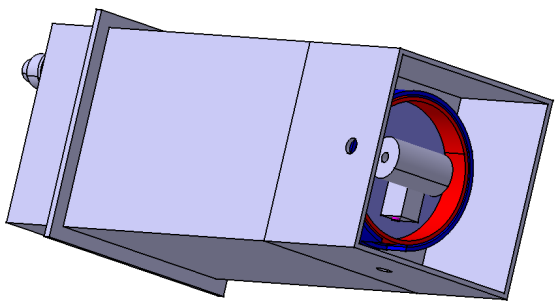

Figure V.11 : Internal view of the production plug for the horizontal beam scenario

safety authorities.

The main flow of gas originates from the gas injected into the ion source. The present ion sources need a flow not exceeding 10^{-3} mbar.l.s^{-1}. For all the following calculations, this has been increased by a factor of 10. The flow of gas considered represents a volume of 80 litres at 800 mb after 3 months of production.

The principles of the storage system are presented in figure V.12. The tanks 1 and 2 have a volume of 200 litres. Before the first run, the tanks 1 and 2 are pumped down to a pressure of 10 mbar.

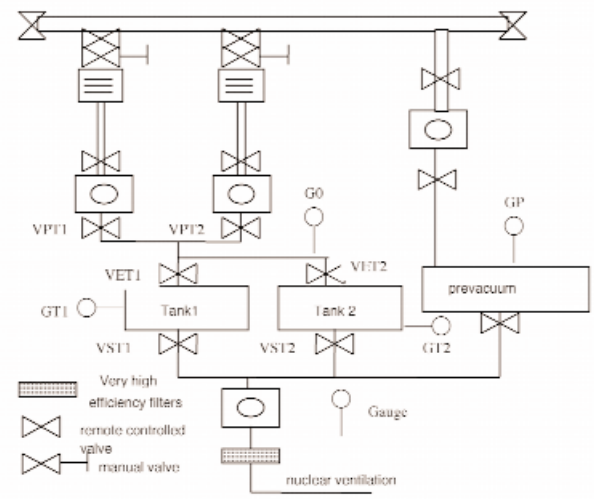

Figure V.12 : Principles of the gas storage system.

T=0	T=1 month	T=30 year
2.51 10^{13} Bq	6.9 10^{10} Bq	2.8 10^{8} Bq

Table V.7 : Estimation of the activity of noble gases in the target for different times (just after the production, 1month after the end of production and 30 years later). The target was assumed to be irradiated for 3 months.

After this preliminary pumping, the valves VST1 and VST2, VET1 and VET2 are closed. The volume of the tube between the primary pumps and VET1 and 2 is considered as a buffer. When the gauge G0 detects a pressure greater than 800 mbar, the valve VET1 is triggered and the buffer volume is extracted into the tank. The VET1 is then closed when the pressure measured by the gauge G0 is equal to the pressure measured in the tank with the GT1 gauge.

After three month of irradiation, the valves of tank 1 are closed and the storage can continue using tank 2, allowing the activity in tank 1 to decay. After a waiting time (still to be defined, as mentioned above) and following an analysis of residual activity, the gas in tank 1 is exhausted through the high efficiency filters of the nuclear ventilation system.

Any leakage of air into one of the chambers of the system would induce a rapid rise of the pressure, which would be detected on the gauge G0. In such an event, both the primary beam and the vacuum pumping would immediately be stopped.

Water activation

This problem has been studied at ISAC facility, and the same system will be installed in LINAG. It consists in a closed loop passing through a heat exchanger. The water of the primary circuit is drained to a buffer volume where it can be monitored prior to be released to outside drains.

Table V.8 : The in-target yields calculated for a 40 MeV, 5 mA deuteron beam striking 7 mm of C followed by 56 slices of UC_2 1 mm thick spaced by 0.5 mm. [Density $\rho(UC_2)$ = 11 g/cm³. Beam size is 10 mm diameter.]

	Ycumul	Yparent	Ydirect		Ycumul	Yparent	Ydirect
Ni66	1,22E+06	1,19E+06	2,65E+04	**Ru111**	2,55E+11	4,57E+10	2,09E+11
Ni67	7,03E+06	6,39E+06	6,40E+05	**Rh111**	4,11E+11	2,55E+11	1,56E+11
Ni68	9,14E+06	6,71E+06	2,43E+06	**Tc112**	8,41E+09	7,36E+08	7,67E+09
Ni69	1,14E+07	5,69E+06	5,71E+06	**Ru112**	6,95E+10	8,41E+09	6,11E+10
Ni70	1,29E+07	3,33E+06	9,58E+06	**Rh112**	2,00E+11	6,95E+10	1,31E+11
Cu70	6,80E+06	1,29E+07	-6,11E+06	**Pd112**	2,00E+11	2,00E+11	0,00E+00
Ni71	2,60E+10	2,60E+10	9,99E+06	**Tc113**	2,56E+09	5,52E+07	2,50E+09
Cu71	2,60E+10	2,60E+10	4,44E+06	**Ru113**	6,44E+10	2,56E+09	6,19E+10
Ni72	9,27E+06	4,22E+05	8,84E+06	**Rh113**	1,71E+11	6,44E+10	1,07E+11
Cu72	1,87E+07	9,27E+06	9,42E+06	**Pd113**	1,71E+11	1,71E+11	5,55E+07
Zn72	2,02E+07	1,87E+07	1,50E+06	**Ru114**	8,52E+10	4,58E+08	8,47E+10
Ni73	1,42E+07	2,58E+05	1,39E+07	**Rh114**	1,68E+11	8,52E+10	8,32E+10
Cu73	5,49E+07	1,42E+07	4,07E+07	**Pd114**	2,22E+11	1,68E+11	5,34E+10
Zn73	2,61E+10	5,49E+07	2,60E+10	**Ag114**	2,22E+11	2,22E+11	3,70E+06
Ni74	6,27E+06	3,51E+04	6,23E+06	**Ru115**	3,23E+09	5,51E+07	3,17E+09
Cu74	5,09E+07	6,27E+06	4,46E+07	**Rh115**	1,15E+11	3,23E+09	1,12E+11
Zn74	2,61E+10	5,09E+07	2,60E+10	**Pd115**	2,98E+11	1,15E+11	1,83E+11
Ga74	2,61E+10	2,61E+10	1,48E+06	**Ag115**	2,18E+11	2,98E+11	-8,05E+10
Cu75	4,85E+07	2,19E+06	4,63E+07	**Rh116**	5,96E+10	2,71E+10	3,25E+10
Zn75	1,39E+08	4,85E+07	9,09E+07	**Pd116**	1,42E+11	5,96E+10	8,28E+10
Ga75	1,51E+08	1,39E+08	1,16E+07	**Ag116**	1,42E+11	1,42E+11	8,51E+07
Cu76	3,27E+07	5,78E+05	3,21E+07	**Rh117**	3,95E+09	1,78E+08	3,77E+09
Zn76	2,13E+08	3,27E+07	1,80E+08	**Pd117**	8,93E+10	3,95E+09	8,54E+10
Ga76	2,66E+08	2,13E+08	5,30E+07	**Ag117**	7,11E+10	8,93E+10	-1,82E+10
Cu77	4,02E+07	2,20E+05	4,00E+07	**Pd118**	1,43E+11	1,71E+09	1,42E+11
Zn77	5,85E+08	4,02E+07	5,45E+08	**Ag118**	1,03E+11	1,43E+11	-4,02E+10
Ga77	1,04E+09	5,85E+08	4,59E+08	**Cd118**	1,46E+11	1,03E+11	4,32E+10
Cu78	2,62E+07	5,15E+04	2,62E+07	**In118**	1,46E+11	1,46E+11	0,00E+00
Zn78	1,09E+09	2,62E+07	1,07E+09	**Pd119**	1,08E+11	2,64E+10	8,19E+10
Ga78	3,18E+09	1,09E+09	2,09E+09	**Ag119**	2,44E+11	1,08E+11	1,36E+11
Ge78	2,97E+10	3,18E+09	2,65E+10	**Cd119**	2,69E+11	2,44E+11	2,46E+10
Zn79	1,10E+09	9,78E+06	1,09E+09	**In119**	8,70E+10	2,69E+11	-1,82E+11
Ga79	3,31E+10	1,10E+09	3,20E+10	**Pd120**	5,48E+10	4,70E+07	5,48E+10
Ge79	3,33E+10	3,31E+10	1,58E+08	**Ag120**	1,90E+11	5,48E+10	1,35E+11
As79	3,67E+10	3,33E+10	3,43E+09	**Cd120**	2,73E+11	1,90E+11	8,29E+10
Zn80	3,43E+08	9,25E+05	3,42E+08	**In120**	2,73E+11	2,73E+11	7,40E+06
Ga80	5,16E+09	3,43E+08	4,81E+09	**Ag121**	1,63E+11	6,64E+08	1,62E+11
Ge80	6,54E+10	5,16E+09	6,02E+10	**Cd121**	2,43E+11	1,63E+11	8,06E+10
As80	9,20E+10	6,54E+10	2,67E+10	**In121**	5,79E+09	2,43E+11	-2,37E+11
Zn81	1,11E+08	1,03E+05	1,11E+08	**Ag122**	5,38E+10	1,37E+08	5,37E+10
Ga81	4,97E+09	1,11E+08	4,85E+09	**Cd122**	2,47E+11	5,38E+10	1,93E+11

Ge81	2,16E+10	4,97E+09	1,66E+10	**In122**	2,47E+11	2,47E+11	4,18E+08
As81	8,02E+10	2,16E+10	5,86E+10	**Ag123**	1,05E+11	1,76E+07	1,05E+11
Ga82	3,74E+09	3,05E+07	3,71E+09	**Cd123**	2,97E+11	1,05E+11	1,91E+11
Ge82	9,64E+10	3,74E+09	9,27E+10	**In123**	2,58E+11	2,97E+11	-3,90E+10
As82	1,08E+11	9,64E+10	1,21E+10	**Ag124**	2,63E+10	1,40E+06	2,63E+10
Ga83	1,29E+09	3,07E+06	1,29E+09	**Cd124**	8,46E+10	2,63E+10	5,83E+10
Ge83	3,85E+10	1,29E+09	3,72E+10	**In124**	1,14E+11	8,46E+10	2,96E+10
As83	1,97E+11	3,85E+10	1,59E+11	**Ag125**	5,75E+07	6,79E+04	5,74E+07
Se83	6,85E+10	1,97E+11	-1,29E+11	**Cd125**	8,13E+10	5,75E+07	8,12E+10
Ga84	2,82E+08	2,15E+05	2,82E+08	**In125**	2,96E+11	8,13E+10	2,14E+11
Ge84	3,97E+10	2,82E+08	3,94E+10	**Ag126**	3,10E+03	6,55E-17	3,10E+03
As84	1,27E+11	3,97E+10	8,70E+10	**Cd126**	7,83E+10	3,10E+03	7,83E+10
Se84	4,52E+11	1,27E+11	3,26E+11	**In126**	1,88E+11	7,83E+10	1,10E+11
Br84	4,53E+11	4,52E+11	4,81E+08	**Sn126**	1,11E+06	1,88E+11	-1,88E+11
Ge85	2,36E+10	2,60E+10	-2,40E+09	**Ag127**	3,90E+02	2,20E-05	3,90E+02
As85	2,22E+11	2,36E+10	1,98E+11	**Cd127**	1,35E+08	3,90E+02	1,35E+08
Se85	2,81E+11	2,22E+11	5,95E+10	**In127**	1,41E+11	1,35E+08	1,41E+11
Br85	2,94E+11	2,81E+11	1,30E+10	**Sn127**	1,68E+11	1,41E+11	2,66E+10
As86	7,62E+10	2,00E+09	7,42E+10	**Sb127**	3,30E+11	1,68E+11	1,62E+11
Se86	5,33E+11	7,62E+10	4,57E+11	**Cd128**	4,20E+07	2,33E+01	4,20E+07
Br86	6,72E+11	5,33E+11	1,39E+11	**In128**	1,43E+11	4,20E+07	1,43E+11
As87	1,64E+10	1,24E+08	1,63E+10	**Sn128**	4,83E+11	1,43E+11	3,40E+11
Se87	3,41E+11	1,64E+10	3,24E+11	**Sb128**	4,37E+10	4,83E+11	-4,40E+11
Br87	6,37E+11	3,41E+11	2,97E+11	**Cd129**	1,57E+07	6,98E-01	1,57E+07
Kr87	6,82E+11	6,37E+11	4,50E+10	**In129**	2,21E+10	1,57E+07	2,21E+10
Se88	3,65E+11	5,46E+09	3,59E+11	**Sn129**	3,77E+11	2,21E+10	3,54E+11
Br88	7,95E+11	3,65E+11	4,30E+11	**Sb129**	6,96E+11	3,77E+11	3,19E+11
Kr88	1,04E+12	7,95E+11	2,41E+11	**Cd130**	2,35E+06	4,10E+01	2,35E+06
Rb88	1,04E+12	1,04E+12	6,29E+08	**In130**	8,21E+09	2,35E+06	8,21E+09
Se89	1,10E+11	1,14E+09	1,09E+11	**Sn130**	4,65E+11	8,21E+09	4,57E+11
Br89	8,46E+11	1,10E+11	7,35E+11	**Sb130**	4,65E+11	4,65E+11	-4,81E+08
Kr89	1,13E+12	8,46E+11	2,88E+11	**In131**	4,41E+09	1,81E+05	4,41E+09
Rb89	1,16E+12	1,13E+12	2,90E+10	**Sn131**	3,85E+11	4,41E+09	3,80E+11
Sr89	9,79E+11	1,16E+12	-1,83E+11	**Sb131**	1,20E+12	3,85E+11	8,13E+11
Se90	3,49E+10	2,90E+07	3,49E+10	**In132**	2,12E+10	5,97E+07	2,12E+10
Br90	5,77E+11	3,49E+10	5,42E+11	**Sn132**	6,65E+11	2,12E+10	6,44E+11
Kr90	1,26E+12	5,77E+11	6,86E+11	**Sb132**	7,06E+11	6,65E+11	4,07E+10
Rb90	1,13E+12	1,26E+12	-1,38E+11	**Te132**	2,18E+12	7,06E+11	1,47E+12
Sr90	1,19E+10	1,13E+12	-1,11E+12	**In133**	2,43E+09	2,77E+06	2,42E+09
Se91	6,17E+09	5,55E+06	6,17E+09	**Sn133**	2,22E+11	2,43E+09	2,20E+11
Br91	3,58E+11	6,17E+09	3,52E+11	**Sb133**	1,33E+12	2,22E+11	1,10E+12
Kr91	1,26E+12	3,58E+11	9,05E+11	**Te133**	1,83E+12	1,33E+12	5,02E+11
Rb91	1,64E+12	1,26E+12	3,78E+11	**Sn134**	5,99E+10	1,61E+08	5,97E+10
Sr91	1,65E+12	1,64E+12	3,92E+09	**Sb134**	4,96E+11	5,99E+10	4,36E+11
Y91	1,29E+12	1,65E+12	-3,53E+11	**Te134**	2,74E+12	4,96E+11	2,25E+12
Br92	7,73E+10	6,50E+08	7,67E+10	**I134**	3,12E+12	2,74E+12	3,76E+11
Kr92	1,11E+12	7,73E+10	1,03E+12	**Sb135**	3,41E+11	6,24E+09	3,34E+11
Rb92	1,69E+12	1,11E+12	5,75E+11	**Te135**	1,82E+12	3,41E+11	1,48E+12

Sr92	1,77E+12	1,69E+12	8,23E+10	**I135**	2,98E+12	1,82E+12	1,16E+12
Y92	1,77E+12	1,77E+12	3,70E+07	**Sb136**	7,87E+10	4,65E+08	7,82E+10
Br93	4,24E+10	1,88E+07	4,24E+10	**Te136**	1,22E+12	7,87E+10	1,14E+12
Kr93	6,57E+11	4,24E+10	6,14E+11	**I136**	1,89E+12	1,22E+12	6,70E+11
Rb93	1,67E+12	6,57E+11	1,02E+12	**Te137**	5,25E+11	1,26E+10	5,12E+11
Sr93	2,03E+12	1,67E+12	3,53E+11	**I137**	1,92E+12	5,25E+11	1,39E+12
Y93	2,03E+12	2,03E+12	1,26E+09	**Xe137**	2,67E+12	1,92E+12	7,57E+11
Kr94	2,69E+11	2,59E+09	2,66E+11	**Te138**	2,08E+11	1,33E+09	2,06E+11
Rb94	1,19E+12	2,69E+11	9,23E+11	**I138**	1,27E+12	2,08E+11	1,06E+12
Sr94	1,83E+12	1,19E+12	6,36E+11	**Xe138**	2,44E+12	1,27E+12	1,17E+12
Y94	1,84E+12	1,83E+12	1,11E+10	**Cs138**	2,51E+12	2,44E+12	6,99E+10
Kr95	4,15E+10	3,73E+07	4,15E+10	**I139**	7,64E+11	3,97E+10	7,24E+11
Rb95	9,01E+11	4,15E+10	8,59E+11	**Xe139**	2,16E+12	7,64E+11	1,39E+12
Sr95	2,26E+12	9,01E+11	1,36E+12	**Cs139**	2,40E+12	2,16E+12	2,44E+11
Y95	2,34E+12	2,26E+12	7,33E+10	**I140**	2,91E+11	6,10E+09	2,85E+11
Rb96	4,20E+11	1,12E+10	4,09E+11	**Xe140**	1,84E+12	2,91E+11	1,55E+12
Sr96	2,37E+12	4,20E+11	1,95E+12	**Cs140**	2,29E+12	1,84E+12	4,48E+11
Y96	2,45E+12	2,37E+12	7,59E+10	**Ba140**	2,35E+12	2,29E+12	6,01E+10
Rb97	1,07E+11	2,63E+08	1,07E+11	**I141**	8,42E+10	1,82E+09	8,23E+10
Sr97	1,18E+12	1,07E+11	1,08E+12	**Xe141**	1,10E+12	8,42E+10	1,01E+12
Y97	1,73E+12	1,18E+12	5,51E+11	**Cs141**	1,91E+12	1,10E+12	8,12E+11
Zr97	2,40E+12	1,73E+12	6,70E+11	**Ba141**	2,04E+12	1,91E+12	1,27E+11
Rb98	7,98E+10	8,53E+07	7,97E+10	**La141**	2,04E+12	2,04E+12	1,11E+08
Sr98	1,05E+12	7,98E+10	9,69E+11	**Xe142**	5,14E+11	1,38E+10	5,00E+11
Y98	1,96E+12	1,05E+12	9,10E+11	**Cs142**	1,52E+12	5,14E+11	1,01E+12
Zr98	2,68E+12	1,96E+12	7,24E+11	**Ba142**	1,92E+12	1,52E+12	3,97E+11
Nb98	2,68E+12	2,68E+12	7,40E+08	**La142**	1,92E+12	1,92E+12	1,70E+09
Rb99	5,56E+09	6,35E+06	5,55E+09	**Xe143**	7,23E+10	2,45E+09	6,98E+10
Sr99	3,77E+11	5,56E+09	3,72E+11	**Cs143**	1,01E+12	7,23E+10	9,33E+11
Y99	1,84E+12	3,77E+11	1,46E+12	**Ba143**	1,79E+12	1,01E+12	7,85E+11
Zr99	2,50E+12	1,84E+12	6,65E+11	**La143**	1,80E+12	1,79E+12	1,47E+10
Nb99	1,60E+12	2,50E+12	-9,01E+11	**Xe144**	4,02E+10	3,34E+07	4,02E+10
Rb100	4,09E+08	1,20E+05	4,09E+08	**Cs144**	6,62E+11	4,02E+10	6,22E+11
Sr100	1,00E+11	4,09E+08	9,96E+10	**Ba144**	1,60E+12	6,62E+11	9,41E+11
Y100	1,35E+12	1,00E+11	1,25E+12	**La144**	1,75E+12	1,60E+12	1,47E+11
Zr100	2,67E+12	1,35E+12	1,32E+12	**Ce144**	4,90E+11	1,75E+12	-1,26E+12
Nb100	2,75E+12	2,67E+12	8,35E+10	**Xe145**	4,27E+09	3,84E+06	4,27E+09
Rb101	1,41E+07	7,35E+02	1,41E+07	**Cs145**	1,86E+11	4,27E+09	1,82E+11
Sr101	1,57E+10	1,41E+07	1,57E+10	**Ba145**	1,14E+12	1,86E+11	9,57E+11
Y101	6,50E+11	1,57E+10	6,35E+11	**La145**	1,58E+12	1,14E+12	4,41E+11
Zr101	2,12E+12	6,50E+11	1,47E+12	**Ce145**	1,59E+12	1,58E+12	4,18E+09
Nb101	2,45E+12	2,12E+12	3,30E+11	**Cs146**	3,87E+10	3,07E+08	3,84E+10
Mo101	2,45E+12	2,45E+12	3,37E+09	**Ba146**	7,38E+11	3,87E+10	6,99E+11
Sr102	2,06E+09	1,71E+06	2,06E+09	**La146**	1,13E+12	7,38E+11	3,91E+11
Y102	1,99E+11	2,06E+09	1,97E+11	**Ce146**	1,37E+12	1,13E+12	2,38E+11
Zr102	1,82E+12	1,99E+11	1,63E+12	**Cs147**	4,72E+09	5,40E+06	4,72E+09
Nb102	2,35E+12	1,82E+12	5,21E+11	**Ba147**	2,76E+11	4,72E+09	2,71E+11
Mo102	2,74E+12	2,35E+12	3,91E+11	**La147**	8,92E+11	2,76E+11	6,16E+11

Zr103	1,09E+12	6,96E+10	1,02E+12	**Ce147**	1,06E+12	8,92E+11	1,65E+11
Nb103	2,32E+12	1,09E+12	1,23E+12	**Cs148**	8,06E+08	5,97E+05	8,06E+08
Mo103	2,47E+12	2,32E+12	1,49E+11	**Ba148**	8,23E+10	8,06E+08	8,15E+10
Tc103	2,49E+12	2,47E+12	2,67E+10	**La148**	5,18E+11	8,23E+10	4,36E+11
Zr104	3,63E+11	5,34E+09	3,58E+11	**Ce148**	9,99E+11	5,18E+11	4,81E+11
Nb104	9,64E+11	3,63E+11	6,01E+11	**Pr148**	1,03E+12	9,99E+11	2,89E+10
Mo104	2,07E+12	9,64E+11	1,10E+12	**Ba149**	1,55E+10	1,39E+07	1,55E+10
Tc104	2,12E+12	2,07E+12	5,71E+10	**La149**	2,60E+11	1,55E+10	2,44E+11
Zr105	6,97E+10	1,19E+09	6,85E+10	**Ce149**	6,64E+11	2,60E+11	4,04E+11
Nb105	7,63E+11	6,97E+10	6,93E+11	**Pr149**	7,15E+11	6,64E+11	5,13E+10
Mo105	1,56E+12	7,63E+11	7,98E+11	**Ba150**	1,78E+09	1,58E+06	1,78E+09
Tc105	1,64E+12	1,56E+12	7,76E+10	**La150**	7,18E+10	1,78E+09	7,00E+10
Ru105	1,64E+12	1,64E+12	1,85E+08	**Ce150**	4,07E+11	7,18E+10	3,35E+11
Nb106	1,95E+11	2,39E+08	1,95E+11	**Pr150**	4,95E+11	4,07E+11	8,86E+10
Mo106	9,71E+11	1,95E+11	7,76E+11	**Ce151**	1,63E+11	1,47E+10	1,49E+11
Tc106	1,03E+12	9,71E+11	6,03E+10	**Pr151**	3,34E+11	1,63E+11	1,70E+11
Ru106	2,30E+11	1,03E+12	-8,02E+11	**Ce152**	8,84E+10	1,91E+09	8,64E+10
Nb107	7,36E+10	6,38E+06	7,36E+10	**Pr152**	2,60E+11	8,84E+10	1,72E+11
Mo107	5,52E+11	7,36E+10	4,79E+11	**Nd152**	3,04E+11	2,60E+11	4,36E+10
Tc107	9,64E+11	5,52E+11	4,12E+11	**Pr153**	1,25E+11	1,85E+10	1,06E+11
Ru107	9,90E+11	9,64E+11	2,60E+10	**Nd153**	1,61E+11	1,25E+11	3,66E+10
Rh107	9,90E+11	9,90E+11	-3,70E+07	**Pm153**	2,14E+11	1,61E+11	5,30E+10
Mo108	3,00E+11	3,17E+10	2,69E+11	**Pr154**	3,16E+10	2,63E+09	2,89E+10
Tc108	3,77E+11	3,00E+11	7,72E+10	**Nd154**	9,46E+10	3,16E+10	6,31E+10
Ru108	4,82E+11	3,77E+11	1,04E+11	**Pm154**	9,58E+10	9,46E+10	1,23E+09
Rh108	4,82E+11	4,82E+11	-3,70E+07	**Nd155**	4,01E+10	1,00E+10	3,01E+10
Mo109	1,08E+11	5,01E+08	1,07E+11	**Pm155**	4,62E+10	4,01E+10	6,08E+09
Tc109	2,13E+11	1,08E+11	1,05E+11	**Sm155**	4,63E+10	4,62E+10	9,99E+07
Ru109	2,91E+11	2,13E+11	7,83E+10	**Nd156**	4,31E+10	1,74E+09	4,14E+10
Rh109	3,17E+11	2,91E+11	2,60E+10	**Pm156**	5,05E+10	4,31E+10	7,43E+09
Mo110	2,04E+10	3,64E+07	2,04E+10	**Sm156**	5,09E+10	5,05E+10	3,96E+08
Tc110	7,20E+10	2,04E+10	5,16E+10	**Pm157**	6,46E+10	5,75E+10	7,09E+09
Ru110	2,31E+11	7,20E+10	1,58E+11	**Sm157**	6,56E+10	6,46E+10	9,69E+08
Rh110	1,19E+05	2,31E+11	-2,31E+11	**Sm158**	6,04E+09	4,64E+09	1,40E+09
Tc111	4,57E+10	5,71E+09	4,00E+10				

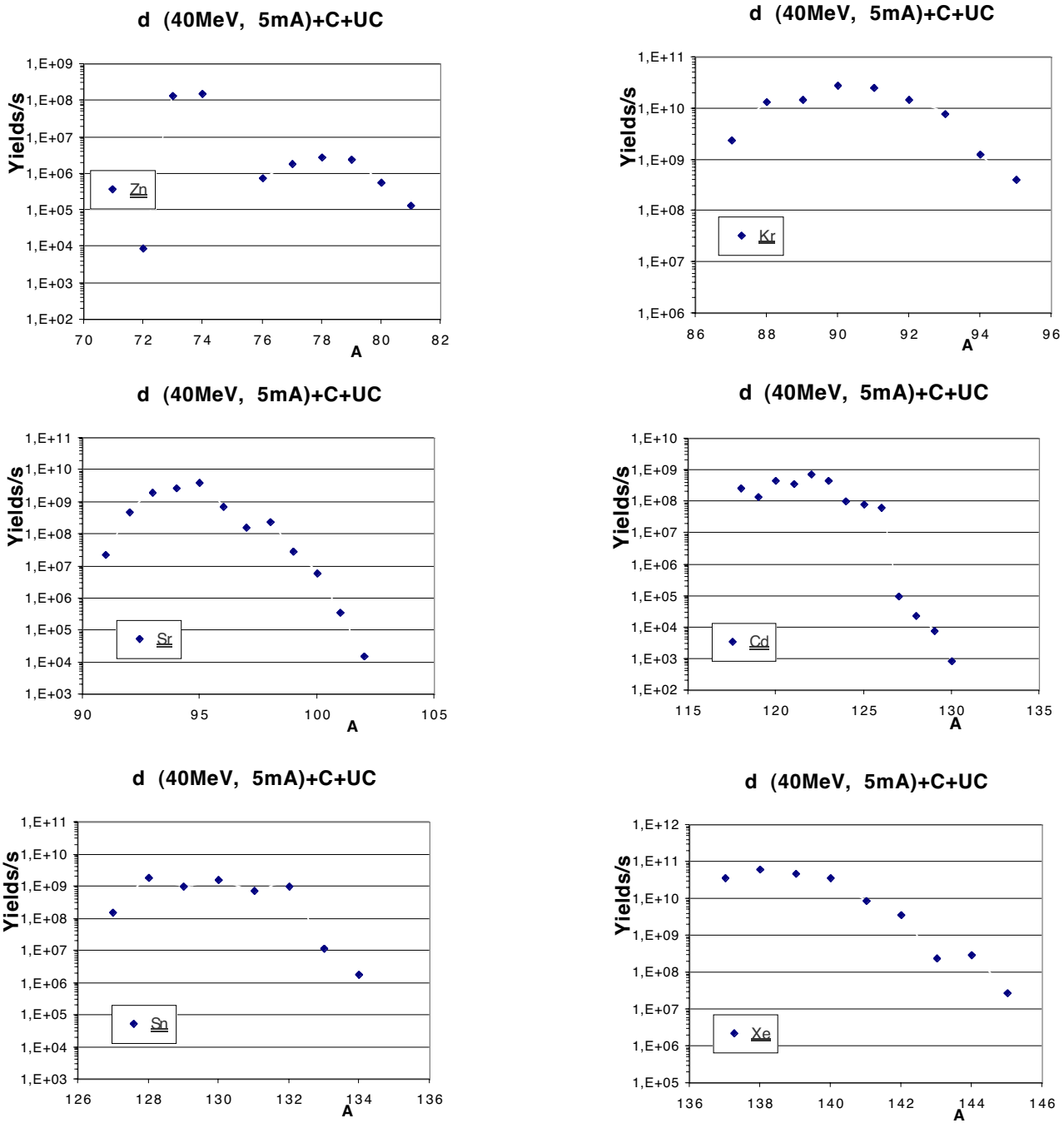

Figure V.13-18 : The expected radioactive beam intensities after diffusion, effusion, ionisation and acceleration.

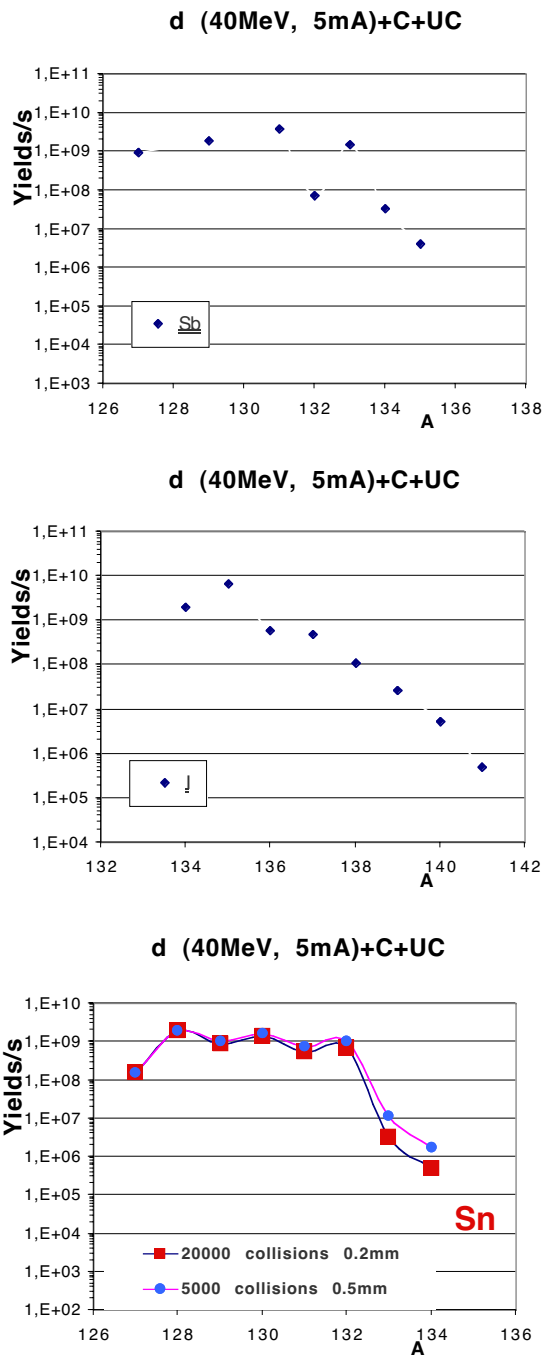

Figure V.19-21 : The expected radioactive beam intensities after diffusion, effusion, ionisation and acceleration. For Sn, two different effusion efficiencies are considered.

References

1) SIRIUS : proposed target station and handling facilities : http://www.ganil.fr/eurisol/targetgroupmeetings/Papers_27_28-02-02.html, Roger Bennett, EURISOL meeting 2002.

2) ISAC target laboratory and facilities : http://www.ganil.fr/eurisol/targetgroupmeetings/Papers_27_28-02-02.html, Paul Schmorr, EURISOL meeting 2002.

3) M.G. Saint Laurent et al., SPIRAL phase II European RTD report, GANIL R 01-03 2001.

4) D. Ridikas thesis, GANIL T99-04, 1999.

5) P. Grand and A.N. Goland, Nucl. Instr. Meth. 145 (1977) 49.

6) SYSTUS code, http://www.esi-group.com/products/systus/overview.html

7) POCO graphite, http://www.poco.com/

8) J.C. Putaux et al., Nucl.Instr. Meth., B126 (1997) 113.

9) P.V. Logatchev, L.B. Tecchio et al., Graphite neutron target for exotic beams, SPES internal report, Legnaro 2000

10) S. Borg et al., Nucl. Instr. Meth. 91 (1071) 109.

11) D. Ridikas, W. Mittig and A.C.C. Villari, Comparative study of the direct and converter methods for high fission yields, GANIL-P-2000-31. 2000, to be published in Nuc. Phys., proceedings of RNB 2000.

12) M. Olivo, et al., AIP conference proceedings n°600 (2001) 246

13) S. Sundell, H. Ravn and the ISOLDE Collaboration, NIM B 70 (1992) 160

14) V.I. Mishin, V.N. Fedoseyev, H.-J. Kluge, V.S. Letokhv, H.L. Ravn, F. Sheerer, Y. Shirakabe, S. Sundell, O. Tengblad NIM B 73 (1993) 550

15) Laurent Maunoury, Thesis GANIL T 98 01 2001.

16) Nathalie Lecesne, Thesis GANIL T 97 02 1997.

17) A.C.C. Villari et al., Proceedings of RNB 2000, Nuclear Physics A

18) R. Leroy et al., Proceedings of the 9th International Conference on Ion Sources, Rev. Sci. Instrum. (2001)

19) F. Landré-Pellemoine, Thesis, Université de Caen, (2001)

20) P. Jardin et al., Rev. Sci. Instrum. 73 (2002) 789

21) G. Gaubert et al., to be submitted to Rev. Sci. Instrum.

22) P. Jardin et al., to be published in the Proceedings of the14th EMIS Conference, Victoria, May 2002

23) J.L. Belmont et al, Proceedings of the International workshop on the physics and techniques of secondary nuclear beams, Dourdan, France. Editions Frontières (1992)

24) N. Chauvin, thesis, Université Joseph Fourier Grenoble (2000)

25) Roussière B. et al., Release properties of UCx and molten U targets preprint IPNO-DR-2002-002. - 2002.

Chapter VI : Security and Radioprotection

VI.1) SHIEDLING AND ACTIVATION OF THE ACCELERATOR : comparison with the IFMIF project

A detailed discussion of the problem of radioprotection in the case of acceleration of deuterons can be found in the report IFMIF (International Fusion Materials Irradiation Facility) edited by Marcello Martone, ENDF/B-VI Library, NBL-USA. This report uses largely the results of the FMIT (Fusion Material Irradiation Test) working group. IFMIF is a project with a linear accelerator for very high intensity (125 mA) beams of deuterons at an energy of 40 MeV. Hence the problems are similar to those expected for the LINAG I project, with 5 mA of deuterons of 40 MeV.

It is therefore useful to summarize the conclusions of the IFMIF report. The basic assumptions and conclusions were the following :

- Based upon beam dynamics simulation work for the APT project and operational experience with the LAMPF linac at Los Alamos, it will be possible to build a CW, high-current ion linac and HEBT with beam losses at the nA/m level. This is the target for the IFMIF preliminary and final designs. However, until an upper limit on probable beam losses can be estimated with confidence, activation analyses will use the more conservative assumption of µA/m beam losses, as established by the FMIT program.
- Access to the accelerator vault, beam turning vault, beam steering vault, beam calibration dump and target interface vault cannot be permitted during accelerator operation.
- All accelerator components will be accessible within 24 hours after beam turn-off. This requirement will be lowest (~1 h) in the injector area and highest in the downstream sections of the HEBT.
- Hands-on maintenance will be possible throughout the accelerator beam line, with the possible exception of the beam steering vault, beam calibration dump and target interface vault. Therefore, the design of these latter accelerator components will be done assuming remote maintenance similar to the FMIT solution.
- Tune-up of the beamline should be at the lowest relevant power level (initially ~ 0.01% duty factor) for the shortest possible time. One should maximize the use of H_2 for tune-up operations, before using D_2.

(In the above discussion, hands-on maintenance is defined to be maintenance without using remote manipulators. Local shielding, special handling or tooling such as long-reach instruments and limited access for personnel are within the definition of hands-on maintenance).

When we compare this IFMIF project with the LINAG-I project, all differences with respect to IFMIF are in the direction of decreased radioprotection problems. To start with, the intensity projected for IFMIF is a factor of 25 higher. Owing to the much lower intensity of LINAG, not only are the absolute values lower, but lower space charge effects are expected, which should imply lower beam losses. A more detailed evaluation is presented below.

Accelerator radiation protection plan

The neutron yield from beam loss depends on the target material and the angle of incidence. For example, the dashed curve of figure VI.1 shows the number of neutrons generated per lost deuteron, as a function of the lost deuteron energy, via D-D reactions between the incoming beam and deuterium ions embedded in the surface of a copper structure, assuming that the embedded deuterium ions have reached a saturation density of 1.7 x 10^{22} cm^{-3} throughout the full pene-

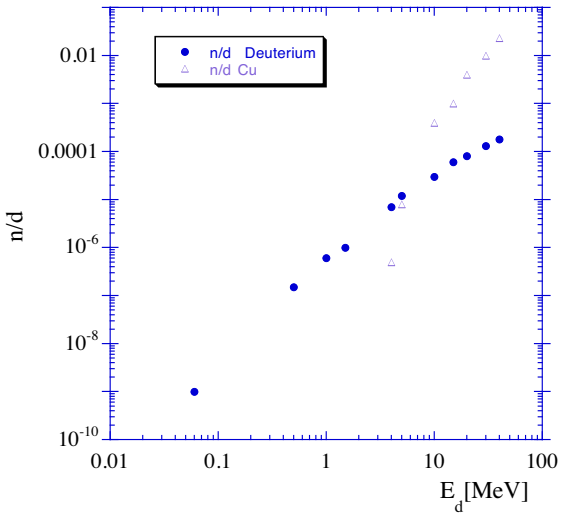

Figure VI.1 : Neutrons produced per lost deuteron via D-D fusion and direct interaction of the deuterium with copper ; the density of deuterium is assumed fully saturated in Cu

tration depth of the lost ions [50]. Note that this volumetric density corresponds to about half that of liquid or solid deuterium.

The RFQ will be made of Cu, whereas the linear accelerator will be of Nb. The neutron yield from deuterons on Nb is much less studied than for Cu. However, the results for Cu over-estimate the yield, owing to a lower Coulomb barrier. Data points available give a factor of 2 lower yield for Nb as compared to Cu (see thesis of N. Pauwels). We will use data for copper in what follows. For deuterons lost at low energy, the resulting fusion neutrons are nearly monoenergetic at 2.5 MeV and are approximately isotropic in angle. As the deuteron energy increases, the peak neutron energy increases correspondingly and strong energy/angle correlations develop. The solid curve shows the number of neutrons generated via direct interaction between the deuteron and copper, in which the neutron is essentially stripped away from the proton. The results indicate that : (1) the D-D cross section is greater than the stripping cross section for deuterons of energy less than 5 MeV, and (2) six orders of magnitude more neutrons are generated per lost deuteron at 40 MeV than at 100 keV.

The radiation and activation which arise from beam losses are strongly affected by the amount of loss, the energy of deuterons that are lost, and the location of the losses.

Here we used the following estimates:

VI.1.1) Ion Source

At the exit of the ion source the loss is estimated to be 3% of the nominal intensity ; this is the same value as in the IFMIF report. The energy of the deuterons at the exit is 20 keV/nucleon, instead of 50 keV/nucleon for IFMIF. A recent measurment at SILHI with a 170-mA deuteron beam at 95 keV gave 75% transmission (draft report DSM/DAPNIA/SACM 2002/19). This should be greatly improved at the much lower intensity projected due to lower space charge effects. Hence we will remain with the 3% estimate of IFMIF. A radiation level of 11.5 μSv/h was observed at the beam stop, at a distance of 60 cm, after 2 hours of functioning. We expect a factor of 33 less due to a beam loss of 3% instead of the 100% stopped beam, another factor of 34 less due to the lower projected beam intensity, and a factor of 10 less due to the lower beam energy. So the expected radiation level is a thus a total factor of 11200 less than in this experiment. In ion source tests with full intensity stopped at the exit of the source, the reduction factor will be 340.

VI.1.2) The RFQ

The losses in the RFQ are estimated to be 1μA/m; this corresponds to a total loss in the RFQ of 6 μA or about 0.1 %. In the report on an RFQ for SPIRAL II by the SEA Saclay (report DSM/DAPNIA/SEA 01/62, and draft report DSM/DAPNIA/SACM 2002/19) the transmission was 100%. A recent calculation, including geometrical errors, gave a total loss of $5\ 10^{-5}$, thus a factor of 20 lower than the value estimated. The material is Cu, so the saturation density cited applies as the upper limit. No significant reaction rate on Cu is possible, because of the low exit energy of 1.5 MeV, much below the barrier.

VI.1.3) The Linear Accelerator

The technical specification of the superconducting structure of the linear accelerator is not compeletly defined. For consideration here we will suppose that it will be made out of about 1 mm thick superconducting Nb. The beam will be stopped at all energies in this material. Superconducting Nb must have a very low (at the ppm level) H or D contamination, at a level below a value that will contribute significantly. So only deuterium build-up on the cold surfaces of the accelerator structure could be the origin of d+d reactions. The total flux of the ion source is estimated to be ≤ 0.01 mbar.l/s. Supposing that all this is neutral and not pumped in the vicinity of the ion source, at the distance of the accelerator this will only result in $2.5\ 10^{-9} g/cm^2$ after 200 days of continuous running, a negligible quantity.

The cooling power of the superconducting accelerator implies a maximum loss of beam power of ≤ 0.5 W/cavity, or ≤ 2 W/m, to avoid evaporation of the liquid He and resultant quenching. This value was used to estimate the maximum permissable beam loss as a function of energy. It corresponds to 1.3 μA at the entrance to the accelerator, and to 0.05 μA at the exit. (The angular distributions of neutrons that are needed for the calculation of the dose at a given distance from the accelerator, and for determining the necessary shielding, were taken from the thesis of N. Pauwels, and interpolated or extrapolated when necessary).

With the estimates and assumptions listed above, we can calculate the neutron yield along the accelerator, as illustrated by figure VI.2.

With these numbers, and the angular distributions discussed before, we can calculate the dose rate at a given distance. With a shielding coefficient for ordinary concrete of

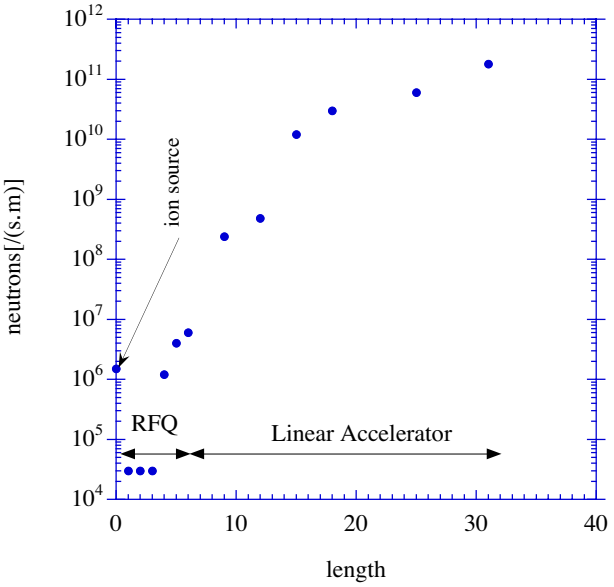

Figure VI.2 : Neutron yield in units per second and per meter of length of the accelerator. For the ion source the unit is the yield per second.

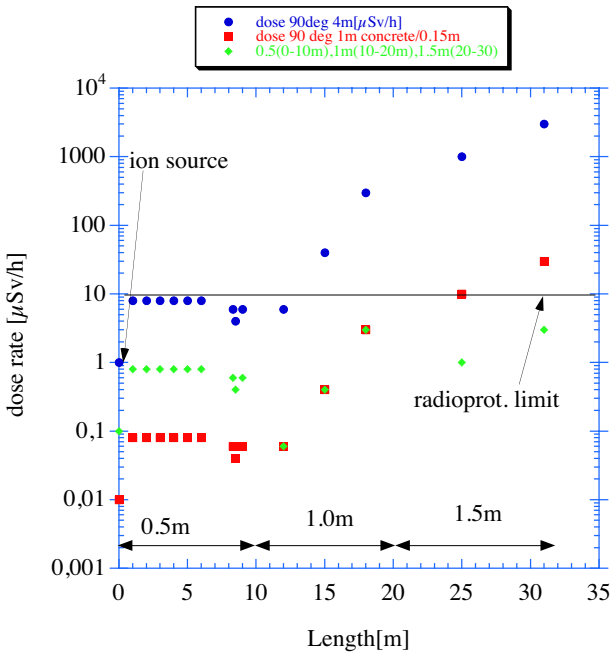

Figure VI.3 : Dose rate at 4 m distance, with and without shielding.

l=15 cm we can than estimate the dose rate after shielding. Two examples are shown, one with a constant thickness of 1 m, and a more realistic one with a thickness varying from 0.5 m at the low energy end to 1.5 m at the high energy end. The dose rate for the ion source shown corresponds to the 3% of beam loss discussed above, but even during tests of the ion source with full intensity stopped at 40 keV, the shielding of 0.5 m is sufficient, as can be seen from figure VI.3.

VI.2) ACTIVATION OF THE ACCELERATOR AND ITS ENVIRONEMENT

The activation problem can be divided into different parts, as can the shielding :

VI.2.1) Ion source

The activation in the ion source section is limited to the production of tritium, because of the low energy, and activation due to neutrons from the reaction d(d,n)^{3}He. Owing to isospin symmetry of nuclear forces, the reactions d(d,n)3He and d(d,p)t have the same cross sections. Hence the estimates of neutron yield presented above can be applied directly.
Tritium production :

With 3% of losses at 40 keV, the production of tritium is about 3 x 10^5/s, using the saturation density of deuterium in the stopper as before. With full intensity this leads to 10^7/s, limited to tuning or testing of the ion source.

Activation of surrounding material :

The neutron energy is 2.5 MeV, so neutron capture reactions are mainly possible. No detailed estimation of activation was done ; however the neutron yield is so low that this should not be a major problem.

VI.2.2) RFQ

The maximum of the deuteron energy is still only 1.5 MeV in the RFQ, so the main reactions will be neutron capture, as for the ion source. The total tritium production can be estimated to 1.3.x 10^7/s in the RFQ. No detailed estimation of activation by the neutrons was done ; however the neutron yield is so low that this should not be a problem. The summed tritium production for the RFQ and the ion source in running conditions is thus estimated to be below 1.5 x 10^6/s. This leads to a saturation decay rate of tritium of about 0.5 x 10^5/s after some years of running 200 days/year, much below the authorisation level of of 10^9 Bq. It is also much lower than

that presently found in the SPIRAL device when ^{13}C of maximum intensity is stopped in a C target.

VI.2.3) LINAC

As was discussed before, contribution from the D+D reaction can be neglected. The activation will originate from d+Nb reactions, either by reactions with the Nb, or the activation of surrounding material by neutrons produced in the d+Nb reaction. Activation data were measured by I.O. Konstantinov et al., Atomnaya Energiya, Vol. 60, no 5, (1986) 332. Main activities are from ^{89}Zr (78.4h) and ^{92m}Nb(10.15days). This is illustrated by figure VI.4.
No data are available at higher energy. As can be seen, the activation for deuterons is higher at energies below about 14

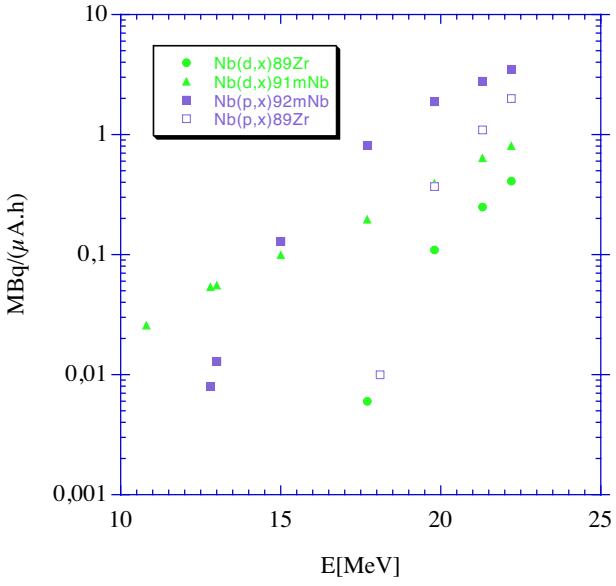

Figure VI.4 : Activation in units of MBq/μAh of thick Nb as a function of energy for deuterons and protons (data from I. Konstaninov et al.)

MeV, and is a factor 5 higher for protons at the maximum energy measured here of 22 MeV. The present data may be extrapolated to higher energy, yielding about 20 MBq/(μA.h) with an estimated error of a factor of 2. The highest activation is then in the high energy end, where the maximum possible loss without quench is below 10 nA per cavity. Thus the activation can be estimated to be less than 0.2 MBq/h per cavity. This value will saturate at about 50 MBq for a beam time of more than 10 days.

This value may be compared to calculations with the LAHET code. The value given by the code for 1 year of running with a beam of d of 40 MeV and 10 nA is 20 MBq, before cooling down. After 3 months, this value decreases by a factor of 18. This value of 20 MBq results in a dose rate at a distance of 1 m of about 4.3 μSv/h per cavity, at a distance of 1 m, before cooling down. After 3 months of cooling, this falls to 3 x 10^{-2} μSv/h and to 6.7 x 10^{-3} Sv/h after 1 year.

If we consider pure Cu instead of Nb, under the same conditions, the dose rate is 34 μSv/h after 1 year of running, before cooling down, and 6.2 μSv/h after 1 year. If a thin Nb-on-Cu structure is used, the activation will be between the values for pure Nb and pure Cu, depending on the thickness of the Nb layer.

VI.2.4) The High Energy Beam Transport Line (HEBT)

The HEBT activation can be estimated in the same way as was done in the IFMIF project and the FMIT program. The numbers given there have to be divided by the intensity ratio of 125 mA/5 mA = 25. For the values below, this has been done.

It was assumed during the FMIT program that the HEBT would lose 10 μA per bending magnet and 3 μA per metre in the straight sections. Because deuterons with sufficient energy will directly activate iron by producing various isotopes of radioactive cobalt, aluminium beam tubes were substituted throughout the HEBT, leading to a ten-fold reduction in the direct activation, and with a much shorter half-life. In this case, the FMIT analysis indicates that for 20 years of operation with a 35 MeV deuterium beam, followed by a 16 hour shut down, the radiation levels are on the order of 2.4 mSv per hour, at 30 cm from the loss point in a bending magnet. After one week, these levels are reduced to the 2–100 μSv per hour level, the dominant source being copper windings in the magnet. These HEBT results are without any shielding. The FMIT analysis concludes that hands-on maintenance will be possible through the use of copious shielding. The beam tube and magnets can be shielded with borated polyethylene to keep the neutrons localized. In addition, lead shielding is required to protect personnel from the gamma rays generated by the activated materials. More work is required, both in beam loss studies and in activation analysis, to obtain more reliable radiation level estimates and improved shielding designs.

VI.2.5) Beam accidents

Accidental beam losses and the radiation induced by such incidents require special operating procedures to be written and scrupulously followed at the time of the incident. The probability of sustained, large beam losses for times >1–10 ms is remote, because several layers of sensing will be used, using different physical principles and multiple shut-down methods. Accident scenarios include :
- failure of beam to shut off, beam delivery actually on target as expected,
- failure of beam turning element plus failure of beam shut-off fast-protect system :
- 90-degree bend in beam leading to the target,
- final neutron-backstreaming control bend in HEBT,
- beam steering magnet,
- focusing elements,
- abnormal beam spot on target;
- abnormal beam power deposit in C-target, and
- failure of beam loss monitoring system to detect abnormal beam loss and shut down beam.

VI.2.6) Shielding for the target/ion-source

Here we want just to discuss the shielding that is necessary around this device in order to have a radiation level below 10 µSv/h in the area immedietely arround this device. Exact values of the shielding thickness will depend on the detailed material composition of this device, which is not yet completely available. We give here values of the shielding that represent an upper limit used for dimensions and cost estimates, and it will probably be possible to decrease these values after a more detailed analysis. If 5 mA deuteron beam at 40 MeV impinges on a C target, the dedicated area should be surrounded about 4 m of ordinary concrete at 0°, to limit the dose rate below 10 uSv/h at 5 m distance; and 2.5 m for the same level at 90° at 4 meters away.

VI.2.7) The authorisation procedures

The authorisation procedures are described in some detail in the references [ref. 1-7]. The discussion below is mainly based on information given to us by P. Royet, who is working on the project for the DOS (Dossier des Options de Surete) for SPIRAL II. Following his conclusions, obtained in collaboration with external specialists, the publication of the authorisation decree could be expected, if there is no major delay, in mid-2005.

We will here only mention the related schedule that has been established (see table VI.1). This schedule can be considered as ambitious but possible. It will depend on the funding authorities, as to which stage of agreement will be considered necessary before funding can begin. Two stages seem possible : (i) the end of the exchange of remarks for the DOS, or (ii) after the drafting of the preliminary safety report, which implies an informal agreement of the Security Authorities. In the general schedule given in chapter IX, we supposed that funding starts at this point, i.e. the beginning of 2004. (note that the start of construction of the building implies at least this level of agreement, because security requirements may change the layout of the building).

The DOS and the preliminary safety report will need quite a detailed analysis of the security options for the target/ion-source. Detailed analysis of standard operation and possible failures and their impact is necessary. A higher level of agreement of the AS, prior to funding, could be the official agreement on the preliminary safety report, which is expected one year later. In the schedules given below we will suppose the first, more optimistic assumption, corresponding to funding commencing at the start of 2004.

References

1) "SPIRAL II : Preliminary design study "Rapport GANIL R 01 04 du 28 novembre 200, High Intensity Beams at Ganil and Future Opportunities : LINAG,Rapport Ganil R 01 02
2) "Les dossiers d'options de sûreté d'installations nucléaires de base " Annexe à la lettre DSIN/FAR/SD3/50488/00 du 26 juin 2000
3) "Constitution d'un dossier d'options de sûreté d'une installation nucléaire de base "Recommandation n°9 du manuel CEA de la sûreté nucléaire (DSNQ/MS/RE/009)
4) Arrêté du 31 décembre 1999 fixant la réglementation technique générale destinée à prévenir et limiter les nuisances et les risques externes résultant de l'exploitation des installations nucléaires de base
5) Décret n°63-1228 du 11 décembre 1963 modifié relatif aux installations nucléaires
6) Décret n°95-540 du 4 mai 1995 relatif aux rejets d'effluents liquides et gazeux et aux prélèvements d'eau des installations nucléaires de base
7) Arrêté du 26 novembre 1999 fixant les prescriptions techniques générales relatives aux limites et aux modalités des prélèvements et des rejets soumis à autorisation, effectués par les installations nucléaires de base

	SPIRAL II SHEDULE OF ADMINISTRATIVE AUTHORISATIONS													
	2002 T3	2002 T4	**2003** T1	2003 T2	2003 T3	2003 T4	**2004** T1	2004 T2	2004 T3	2004 T4	**2005** T1	2005 T2	2005 T3	2005 T4
Draft of the DOS	—	—												
Examination of the DOS by the AS			—	—										
Exchange and integration of remarks				—										
Draft of the preliminary Safety report				—	—	—	—							
Examination of the draft by the AS								—	—	—				
Exchange and integration of remarks									—	—				
Aproval of the <u>preliminary Safety report</u>											**X**			
Draft of the Application of Modification the INB (DAM) and of the Autorisation of Rejection of radioactive discharge (DAR)			—	—	—	—								
Examination of the DAM and DAR by the AS							—	—	—					
Exchange and integration of remarks								—	—					
Public Inquiries concerning the DAR & DAM										—				
Examination by the CIINB											**X**			
Publication of the decree of authorisation of rejection												**X**		
Publication of the decree of authorisation of SPIRAL 2												**X**		

Glossary:

DOS: Dossier des Options de Sureté,
AS: Autorités de Sureté
INB:Installation Nucléaire de Base
CIINB: Commission Interministrielle des INB

Table VI.1 : Schedule of administrative Security Authorisations

Chapter VII : Siting, postacceleration and coupling to experimental areas.

In considering the implantation of LINAG on the GANIL site a number of factors must be taken into account. In particular, the various post acceleration options as well as future developments should be considered. Furthermore these constraints need to be examined in the light of the interests and requirements of the user community. Beyond describing the siting of LINAG itself, the present section outlines the features of the proposed facility, when coupled to the existing accelerator complex offers.

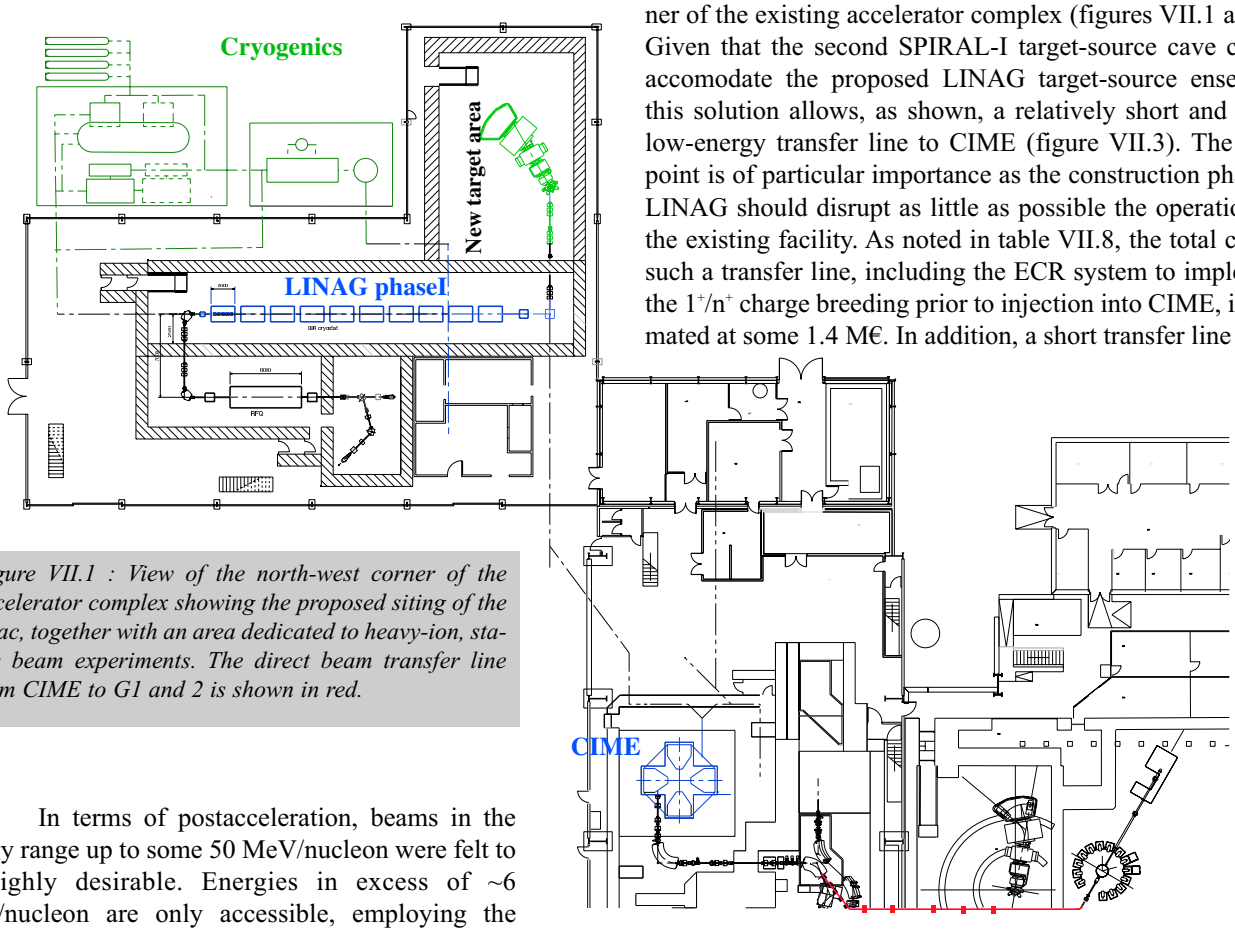

Figure VII.1 : View of the north-west corner of the accelerator complex showing the proposed siting of the linac, together with an area dedicated to heavy-ion, stable beam experiments. The direct beam transfer line from CIME to G1 and 2 is shown in red.

In terms of postacceleration, beams in the energy range up to some 50 MeV/nucleon were felt to be highly desirable. Energies in excess of ~6 MeV/nucleon are only accessible, employing the machines currently available on site, using the existing coupled cyclotrons ; either via the C02 injection cyclotron or a purpose built RFQ. Energies around the Coulomb barrier and somewhat above – ~1.7–6 MeV/nucleon – will be most efficiently achieved via reacceleration of high charge state (n^+) beams with the CIME cyclotron.

At very low-energies, the interest within the community to pursue decay studies etc... , mitigates for the provision of beams of some 100 keV – that is, typical source extraction energies. It should be noted that such a facility is also essential in order to provide for the installation of a beam identification station, such as that employed on SPIRAL-I [ref 1].

The desirability to retain these postacceleration options argues for the siting of LINAG on the north-west corner of the existing accelerator complex (figures VII.1 and 2). Given that the second SPIRAL-I target-source cave cannot accomodate the proposed LINAG target-source ensemble, this solution allows, as shown, a relatively short and direct low-energy transfer line to CIME (figure VII.3). The latter point is of particular importance as the construction phase of LINAG should disrupt as little as possible the operations of the existing facility. As noted in table VII.8, the total cost of such a transfer line, including the ECR system to implement the $1^+/n^+$ charge breeding prior to injection into CIME, is estimated at some 1.4 M€. In addition, a short transfer line to the

existing SPIRAL-I low-energy experimental area (LIRAT) may be easily implemented.

Whilst the proposed siting of LINAG requires the implementation of a relatively long (~120m), low-energy beam transfer line to the C02 injection cyclotron (Fig VII.2) or dedicated RFQ-injector (~60m), the transporting of 1^+ charge state beams greatly simplifies the task. The developments and costs (including the 1^+- n^+ charge breeder) associated with these solutions are moderate : some 3 M€ in the case of injection via C02 and 6 M€ if a purpose built RFQ-injector is included (table VII.8) [ref 2].

Importantly the proposed implantation outlined in figure VII.1 provides ample flexibility in the extension of the linac to higher energies ref.1), for example by adding cavities in a structure running along the northern side of GANIL parallel to the existing buildings, as shown for example figure VII.4. This provides the most flexibility in the siting of the associated experimental areas for high-energy, in-flight fragmentation or ISOL production schemes. The layout of LINAG and its siting can also easily accomodate an eventual second source + RFQ ensemble to provide for improved future high-energy, heavy-ion operations (A>60). Moreover, the absence of any existing structures at the injection end of the linac would allow for its use as an eventual postaccelerator, for any future ISOL based project such as EURISOL.

The choice of a linear accelerator also capable of accelerating heavy ions at high intensities opens up a wealth of possibilities in terms of stable beam experiments. In particular, great interest has been expressed within the community to have access to high-intensity, heavy-ion beams around the Coulomb barrier for the production and spectroscopy of heavy elements as well as that of medium to high mass proton-rich systems. Given that from the technical standpoint operations centred on the production of fission fragment beams might be expected at most to occupy some 50% of the possible running time, a very significant amount of time could be devoted to stable beam operations. Given the proposed siting of LINAG injection of stable beams from the linac into the existing experimental areas would be complex and expensive and would severely limit the parallel beam operations discussed below. Moreover the handling of very high-intensity beams in the existing areas is most probably not feasible. It is thus suggested that a purpose built area, such as that proposed in figure VII.1, should be considered as an integral part of the facility. A location on the north side of the LINAG building is preferable as it allows for the later expansion, if necessary, of the area ; a location on the southern side of the building would be unduly restrictive owing to the need to maintain free heavy vehicle access to the nouthern end of the existing buildings.

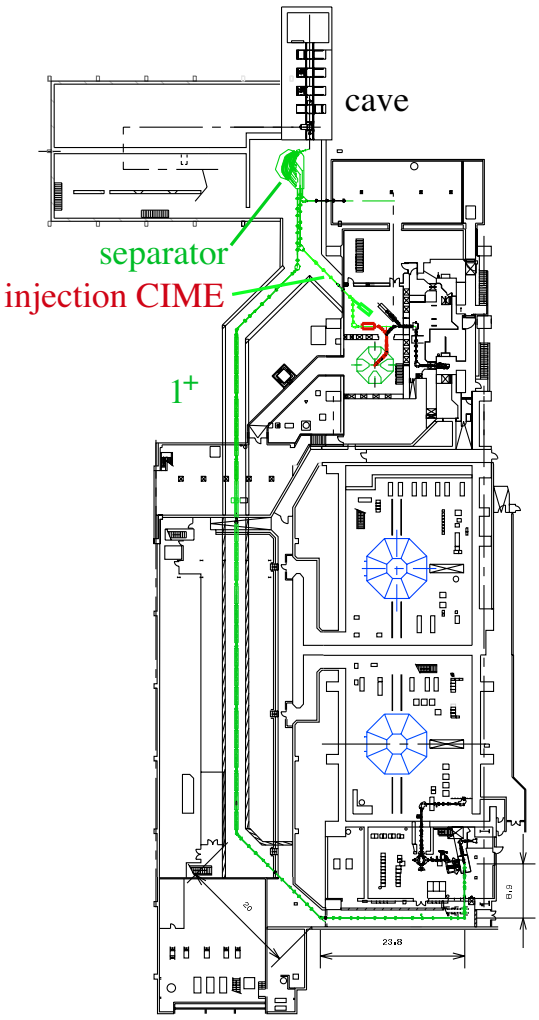

Figure VII.2 : Layout at the below ground level of the LINAG target-ion source cave and beam transport to the low-energy area, CIME and the C02 injection cyclotron.

Owing to the diverse range of experimental programmes currently undertaken and envisaged by the GANIL user community, together with the oversubscription on available beamtime, it is strongly felt that any new developments, such as LINAG, should facilitate (or at the very least forsee) parallel beam operations ; that is, the simultaneous delivery of different beams to different experiments. A key feature to any such operations will be the construction of a direct beamline from CIME to the G1 and G2 areas that bypasses the α-spectrometer (figure VII.1). At present this project is under

study at GANIL in the context of providing parallel stable beam operations with CIME. With the advent of secondary beams produced with LINAG, this beamline would thus facilitate the furnishing of reaccelerated beams via CIME to G1 or G2, whilst the coupled cyclotrons provide stable or SISSI fragmentation beams to any of the remaining experimental areas (SPEG, LISE, INDRA, G4, D1 and 2). In the case of the implementation of an experimental area dedicated to stable beam operations with LINAG, the coupled cyclotrons could function as just described, or as the driver for SPIRAL-I.

Arguably the most diverse range of operations may be achieved if more than one radioactive species extracted from the LINAG target-source ensemble could be selected. Such multibeam extraction would require the development of a relatively sophisticated separator: either a magnetic spectrometer, such as the BRAMA device [ref 3] (conceived in

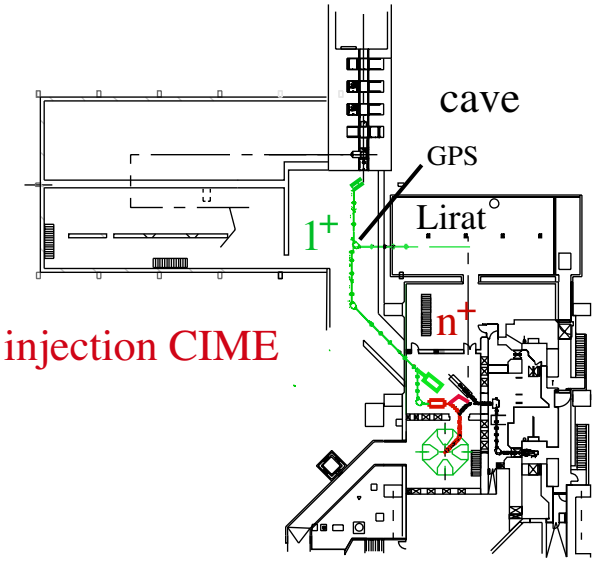

Figure VII.3 : Details of the porposed layout of the the LINAG target-ion source cave and the feeding of the low-energy area and CIME.

the context of the original US ISL laboratory project) shown in figure VII.2, or a Wien filter (or General Purpose Spectrometer, CERN-Isolde). Ideally then, as the layout in figure VII.2 indicates, three different ions falling within the acceptance range of the separator could be fed simultaneously to the low-energy area and to CIME as well as the coupled cyclotrons for reacceleration. A detailed design study for such a separator remains to be undertaken, however it is clear that if the feasibility of such a device can be demonstrated, its eventual inclusion would enhance considerably the capabilities of the facility.

VII.1) POST ACCELERATION OPTIONS

In the following discussion, we examine the different options for reacceleration based on the existing machines, namely, CIME, CSS1 and CSS2. As such the following energy regimes would be accessible :
- CIME : from 1.7 MeV /n to 6 MeV/nucleon
- CIME+CSS2 : up to 40 MeV/nucleon
- CO2 + CSS's : from 5 MeV/n up to 45 MeV/nucleon.
- RFQ + CSS's : up to 45 MeV/nucleon with a much better transmission.

VII.1.1) Post acceleration in using the CIME cyclotron

The maximal energy depends on the charge to mass ratio of the ions (table VII.1).

VII.1.2) Re injection of the CIME beams into CSS2

The installation of additional transfer lines in the vicinity of CSS2 requires major modification to the building,

Isotope	Charge state Q1	E_{max} from CIME
$^{132}_{50}Sn$	15^+	3.4 MeV/nucleon (h=4)
	20^+	6.0 MeV/ nucleon (h=3)

Table VII.1 : On acceleration with CIME: The maximum energy depends on the charge state provided by the source. Q=15⁺ to 20⁺ is a very conservative figure. (Q=25⁺ may be possible with the near future source).

particularly shielding around CSS2 (access to CSS2 and CIME). Moreover, the energy dispersion at the exit of CIME cyclotron would produce a debunching of the beam. As such, the transfer line should not exceed 50 m in order to avoid a reduction in the transmission. The shortest beam transfer line we can envisage would require major modification of the building. Putting outside these difficulties a study was carried

out to examine the possibility of re-injection of the beam from CIME into CSS2.

The principle conclusions were :
- It is not possible to inject the beam from CIME into CSS2 without stripping and without modifying the cyclotron CSS2.
- Only one case of direct re-injection of a beam from CIME into CSS2 is possible : CIME operating in harmonic 5, magnetic field lower than the present lowest limit, and CSS2 in harmonic 4. This considerably restricts the operating range of CIME to ions with $0.175 < Q/A < 0.25$ in the frequency range $9.6\ \text{MHz} \leq f_{hf} \leq 13.6\ \text{MHz}$. This leads, as illustrated in TableVII.2 to :
- an increase in the maximum energy while the injection radius of CSS2 would need to be changed. The restricted frequency range of the coupled cyclotrons would allow operation only with : H=4 in CIME and H=3 in CSS2 for energies ranging from 10 to 21 MeV/nucleon.

This solution allows energies of 40 MeV/nucleon to be reached. However, to retain standard stable beam operation with C0+CSS2+CSS2, it will also be necessary to reduce the ejection radius of CSS1 to 2.81m. Similar modifications have been carried out as part of the OAE project [ref 4] and necessitated a 6-month shutdown.

Conclusions for CIME+ CSS2 acceleration.

Implementing such an acceleration scheme implies the construction of a 60 m long beam line from CIME to CSS2 in a very crowded environment. It should be underlined that the installation of such an additional transfer line will require major modifications to the accelerator building (enlargement), and will impose constraints on the shielding around CSS2. Such modifications will be very costly and, moreover, as was already recommended in the report "Long Term Future of GANIL Accelerator", the re-injection of the CIME beam into one of the CSS should not be considered.

Isotope	Emax from CIME	Stripping efficiency	Emax from CSS2	Transmission
$^{93}_{36}Kr$	3.3 MeV/nucleon	25% ($Q=27^{+}$)	21 MeV/ nucleon	< 4.5%
$^{132}_{50}Sn$	3.3 MeV/ nucleon	20% ($Q=35^{+}$)	21 MeV/ nucleon	< 3.5%

Table VII.2 : CIME (H=5) +CSS2 (H=4).

Isotope	E_{max} from CIME *(H=4)*	Stripping efficiency	E_{max} from CSS2 *(H=3)*	Transmission
$^{93}_{36}Kr$	5.2MeV/nucleon	28% ($Q=30^{+}$)	39MeV/ nucleon	< 5.6%
$^{132}_{50}Sn$	4.4MeV/ nucleon	21% ($Q=38^{+}$)	33MeV/ nucleon	<4.2%
	5.2MeV/ nucleon	6.2 % ($Q=42^{+}$)	39MeV/ nucleon	<1.2 %

Table VII.3 : CIME (H=4)+CSS2 (H=3), and a modified injection radius (RC2=1.125m) for CSS2.

VII.1.3) Post acceleration with C0+CSS1+CSS2

It is possible to transport the radioactive ion beams directly from the production target to one of the C0 injector cyclotrons. This would offer the advantage of simplicity, since no modifications would need to be made to the existing accelerators, apart from the addition of appropriate diagnostics. This solution would, in principle, offer the entire range of energies currently available with stable ions ; that is, from ≈ 1 to 45 MeV/nucleon.

The maximum energy for the optimum stripping efficiency is restricted to 35 MeV/nucleon for neutron-rich nuclei around A=100 (see table VII.4). Given the poor transmission of the injectors (15 % for C02 and 30 % for CO1) and L1 beam line (60 %), together with the stripping efficiency, the overall transmission is quite small.

Isotope	E_{max} from C02	E_{max} from CSS1	Stripping efficiency	E_{max} from CSS2	Transmission
$^{93}_{36}Kr$	0.38 MeV/n	5.3 MeV/n	27% ($Q=28^+$)	36 MeV/n	< 2.2%
	0.5 MeV/n	7.49 MeV/n	5.4% ($Q=34^+$)	50 MeV/n	<0.5%
$^{132}_{50}Sn$	0.39 MeV/n	5.5 MeV/n	22% ($Q=40^+$)	36 MeV/n	< 2.0%
	0.48 MeV/n	6.8 MeV/n	2.0 % ($Q=45^+$)	45 MeV/n	< 0.16%

Table VII.4 : C02 (H=3)+CSS1(H=5)+CSS2 (H=2)

Choice of the cyclotron injector

Two injection cyclotrons already exist - C01 and C02. We note that CO1 is already equipped with a 100 kV high voltage platform.

The C01 cyclotron is, however, not suitable for several reasons :

- 100 kV will be difficult to achieve for a 1^+ source system : as a large high voltage platform in the very radioactive environment of the production cave is not desirable.
- A very high stability is difficult to achieve at 100 kV.
- The coupling between the $1+/n^+$ sources requires a stability of better than 5V.
- The CO1 cyclotron is needed for the acceleration of high intensity beams for SPIRAL I or SISSI. We do not therefore recommend that the injection energy be reduced to 30 kV as the high intensity capability of the C01 cyclotron depends on the high voltage platform and injection line.

The C02 cyclotron which is equipped with a 25 kV platform could be adapted to allow the re-ionization of 1^+ radioactive beam. A second platform could then be built for the n^+ source and an injection beam line would also be added. In this way, the existing n^+ source will be conserved for stable metallic ion production. The modifications (displacement and/or enlargement) of the existing platform would not be significantly cheaper.

The transfer beam line from the LINAG cave to C02 injector

As described above, a transport line would have to be provided for the low-energy beams over a distance of about 120 meters (figure VII.2).

Other projects have already examined such a scenario (PIAFE, Grenoble [ref 5] and DRIBS, Dubna [ref 6]). The relatively cheap technology developed for the PIAFE project seems well adapted to our needs. It uses iron free magnetic quadrupoles. Such technology could be applied in the 80 m long straight section. The second section (40 m) includes a number of bends and the use of periodic FODO channels is not possible.

Beam characteristics	Charge state : 1^+ Mass : 75uma<M<150 uma Energy < 30 keV
FODO channel	Length : 3 m Betatron phase advance : 50°
Magnetic quadrupoles Girders	Length : 7 m Radius : 49 mm I<1500A Bpole<0.0125T Alignment tolerance 0.3mm RMS (±0.5mm) Length : 3 m Mass : 1500kg Alignment tolerance 0.3mm RMS (±0.5mm)
Vacuum	P=10^{-8}mbar Ionic pump (45l/s) every 18 m +turbomolecular pump
Monitor + Corrector (steerer)	Every 9 m (PIAFE 18m)

Table VII.5 : Target-source to C02 low-energy beam transport line.

Technical considerations

Sensitivity to magnetic field

The solution adopted for PIAFE (FODO mesh consisting of iron-free quadrupoles) should be studied in more detail owing to the possible effects of the CSS leakage fields.

Charge exchange

The high sensitivity of the low-energy beams to the surrounding magnetic fields and to charge exchange mechanisms on the residual gas dictates that 1^+ ions are transported.

At low energy the cross section of charge exchange process depend mainly on the charge state and the first ionization potential of the residual gas.

The cross-section can be approximated by the formula of Schlachter :

$$\sigma_{q,q-1} = 1.43\ 10^{-12} q^{1.17} I_1^{-2.76} cm^2$$

Where I1 is the first ionization potentiel in eV of the atom and q the charge state.

The transmission T is then given by :

$$T = \exp\left[-\rho\, L\, \sigma_{q,q-1}\right] = \exp\left[-\frac{k_B\, T}{P} L\, \sigma_{q,q-1}\right]$$

Using T= 20°C and L=120m , we can evaluate the transmission as a function of the partial pressure of He and N (I1=14.534 eV for N, I1=24.587 eV for He). We note that residual Nitrogen gas induces higher beam losses than Helium.

Considering Nitrogen, a transmission around 80 % would require a vacuum better than 10^{-7} mbar for a 1^+ beam, while a value of 3.310^{-9} would be needed to achieved such a transmission for $q=20^+$ (figure VII.5). Therefore the transport of a multicharged ion beam over 120 m could be very expensive as far as the vacuum technology is concerned. For the transport of a monocharged ion beam 10^{-8} would be sufficient to achieve 97 % transmission.

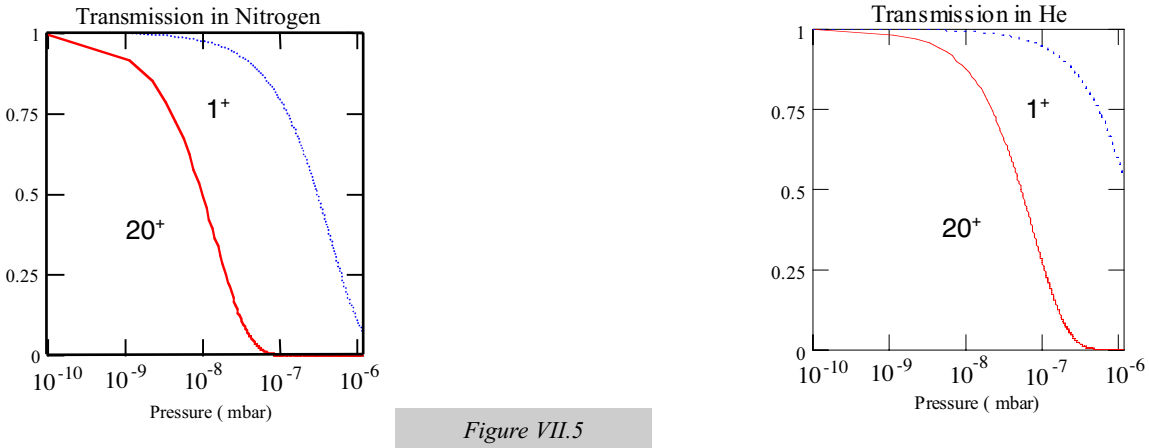

Figure VII.5

Finally, we note that as demonstrated, by the study of the PIAFE low energy beam line the emittance increase due to collisions should not play any role for pressures in the range 10^{-7} to 10^{-8} mbar.

Post acceleration with RFQ+CSS1 + CSS2.

The construction of a dedicated radio-frequency quadrupole (RFQ) injector presents several advantages compared to the reinjection of 1^+ ions into C02.

- The transport beam line needed between the 1^+ and n^+ source could be much shorter (60 m versus 120 m).
- Easier tuning of the injector (2 hours compared to 8 hours).
- The transmission presently achieved with the C02 injector could be increased by a factor 5.
- The RFQ could be employed to produce beams in the energy domain of interest for nuclear astrophysics and would be more suited for such experiments (rapid energy change) than the C02 injector.
- The RFQ, could also be used as a third injector for stable beams. This would allow beams provided by C01 or C02 to be directed to IRRSUD, while accelerating other beams with the RFQ for nuclear physics.
- The RFQ could also be used to increase significantly the intensity of stable beams using CSS1. This could be of some interest, for instance, for super heavy element production.

The principle drawbacks are :

- The additional cost compared to C02 has been evaluated at some 3 M€.
- A detailled study for such an RFQ would require additional time and manpower.

A good example of a modern variable frequency RFQ is that used at ISL BERLIN [ref 7].

	ISL Berlin	GANIL needs
Operating frequency range (MHz)	80 ≤ F ≤ 120	77 ≤ F ≤ 112 (h= 8 to 11)
Maximum electrode voltage (kV)	50	50
Structure length (m)	3	≈ 8
Beam aperture diameter (mm)	5	
Input energy range (keV/n)	9 ≤ W ≤ 36	2.5 ≤ W ≤ 15
Output energy range (MeV/n)	0.09 ≤ W ≤ 0.36	0.275 ≤ W ≤ 1
Beam pulse width (ns)	≤ 1	≤ 1
Normalised acceptance (≠.mm.mrad)	0.5	0.5 - 1
Output ΔE/E	≤ 10^{-2}	≤ 10^{-2}

Table VII.6 : Characteristics of the proposed RFQ compared to that at ISL Berlin.

Isotope	E_{max} from RFQ	E_{max} from CSS1	Stripping efficiency	E_{max} from CSS2	Transmission
$^{93}_{36}Kr$	0.38 MeV/n	5.3 MeV/n	27% (Q=28+)	36 MeV/n	< 14%
	0.5 MeV/n	7.49 MeV/n	5.4% (Q=34+)	50 MeV/n	<2.7%
$^{132}_{50}Sn$	0.39 MeV/n	5.5 MeV/n	22% (Q=40+)	36 MeV/n	< 11%
	0.48 MeV/n	6.8 MeV/n	2.0 % (Q=45+)	45 MeV/n	< 1.0%

Table VII.7 : RFQ+CSS1(H=5)+CSS2 (H=2)

A summary of the various post acceleration options discussed here is given in table VII.9. In addition, in table VII.8, we list a number of examples of secondary beams rates together with the stable analogue beams that would be used for tuning the cyclotrons.

	Produced rate [pps]	Extracted from the source	Target Exp.	Charge State	Possible Pilot beams
75Zn	$1.39\ 10^{8}$	$1.4\ 10^{6}$	$4.2\ 10^{4}$	14+/29+	86Kr16+/ 33+
78Zn	$1.09\ 10^{9}$	$1.1\ 10^{7}$	$3.3\ 10^{5}$	14+/29+	84Kr15+/ 31+
88Kr	$1.04\ 10^{12}$	$1.\ 10^{10}$	$3.\ 10^{8}$		
90Kr	$1.26\ 10^{12}$	$1.3\ 10^{10}$	$4.\ 10^{8}$	11+/31+	82Kr10+/ 28+
92Kr	$1.11\ 10^{12}$	$1.1\ 10^{10}$	$3.3\ 10^{8}$		
112Rh	$2.\ 10^{11}$	$2.\ 10^{9}$	$5.\ 10^{7}$		
116Rh	$5.96\ 10^{10}$	$6.\ 10^{8}$	$1.5\ 10^{7}$	16+/38+	66Zn8+/1 9+
132Sn	$6.65\ 10^{11}$	$6.6\ 10^{9}$	$1.6\ 10^{8}$		
138Xe	$2.44\ 10^{12}$	$2.4\ 10^{10}$	$6.\ 10^{8}$		
142Xe	$5.14\ 10^{11}$	$5.1\ 10^{9}$	$1.3\ 10^{8}$	18+/42+	134Xe17+ /40+
150Ce	$4.07\ 10^{11}$	$4.1\ 10^{9}$	$8.\ 10^{7}$		
156Sm	$5.09\ 10^{10}$	$5.1\ 10^{8}$	$1.\ 10^{7}$	20+/46+	78Kr10+/ 23+
158Sm	$6.04\ 10^{9}$	$6.\ 10^{7}$	$1.2\ 10^{6}$		

Table VII.8 : Rates production from source (1 %) and expected rate on target , assuming the following efficiencies: transfer line 80 %, C0 30 %, L1 + CSS1 30 %, stripping 30 to 20 % (most probable charge state), CSS2 to target 80 %. Possible stable pilot beams for tuning are also listed.

Post-acceleration method	Solution proposed Technical remark	Cost estimate	Energy/transmission for Interest $^{132}_{50}Sn$
CIME	- 1+ /n+ beam line - injection in CIME	1.4 M€	Emax= 6 MeV/n Transmission 25%
RFQ +SSC1 +SSC2	-60 m long transport line from target cell of driver - 1+ /n+ beam line - injection in the RFQ - Stripping between SSC1 and SSC2	6 M€	E=35 MeV/n Transmission 10% Emax=45 MeV/n Transmission 1% -RFQ Beam for nuclear astrophysics - Intense stable beam available, for super heavy elements.
C02 + SSC1 + SSC2	-120 m long Transport line from target cell of driver - 1+ /n+ beam line -injection in the CO2 stripping between SSC1 and SSC2	3 M€	Emax=35 MeV/n Transmission 2% E= 45 MeV/n Transmission 0.2%
CIME (H=4) +CSS2 (H=3)	Modification of SSC2 injection radius Major Building modification - 1+ /n+ beam line injection in CIME Stripping **Feasibility not demonstrated**	4 M€	Emax=40 MeV/n Transmission 1%

Table VII.8 : Summary of post acceleration options and estimated costs.

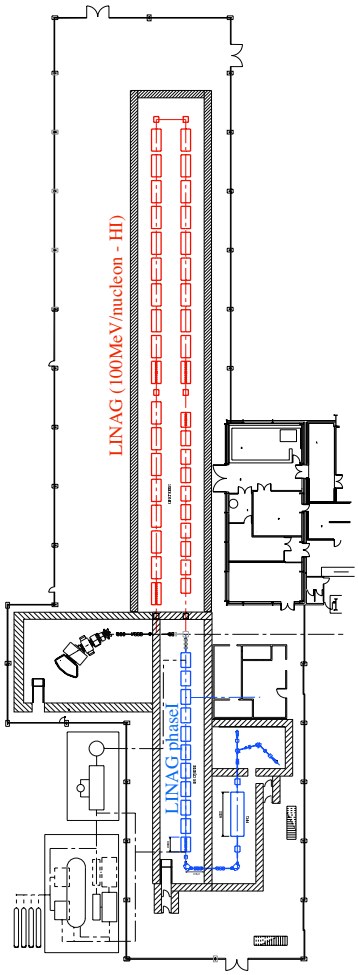

Figure VII.4 : Layout of the future LINAG implantation.

References

1) Commisionning of SPIRAL, the GANIL RIB Facility, M. Lieuvin et al, 16th Conference on Cyclotrons and their Applications, East Lansing, USA, May 2001, AIP Conference Proceedings Vol. 600

2) Variable Frequency RFQ's as Cyclotron Injectors A. Schempp, 16th International Conference on Cyclotrons and their applications, East Lansing, USA, May 2001, AIP Conference Proceedings Vol. 600

3) JM.Nitschke particle accelerator vol. 47, n° 3-4, 1994, p.153

4) Project OAE at GANIL, J. Ferme, 11th Conference on Cyclotrons and their Applications, Tokyo, Japan, October 1986

5) The PIAFE Project at Grenoble : Beam Transport of a Very Low Energy Radioactive Beam, J.-M. De Conto et al, EPAC 1996

6) DRIBs, The Dubna Project for Heavy Ion Beams, Yu. Ts. Oganessian

7) A New Injector Concept : the RFQ-cyclotron Combination at ISL Berlin 14th Conference on Cyclotrons and their Applications, Cape Town, South Africa, October 1995, World Scientific

Chapter VIII : Possible links between LINAG and EURISOL

VIII.1) BACKGROUND TO EURISOL

EURISOL is an RTD project funded by the European Commission to do a "preliminary design study of the next-generation European ISOL radioactive nuclear beam facility", intended to produce RNBs which are some orders of magnitude higher in intensity than those presently available. It should be stressed that the study is site-independent, though calls might be made during the next phase of the project for European laboratories to offer to host the facility. GANIL could, of course, be one contender, and it is therefore sensible to look at the implications of this for the LINAG proposal.

Like LINAG, EURISOL is intended to have a primary beam driver-accelerator, serving a number of target stations, and the RNBs resulting would then be accelerated in a post-accelerator. The latter has been specified as having the ability to accelerate ions up to and including ^{132}Sn to an energy of 100 MeV/u, thus providing the possibility of fragmentation of such neutron-rich nuclei, with the hope of producing acceptable yields of many exotic neutron-rich ion species.

Unlike LINAG, the EURISOL driver of choice is a proton linear accelerator, with both high energy and high beam power : 1 GeV and 1–5 MW. Investigation has shown that this machine could be designed to accelerate other ions of M/q = 2 (up to 500 MeV/u) at some significant extra cost, while M/q = 3 ions would require major changes and much greater cost. Another possibility would be to restrict the M/q = 3 ions to 33 MeV/u, which would require less extensive modification, but would nonetheless imply a cost increase.

EURISOL would probably use (a) medium-power beams (say 100 microamps of 1 GeV protons) directly onto a production target, and also (b) high-power beams, dissipating up to perhaps 1 MW of beam power in a liquid-metal target, such as a mercury-jet target. The target design and heavy shielding needed around the latter targets are beyond the scope of LINAG, but for both projects the targets and shielding for beam powers exceeding 100 kW require careful planning and sufficient space for safe handling of such highly radioactive targets.

VIII.2) SYNERGIES

Firstly, we remark that there would be a significant sharing of technology and the expertise necessary, since both projects have considered superconducting linear accelerators, with the concomitant RF and refrigeration systems, even if the machines were physically different.

Secondly, it could be suggested that the driver for LINAG could also be the driver for EURISOL. However, there are several important points to be considered here. The LINAG driver is a heavy-ion accelerator, while the EURISOL driver is essentially a proton driver, divided into 3 sections. These are (a) the low-energy section consisting of the ion-source on a 100 kV platform, followed by a 5 MeV RFQ, (b) an intermediate-energy section, comprising either a drift-tube linac or a linac with superconducting cavities, up to 85 MeV, and (c) a high-energy section containing 3 types of superconducting linac cavities, optimised for different values of β. For acceleration of M/q = 3 up to 100 MeV/u, a completely different RFQ would be needed, plus additional cavities to extend (or replace) the intermediate section so as to bypass completely the first (low-β) part of the high-energy section. As a result, the two machines are very different, but could in principle, share the final medium- and high-β sections.

It may be more practical to suggest that construction of the LINAC heavy-ion driver, to be used with CIME (as Phase 1) could be followed by construction of the EURISOL post-accelerator (Phase 2), and at some later stage by the much higher power proton driver, together with its heavily shielded multi-MW target area (Phase 3). The difficulty here is of course the high total cost of the EURISOL facility, which would be made even higher with this scenario !

Thirdly, we note that the most promising possibility examined for EURISOL post-accelerator is a superconducting linac, and the precisely the same technology is also proposed for the suggested LINAC driver. These two machines could in fact be one and the same. The proposed (final) LINAG driver should be able to accelerate ions up to mass 100 to an energy of 100 MeV/u, while EURISOL proposes a maximum mass of 132. (The implications of accelerating var-

ious charge-states of ^{132}Sn, with and without charge-breeding, have also been closely studied in the EURISOL context). For ions with M/q = 3 or less, the LINAG driver is very compatible with the EURISOL post-accelerator, though a few additional cavities may be needed to reach 100 MeV/u. The implication here is that LINAG could very well be a first phase of EURISOL, and could easily provide a ready-made post-accelerator for this ambitious European project.

There would be some competition here between the requirements of LINAG (i.e. shielded target, ion-source, and low-energy experimental areas) and those of EURISOL (i.e. possible fragment separator and high-energy experimental areas). However, these are problems relating to building lay-out and planning, and could probably be solved with suitably designed beam lines.

It can also be argued that since the EURISOL driver could be used at times for production of ions which are used only for low-energy experiments, the post-accelerator would be then available as a heavy-ion driver for the LINAG part of the facility, with its own target/ion-source set-up and post-accelerator (e.g. CIME or CSS1 and/or CSS2).

Another aspect of LINAG is that it would provide useful experience in operating an accelerator with up to 5 mA beams, and with design and handling of targets and ion sources with beams of much higher power than those presently available at SPIRAL. Radiation shielding and safe handling of radioactive components and safe disposal of radioactive waste materials and by-products (such as gases) will be an extremely important factor in obtaining permission to operate a facility such as LINAG or EURISOL. Even though the EURISOL proposal is concerned with MW beam power, the experience with the 300 kW beams proposed for LINAG would be very relevant. A demonstrated competence in these areas would be a big advantage to any laboratory proposing to host such a facility.

Chapter IX : Summary of costs and general schedule

The estimated preliminary costs for the project LINAG I are sumarized in the following table. These costs are for the LINAG I, as the production of fission fragments are assumed to be accelerated by CIME and to be used simultaneously in the LIRAT area. They do not include the ion source for heavy ions with M/Q=3, but they do include the building for adding this source. They also include an experimental area for near-Coulomb-barrier physics, but not the beam line and the equipment needed in this area. They do not include post-acceleration with the CSS1-CSS2.

The schedule is given in figure IX.1 pre-supposes that the funding, eventually related to the safety authorisations, will start in January 2004, and that the full amount of funding will be available before end of 2006. The safety authorisations will be necessary to start the construction of the building before mid-2004, in order to be able to start the installation of equipment in time with the schedule. The timing of funding and safety authorisations are the most critical conditions in the schedule shown.

ITEMS	cost (kE)	ITEMS	cost (kE)
Building / Infrastructure	**5850**		
Compressors	240	**Source N+**	**450**
Liquifier	126		
Coulomb Barrier Exp. Area	292	**Beam Transport**	**3360**
Shielding Exp. Area	125	HEBT LINAC-TIS	360
Driver building	1944	TIS-GPS separator	600
Shielding Driver Building	467	Separator GPS	500
Basement Target-Ion Source	374	Separator-n^+ -injection line Cime	1400
Basement Power s/Beam transp.	780	séparateur-LIRAT	200
installation	1500	Identification device in 1^+ n^+ line	300
Linac Driver	**14785**		
D+ source	185	**Radioprotection**	**750**
LEBT	275	beacons, controls	600
RFQ	2635	extension UGS's	150
Sc-LInac			
MEBT	610	**Computer Control**	**250**
Cryogenic modules	8130	Beam lines and TIS (except driver)	250
Cryogenic Plant	2150	**Miscellaneous**	**2000**
diagnostics	400	missions	150
Computer control	400	Layout GANIL (routes,)	100
		aléas (5%)	1750
Target / Ion Sources	**6675**	**R&D during APD**	**1550**
Surroundings	750	driver	400
3 Sources	225	TIS	200
Target	300	APD building architect	300
Plugs (2 operation + 1 R&D)	450	R&D charge breeder (SIRAP)	550
Plug (extraction)	150	2 post-docs	100
Plug (separator)	150		
Handling system	750		**35670**
Storage cells	200		
Test bench	500		
Gas storage	200		
Hot cell and manipulators	2000		
Nuclear ventilation	1000		
TOTAL		35670	

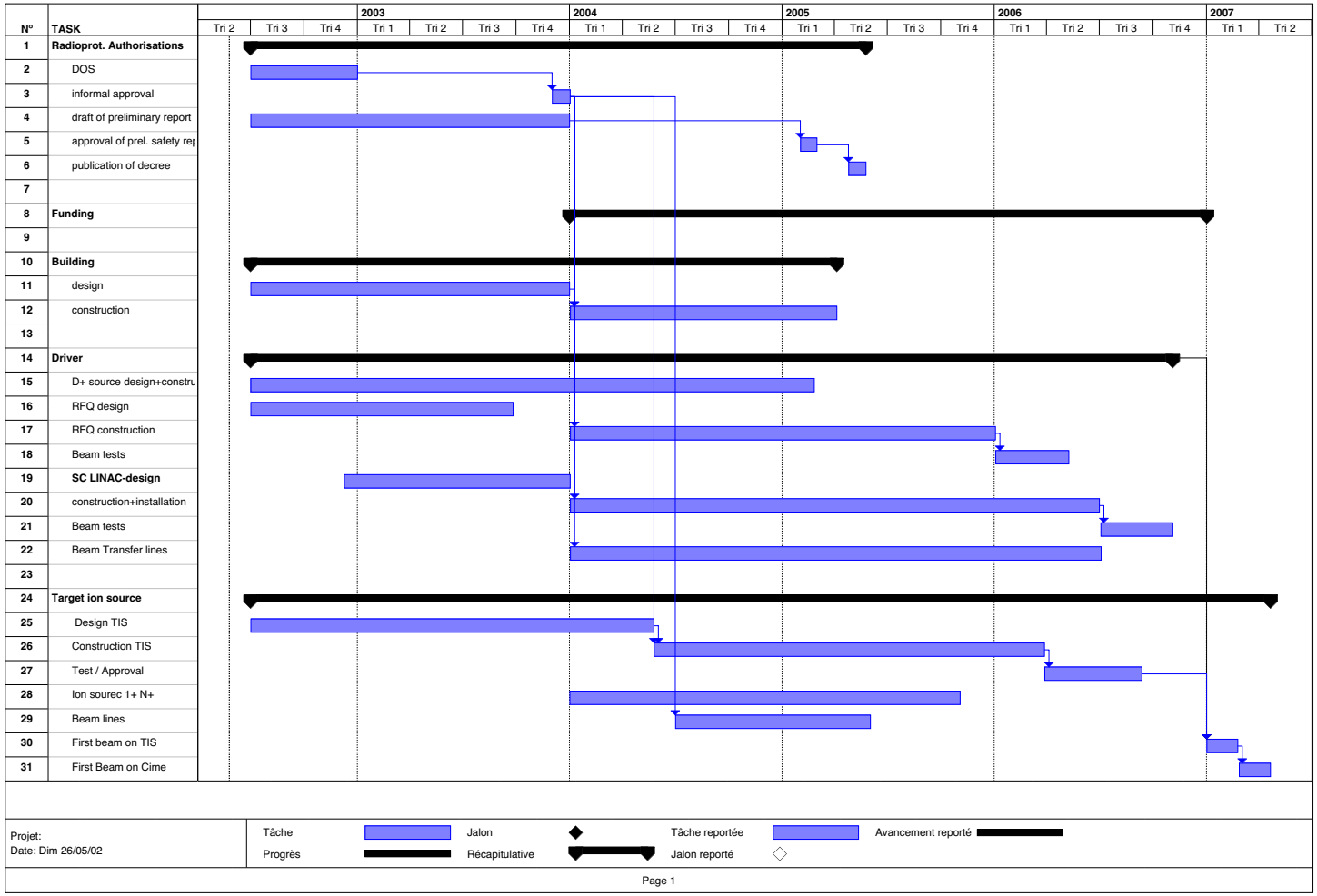

Figure IX.1 : Schedule of the LINAGI project.

Chapter X : Conclusion

In the present report we have studied in some detail technical aspects of the LINAG I project. It integrates the SPIRAL II project that had the aim of adding medium-mass nuclei to those available with SPIRAL. Fission induced by light particles (e, p, d, etc.) was proposed to produce the radioactive ions, with an aim of 10^{13} fissions/s at least.

We have shown here that the LINAG I project can reach even higher fission rates using proven technologies. Using a C-converter and a 5-mA deuteron beam, neutron-induced fission will be 1.3 x 10^{13} fissions/s using standard-density UC_x, and 5.3 x 10^{13} fission/s for high-density UC_2. For both cases, a very small volume (240 cm^3) ion source was selected, in order to have relatively fast diffusion-effusion times for short-lived nuclei. In principle, larger volumes could result in even higher fission rates, up to 2 x 10^{14} fissions/s, for which the heat produced by fission in the ion source reaches 6 kW, the present limit for the SPIRAL targets.

Besides this method of using a converter, direct irradiation of the UC_x with beams of d, ^{3,4}He, ^{6,7}Li, or ^{12}C can be used if the higher excitation gives a higher branching to a given nucleus of interest. This is the case for many nuclei far from the fission "bump". For example, with a deuteron beam limited to 6 kW, this is 0.15 mA impinging directly on UC_x, 5 x 10^{12} fission/s are expected. This method therefore becomes advantageous if the branching ratio to the nucleus is increased by an order of magnitude as compared to low energy fission.

With relatively small supplementary investments (for a heavy ion source and beam lines) studies of fusion-evaporation will be possible. If thin target methods associated with a separator are used, the energy deposited in the target will be the main limitation. With techniques developed for super-heavy research, it was seen that, for example, an N=Z nucleus like ^{80}Zr that has a formation cross section of only 10 μb, could be produced at the exit of a separator with an intensity of more than 10^4/s. This opens up a large domain of research near and at the N=Z line. More generally, heavy ion beams of high intensity for near-Coulomb-barrier physics could be produced. Present high-performance ECR ion sources (PHOENIX, SERSE, etc...) already deliver 1 mA of O ions for M/Q=3, and are close to reaching this value for Ar (≥ 200 μA already). Present values for Kr are in the 10 μA range for M/Q = 3. This would allow us to cover physics near the Coulomb barrier for high intensity beams of A ≤ 86. These characteristics could be complementary to a stable beam accelerator optimised for a higher M/Q ratio.

The linear accelerator as a driver in this project belongs to the technology of high intensity accelerators, which are of strong current interest for various domains and are experiencing rapid technological development. A new RFQ structure has been designed for the project, that greatly reduces costs and fabrication time. This structure was calculated with full beam dynamics for the projected intensity of 5mA of deuterons, taking into account geometrical tolerances. Very low losses were found, of the order of 5 x 10^{-5}. The superconducting linac has been studied in some detail, and suitable quarter-wave resonators using solid-Nb or Nb/Cu could be manufactured without any significant problems. Beam dynamics calculations and cost evaluations were made for a conceptual design, using the Nb/Cu QWR of the Legnaro type, as they perform the required accelerating field at the best price. Power supplies would need to employ the older, slightly less reliable vacuum-tube technology, owing to the high power levels required. Multi-kW power-couplers will need some development for the QWR application, but far higher-power couplers already exist for other S/C cavities. No problems are foreseen with the cryogenic systems required, which have also been examined in some detail. Beam dynamics calculations with space-charge forces and halos for the complete accelerator are in progress.

As a consequence of the high production rates, the radioprotection constraints become a major factor in the project. This implies a change of technology compared with SPIRAL, with higher costs for the target/ion-source and associated infrastructure. The technology of target "plugs", as used at TRIUMF-ISAC, has been chosen. It offers the guarantee of safe handling of the high levels of activity produced.

The Linag I project could be considered as being part of a multi-beam policy of GANIL. It was shown in the chapter on post-acceleration that many possibilities of simultaneous use of beams would be possible. (We note here that several simultaneous beams are already used at GANIL).

Another aspect of LINAG I is its possible synergies with EURISOL. We note that the most promising possibility examined for EURISOL post-accelerator is a superconducting linac, and precisely the same technology for the linac is also proposed for the suggested LINAG I driver. These two

machines could in fact be one and the same, by just adding an appropriate RFQ for bigger M/Q ratios. The proposed (final) LINAG driver should be able to accelerate ions up to mass 100 to an energy of 100 MeV/u, while EURISOL proposes a maximum mass of 132. (The implications of accelerating various charge-states of ^{132}Sn, with and without charge-breeding, have also been closely studied in the EURISOL context). For ions with M/q = 3 or less, the LINAG driver is very compatible with the EURISOL post-accelerator, though a few additional cavities may be needed to reach 100 MeV/u.

The implication here is that LINAG could very well be a first phase of EURISOL, and could easily provide a ready-made post-accelerator for this ambitious European project. It would also provide useful experience in operating an accelerator with up to 5 mA beams, and with design and handling of targets and ion sources with beams of much higher power than those presently available at SPIRAL. Radiation shielding and safe handling of radioactive components and safe disposal of radioactive waste materials and by-products (such as gases) will be an extremely important factor in obtaining permission to operate a facility such as LINAG or EURISOL. Even though the EURISOL proposal is concerned with MW beam power, the experience with the 300 kW beams proposed for LINAG would be very relevant. A demonstrated competence in these areas would be a big advantage to any laboratory proposing to host such a facility.

Contributors :

The LINAG phase I study was co-ordinated by Wolfgang Mittig, Ganil.
Two meetings were organised at Saclay on January 15th, 2002, and on April 30th, 2002. In the first meeting seven sub-groups were formed.

1) Driver
2) Post-acceleration
3) Sources for primary beams
4) Production target/Secondary beam sources
5) Security and Radioprotection
6) Layout of the facility
7) General Infrastructure and Report Edition.

The list of persons who contributed in the different subgroups is given in the table below, and the co-ordinators of these sub-groups are also indicated. By advance, we apologise to those whose names were forgotten in the last rush of the redaction of the present document. Many others contributed by their advice, help and critics.

Name	Lab.	Driver	Post-acceler ation	Primary Sources	Target/ Second. Sources	Securit Radio-Protect.	Layout of facility	General Infrastr. Report
G. Auger	GANIL							Coord.
C. Barué	GANIL	X		X				
P. Bertrand	GANIL	X						
J-L. Biarotte	IPNO	X						
S.Bousson	IPNO	X						
B. Bru	GANIL	X						
F. Chautard	GANIL		X					
F. Clapier	IPNO					Coord.		
C. Commeaux	IPNO	X						
J. Cornell	GANIL							X
F. Daudin	GANIL						X	
M. Di Giacomo	GANIL	X						
P. Dolegeviez	GANIL	X						
R. Duperrier	SACM	X						
M. Duval	GANIL	X						
R. Ferdinand	SACM	X						
G. Gaubert	GANIL				X			
R. Gobain	SACM	X						
Y. Huguet	GANIL						X	
B. Jacquot	GANIL		X					
P. Jardin	GANIL				X			
B. Laune	IPNO		Coord					
N. Lecesne	GANIL				X			
P. Leherissier	GANIL	X		X				
R. Leroy	GANIL			X	X			
J. Lesrel	IPNO	X						
F. Loyer	GANIL							X
MH Moscatello	GANIL	Coord						
G. Olry	IPNO	X						
N. Orr	LPC						Coord.	
M. Painchault	SACM	X						
J.Y. Pacquet	GANIL				X			
V. Panteleev	St-Peter				X			
F. Pellemoine	GANIL				X			
B. Rannou	GANIL					X		
D. Ridikas	SPhN				X			
P. Royet	GANIL					X		
P. Sortais	ISN			Coord.				
MG St-Laurent	GANIL				X	X		
A. Savalle	GANIL		X					
D. Uriot	SACM	X						
F. Varenne	GANIL	X	X					
A.C.C. Villari	GANIL				Coord.			

The list of the 96 persons who participated at least at one of the meetings is given below.

NAMES	First Name	Laboratory	NAMES	First Name	Laboratory
ALAMANOS	Nicolas	CEA	JARDIN	Pascal	GANIL
AUGER	Gérard	GANIL	KORTEN	Wolfram	CEA
AUGER	Françoise	CEA	LAPOUX	V.	CEA
AZAIEZ	Faical	IPNO	LAU	Christophe	IPNO
BAJARD	Marcel	IPNL	LAUNE	Bernard	IPNO
BAJEAT	Olivier	IPNO	LE COZ	Yves	CEA
BARUE	Christophe	GANIL	LECESNE	Nathalie	GANIL
BERTRAND	Patrick	GANIL	LEFORT	Hervé	IPNO
BIARROTTE	Jean-Luc	IPNO	LEHERISSIER	Patrick	GANIL
BLANK	Bertram	CENBG	LERAY	Sylvie	CEA
BLUMENFELD	Yorick	IPNO	LEROY	Renan	GANIL
BOUDARD	Alain	CEA	LESREL	Jean	IPNO
BOUSSON	Sébastien	IPNO	LEWITOWICZ	Marek	GANIL
BRU	Bernard	GANIL	LOPEZ-MARTENS	Araceli	CSNSM
BUTLER	P.A.	Liverpool	LOYER	François	GANIL
CHARTIER	Marielle	Liverpool	LUNNEY	David	CSNSM
CHATTERJEE	Mihir	GANIL	MATERNA	T.	Université Libre de Bruxelles
CHAUTARD	Frédéric	GANIL	MIELOT	Christophe	IPNO
CHBIHI	Abdou	GANIL	MITTIG	Wolfgang	GANIL
CLAPIER	François	IPNO	MORJEAN	Maurice	GANIL
CORNELL	John	GANIL	MOSNIER	Alban	CEA
DAUDIN	François	GANIL	MUELLER	Alex	IPNO
DAUGAS	Jean-Michel	CEA DAM	NALPAS	Laurent	CEA
DAYRAS	Roland	CEA	OLRY	Guillaume	IPNO
DHILLY	Gérard	GANIL	ORR	Nigel	LPC
DI GIACOMO	Marco	GANIL	PAINCHAULT	Michel	CEA
DOLEGIEVIEZ	Patrick	GANIL	PANTELEEV	Vladimir	ST PETERSBOURG
DROUART	Antoine	CEA	PEGHAIRE	Alain	GANIL
DUPERRIER	Romuald	CEA	PELLEMOINE	Frédérique	GANIL
DUVAL	Maurice	GANIL	PINSTON	J.A.	IN2P3
EGELHOF	Peter	GSI	RIDIKAS	Danas	CEA
ESSABAA	Said	IPNO	RIVET	Marie-France	IPNO
FERDINAND	Robin	CEA	ROUSSEL-CHOMAZ	Patricia	GANIL
FORTUNA	G.	LNL	ROYET	Pascal	GANIL
FRANKLAND	John	GANIL	SAINT-LAURENT	MG	GANIL
GAUBERT	Gabriel	GANIL	SAVAJOLS	Hervé	GANIL
GILLIBERT	Alain	CEA	SCHMIDT	KH	GSI
GIOVINAZZO	Jérôme	CENBG	SKAZA	Flore	CEA
GOBIN	Raphaël	CEA	SORLIN	Olivier	IPNO
GOUTTE	Dominique	GANIL	SORTAIS	Pascal	ISN
GREVY	Stéphane	LPC CAEN	STANOIU	Mihai	GANIL
GUILLEMAUD-MUELLER	Dominique	IPNO	STUTTGE	Louise	IRES
HANAPPE	Francis	Université Libre de Bruxelles	TECCHIO	Luigi B.	INFN
HANNACHI	Fazia	CSNSM	THEISEN	Christophe	CEA
HENRY	Sylvain	CERN	TKATCEHNKO	André	IPNO
HOSNI	Faouzi	IPNO	VILLARI	Antonio	GANIL
HUGUET	Yves	GANIL	VOLANT	Claude	CEA

We thank all those who welcomed us in their laboratories, and who gave us very precious and essential information for the SC linac proposal :
LNL : A. Facco, V. Palmieri, A.M. Porcellato, D. Berkovits, V. Zviagintsev, S. Stark, G. Bassato, S. Canella, P. Favaron, G. Bisoffi, A. Pisent
ANL : P. Ostroumov, K. Shepard, G. Zinkan, J. Specht
ISAC/TRIUMF : P. Bricault
We thank Prof. R. Maier and Dr. R.Toelle for communicating us the very helpful reports on the superconducting injector LINAC for Cooler Synchrotron COSY at Juelich, Germany.